Increasing Notch signaling antagonizes PRC2-mediated silencing to promote reprograming of germ cells into neurons

Stefanie Seelk[1]*, Irene Adrian-Kalchhauser[2,3]*, Balázs Hargitai[2], Martina Hajduskova[1], Silvia Gutnik[2], Baris Tursun[1†] and Rafal Ciosk[2†]

[1] Berlin Institute for Medical Systems Biology, Max-Delbrück-Center for Molecular Medicine, Robert-Rössle-Strasse 10, Berlin 13125, Germany

[2] Friedrich Miescher Institute for Biomedical Research, Maulbeerstr. 66, 4058 Basel, Switzerland

[3] Present address: Programm Mensch-Gesellschaft-Umwelt, Department of Environmental Sciences, University of Basel, Vesalgasse 1, 4051 Basel, Switzerland

* These authors contributed equally to this work

[†] Correspondence: rafal.ciosk@fmi.ch; baris.tursun@mdc-berlin.de

Short Title: Notch antagonizes PRC2 for reprograming

Keywords: Notch, GLP-1, PRC2, MES, UTX-1, stem cell, germline, reprograming

Abstract

Cell-fate reprograming is at the heart of development, yet very little is known about the molecular mechanisms promoting or inhibiting reprograming in intact organisms. In the *C. elegans* germline, reprograming germ cells into somatic cells requires chromatin perturbation. Here, we describe that such reprograming is facilitated by GLP-1/Notch signaling pathway. This is surprising, since this pathway is best known for maintaining undifferentiated germline stem cells/progenitors. Through a combination of genetics, tissue-specific transcriptome analysis, and functional studies of candidate genes, we uncovered a possible explanation for this unexpected role of GLP-1/Notch. We propose that GLP-1/Notch promotes reprograming by activating specific genes, silenced by the Polycomb repressive complex 2 (PRC2), and identify the conserved histone demethylase UTX-1 as a crucial GLP-1/Notch target facilitating reprograming. These findings have wide implications, ranging from development to diseases associated with abnormal Notch signaling.

Introduction

Cell-fate decisions are controlled, on the one hand, by intercellular signaling and, on the other hand, by intrinsic mechanisms such as epigenetic chromatin modifications. The Notch signaling pathway is a highly conserved and widespread signaling mechanism (Artavanis-Tsakonas *et al.* 1999; Greenwald and Kovall 2013), which has been implicated in key cell-fate decisions such as the decision between proliferation and differentiation (Liu *et al.* 2010). Notch signaling has also been implicated in cellular reprograming. Upon inhibition of Notch signaling, the oncogenic genes KLF4 and cMyc become dispensable for the generation of induced pluripotent stem cells (iPSCs) from mouse and human keratinocytes (Ichida *et al.* 2014). In this setting, Notch inhibits reprograming. Conversely, Notch signaling promotes transdifferentiation of pancreatic acinar cells to ductal cells (Sawey *et al.* 2007), or the conversion of hepatocytes into biliary cells in liver primary malignancy intrahepatic cholangiocarcinoma (ICC) (Sekiya and Suzuki 2012). Notch signaling can also affect reprogramming in normal development. In *C. elegans*, signaling through the GLP-1 and LIN-12 Notch receptors impedes reprogramming during embryogenesis and, during larval development, signaling through LIN-12 is required for the conversion of a rectal epithelial cell into a motorneuron (Jarriault *et al.* 2008; Djabrayan *et al.* 2012).

The role of epigenetic regulators in cell-fate decisions has been studied mostly in pluripotent cells cultured outside of their normal tissue environment (Meshorer and Misteli 2006; Spivakov and Fisher 2007; Lessard and Crabtree 2010; Orkin and Hochedlinger 2011). Therefore, epigenetic regulation of stem cell identity in intact tissues remains poorly understood. Additionally, the impact of external cues, for example signaling from a stem cell niche to the recipient cell's chromatin remains equally unresolved. By contrast, *C. elegans* has been used as a model to study reprograming in an intact organism (Horner *et al.* 1998; Fukushige *et al.* 1998; Zhu *et al.* 1998; Fukushige and Krause 2005; Ciosk *et al.* 2006; Jarriault *et al.* 2008; Yuzyuk *et al.* 2009; Riddle *et al.* 2013). In this model, germ cells can be directly reprogrammed into neurons by depleting specific chromatin modifiers such as LIN-53 (Rbbp4/7) or components of PRC2, and by concomitant overexpression of the

transcription factor CHE-1, which induces glutamatergic neuronal fate in a process which we refer to as Germ cell Conversion (GeCo) (Tursun *et al.* 2011; Patel *et al.* 2012).

Here, we identify the Notch signaling pathway as a critical player in this reprograming model. This was unanticipated, since signaling through the Notch receptor GLP-1 (henceforth GLP-1^{Notch}) from the somatic gonadal niche is known to maintain germline stem cell/progenitor fate (Kimble and Crittenden 2007). To understand this novel, reprograming-promoting role of GLP-1^{Notch}, we combined genetics with tissue-specific expression profiling. We identified genes regulated by GLP-1^{Notch}, including genes recently shown to maintain the germline stem/progenitor cells (Kershner *et al.* 2014). Additionally, and unexpectedly, we found that many genes activated by GLP-1^{Notch} signaling were also repressed by the cell fate-stabilizing chromatin regulator PRC2. We show that GLP-1^{Notch} and PRC2 have an antagonistic effect on germ cell-fate decisions and demonstrate co-regulation of their common target, *utx-1*. Importantly, UTX-1 is a histone demethylase known to erase the gene-silencing methylation of histone H3 dependent on PRC2 (Maures *et al.* 2011; Jin *et al.* 2011; Vandamme *et al.* 2012). Thus, we propose that the GLP-1^{Notch}–dependent induction of UTX-1 facilitates reprograming by alleviating PRC2-mediated repression of alternative cell fates.

Results

GLP-1^{Notch} enhances conversion of germ cells into neuron-like cells

Germ cells can be converted into neuronal cells in intact *C. elegans* upon overexpression of the neuronal transcription factor CHE-1, simply by depleting the chromatin modifier LIN-53 (Tursun *et al.* 2011; Patel *et al.* 2012). This GeCo phenotype can be followed in living animals by monitoring a reporter GFP expressed from the *gcy-5* promoter, which otherwise is induced in glutamatergic ASE neurons (Altun-Gultekin *et al.* 2001). In contrast to the spontaneous teratomatous differentiation of meiotic germ cells, observed in the absence of specific RNA-binding proteins (Ciosk *et al.* 2006; Biedermann *et al.* 2009; Tocchini *et al.* 2014), GeCo is preferentially observed in the pre-meiotic, proliferating germ cells (Tursun *et al.* 2011; Patel *et al.* 2012). Consistently, removing the proliferating germ cells, by inhibiting the GLP-1^{Notch} signaling, prevents GeCo (Tursun *et al.* 2011). However, because the proliferating germ cells were eliminated, these experiments did not address a possible direct effect of GLP-1^{Notch} signaling on GeCo. We began addressing this issue by examining the gonads of animals carrying the gain-of-function *glp-1* allele (*ar202*) (Pepper *et al.* 2003). These gonads are filled with proliferating germ cells and, upon depleting LIN-53 and overexpressing CHE-1, we observed that significantly more germ cells converted to ASE neurons (Figure 1A, Figure 1–source data 1). We refer to this enhanced GeCo as "GeCo+". Detailed quantification revealed that the GeCo+ gonads contained more than twice the number of converted cells (Figure 1–figure supplement 1A, Figure 1–source data 1). The nuclei of these converted cells were reminiscent of neuronal nuclei and the cells displayed axo-dendritic projection (Figure 1–figure supplement 1B), as previously described (Tursun *et al.* 2011; Patel *et al.* 2012). To confirm that the GeCo enhancement depends on the canonical Notch signaling pathway, rather than an independent function of the GLP-1^{Notch} receptor, we RNAi-depleted the transcriptional effector of GLP-1^{Notch} signaling, *lag-1* (Christensen *et al.* 1996). We exposed animals only after hatching to *lag-1* RNAi in order to avoid sterility, which is caused when animals are subjected to *lag-1* RNAi earlier (Supplemental file 1). RNAi-mediated knock-down of *lag-1* strongly inhibited GeCo (Figure 1B, Figure 1–source

data 1). Importantly, under these experimental conditions, we did not observe any obvious reduction of germ cell numbers (Figure 1C, Figure 1–source data 1), suggesting a proliferation-independent effect of GLP-1^{Notch} signaling on cell-fate conversion. To investigate this further, we tested GeCo efficiency on germ cells proliferating independently of GLP-1^{Notch} signaling. We took advantage of mutants in which, in the absence of two meiosis/differentiation-promoting factors GLD-1 and GLD-2, germ cells proliferate independently of GLP-1^{Notch} (Kadyk and Kimble 1998). Specifically, we examined GeCo in the loss-of-function *gld-1(q497) gld-2(q485)* mutants, which carried either wild-type *glp-1* or the loss-of-function *glp-1(q175)* allele (Austin and Kimble 1987). Both mutant combinations have previously been described to have tumorous germlines and impaired meiotic entry (Kadyk and Kimble 1998; Hansen *et al.* 2004). In contrast to efficient GeCo observed in the *gld-1(q497) gld-2(q485)* gonads, GeCo was strongly diminished in the *gld-1(q497) gld-2(q485); glp-1(q175)* gonads, despite the ongoing germ cell proliferation (Figure 1D, Figure 1–source data 1). Counting the number of germ cells in these gonads revealed only a slight difference (a 15% increase in the numbers in the double vs. triple mutant gonads), suggesting that the strong enhancement of GeCo by GLP-1^{Notch} signaling cannot be explained by increased number of germ cells (Figure 1–figure supplement 2, Figure 1–source data 1). Since it has been proposed that dividing cells have a higher propensity for cellular reprograming (Egli *et al.* 2008; Hanna *et al.* 2009), we also tested whether blocking the cell cycle would affect the observed GeCo enhancement in *glp-1(gf)* gonads. As previously described (Fox *et al.* 2011; Patel *et al.* 2012), we used hydroxyurea (HU) treatment to block the cell cycle in the S phase. Blocking the cell cycle by HU did not diminish the GeCo+ phenotype (Figure 1–figure supplement 3, Figure 1–source data 1). Combined, these results suggest that GLP-1^{Notch} enhances GeCo independently from its role in promoting germ cell proliferation.

GLP-1^{Notch} activates genes mainly on X chromosomes

To understand the effects of GLP-1^{Notch} on GeCo, we set out to identify genes regulated by GLP-1^{Notch} signaling in germ cells. To conduct analysis in morphologically similar tissue, we

again took advantage of the *gld-1 gld-2* double mutants that, combined with either loss-of-function or gain-of-function *glp-1* alleles, have morphologically similar gonads, filled with proliferating, undifferentiated germ cells (Figure 2–figure supplement 1) (Kadyk and Kimble 1998; Hansen *et al.* 2004). We combined *gld-1(q497) gld-2(q485)* mutations with either the temperature-sensitive loss-of-function (lf) *glp-1* allele *(e2144)*, or the temperature-sensitive gain-of-function (gf) *glp-1* allele *(ar202)* (Priess *et al.* 1987; Pepper *et al.* 2003). Because GLD-1 and GLD-2 regulate gene expression at the posttranscriptional level only, we expected that transcriptionally regulated GLP-1^{Notch} targets could be identified in this background.

To analyze gene expression, gonads were dissected from animals grown at the restrictive temperature in two independent experiments, and transcripts were analyzed with tiling arrays (GEO accession number GSE49395). We identified around 100 transcripts that were differentially expressed between the *gld-1 gld-2; glp-1*(lf) (Notch OFF) and *gld-1 gld-2; glp-1*(gf) (Notch ON) gonads (Figure 2A and Figure 2–figure supplement 2, Figure 2–source data 1). These changes were confirmed by quantitative RT-PCR (RT-qPCR) on selected transcripts (Figure 2–figure supplement2A, Figure 2–source data 1). Most differentially expressed transcripts were upregulated in the 'Notch ON' gonads, indicating a predominantly activating role of GLP-1^{Notch} in germ cells. For simplicity, we will refer to the transcripts upregulated at least two fold in the 'Notch ON' gonads as 'Notch–activated'. Some Notch-activated genes, such as *sel-8/Mastermind*, *lst-1,* and *epn-1*/*Epsin*, have been implicated in Notch signaling in other cell types (Doyle *et al.* 2000; Yoo 2004; Tian *et al.* 2004; Singh *et al.* 2011; Kershner *et al.* 2014). However, it remains possible that, rather than being direct GLP-1Notch targets, some of the Notch-activated genes were upregulated as an indirect consequence of increased GLP-1/Notch signaling.

To demonstrate that Notch-activated genes are functionally relevant for germ cell proliferation, we performed RNAi knockdown of Notch-activated genes (n=64) on animals carrying the gain-of-function *glp-1(ar202)* allele, and screened for enhancement or suppression of the tumorous gonad phenotype (Supplementary file 1; for detailed experimental procedure see Materials and Methods). Knocking down some of the Notch-

activated genes (n=17, 26.6%) suppressed the tumorous phenotype, which agrees with predominantly proliferation-promoting role of GLP-1^{Notch}. Interestingly, knocking down a subset of the Notch-activated genes enhanced the tumor (n=8, 12.5%) (Supplementary file 1), suggesting that some of the Notch-activated genes may counteract proliferation. While some of these genes may function autonomously in the germline, others could affect the germline indirectly from the soma. To test this, we RNAi-depleted selected candidates in the *rrf-1 (pk1417)* mutant background, which is permissive for RNAi in the germline but deficient in RNAi in many (but not all) somatic tissues (Kumsta and Hansen 2012). While depleting most candidates in the *rrf-1* background had similar effects on the germline as in the wild type (suggesting germline-autonomous function), in some cases the effects were abolished, suggesting that these genes function in the soma (Figure 2-figure supplement 3, Figure 2–source data 1).

Strikingly, we noticed that Notch-activated genes were enriched on the X-chromosome, the *C. elegans* sex chromosome. 45% of the Notch-activated genes were X-linked, which is four-fold more than expected by chance ($p = 2.99e^{-14}$; Figure 2A and Figure 2–figure supplement 2B, Figure 2–source data 1). When analyzing only genes with higher than baseline germline expression values, the disproportional X-linkage of Notch-activated genes was even more striking (fifteen times more than expected by chance ($p = 2{,}19e^{-38}$; Figure 2A and Figure 2–figure supplement 2B, Figure 2–source data 1). In the *C. elegans* germline, X-linked genes are largely silenced by the *C. elegans* PRC2 (Fong *et al.* 2002). Thus, the X chromosome bias among Notch-activated genes suggested a possible antagonistic relationship between GLP-1^{Notch} and PRC2.

GLP-1^{Notch} and PRC2 have antagonistic functions in the germline

The *C. elegans* PRC2 consists of MES-2, -3, and -6 (Bender *et al.* 2004) and levels of the corresponding transcripts were essentially not altered by GLP-1^{Notch} signaling (*mes-2*: absolute fold change (fc) -1.3747; *mes-3*: fc 1.003; *mes-6*: fc 1.037). To test for a functional relationship between GLP-1^{Notch} and PRC2, we examined genetic interactions between GLP-

1^{Notch} and PRC2 mutants. At 20 °C, both the temperature-sensitive gain-of-function *glp-1(ar202)* and the homozygous loss-of-function *mes-2(bn11)* mutants, derived from heterozygous mothers providing maternal MES-2 (*mes-2* M+Z- mutants), were viable and produced gonads with nearly wild-type appearance. The double *mes-2* M+Z-; *glp-1(ar202)* mutants, however, displayed distal and proximal tumors at the same temperature (Figure 2B; 32/32 examined gonads). PRC2 and GLP-1^{Notch} thus interact functionally, and they appear to do so in a germ cell autonomous manner (Figure 2-figure supplement 3, Figure 2–source data 1).

Given the striking enrichment of Notch-activated genes on the X chromosome, and the genetic interaction between PRC2 and GLP-1^{Notch}, we speculated that GLP-1^{Notch} and PRC2 act on similar genes. To determine whether Notch-activated genes are also PRC2-repressed, we first determined putative PRC2 targets by expression analyses on isolated wild-type, M+Z- *mes-2* or *mes-6* mutant gonads (GEO accession number GSE49395). Consistent with the joint function of MES-2 and MES-6 in the PRC2 complex, a very similar set of genes was upregulated upon the loss of either protein (Figure 2C; henceforth 'PRC2 repressed' genes; also see (Gaydos *et al.* 2012). Indeed, those PRC2-repressed genes overlapped strongly with Notch-activated genes, particularly those linked to the X chromosome. Nearly all of the X-linked Notch-activated genes were also derepressed upon the loss of PRC2 (Figure 2C). This is consistent with the observed genetic interaction and suggests that increased GLP-1^{Notch} signaling can induce expression of specific PRC2-repressed genes. This activation of the PRC2-repressed genes is not due to a global loss of the repressive tri-methylation of Histone H3 at lysine residue 27 (H3K27me3), since, upon examining gonads of different GLP-1^{Notch} mutants, we observed no global loss of H3K27me3 in the germ cells (Figure 2–figure supplement 4).

GLP-1^{Notch} signaling enhances reprogramming

Germ cell conversion to neurons can be triggered not only by LIN-53 depletion but also by the depletion of PRC2 (Patel *et al.* 2012). Potentially, the depletion of LIN-53 could facilitate

reprograming by inhibiting PRC2, since the depletion of LIN-53 results in a global loss of H3K27me3 in the germline (Patel *et al.* 2012). Considering the antagonistic relation between GLP-1^{Notch} and PRC2 on cell proliferation and gene regulation, we wondered whether GeCo triggered by the depletion of PRC2 would be sensitive to Notch signaling. Indeed, GeCo was strongly enhanced in PRC2-depleted (*mes-2*, *mes-3* or *mes-6* RNAi) animals, when they also carried the gain-of-function *glp-1(ar202)* allele (Figure 3A, Figure 3–source data 1). Moreover, similar to the LIN-53–depleted *gld-1(q497) gld-2(q485); glp-1(q175)* gonads (Figure 1D), the loss of GLP-1 effectively prevented GeCo in PRC2–depleted *gld-1(q497) gld-2(q485); glp-1(q175)* gonads (Figure 3B, Figure 3–source data 1). Together, these results suggest that GLP-1^{Notch} stimulates GeCo in PRC2-compromised gonads.

UTX-1 is required for GLP-1^{Notch}-mediated GeCo enhancement

To determine how GLP-1^{Notch} might counteract PRC2, we depleted candidate Notch-activated genes (Supplementary file 1), and examined GeCo efficiency (Figure 4A, Figure 4–source data 1). The strongest suppression of the GeCo+ and GeCo phenotype was observed upon the depletion of *utx-1,* which also suppressed *mes-3* RNAi-mediated GeCo+ in *glp-1(ar202)* (Figure 4–figure supplement 1). Depletion of two other candidates, the uncharacterized C07G1.6 and the aldolase ortholog *aldo-1*, also suppressed GeCo+, albeit less efficiently (Figure 4A). Because UTX-1 was suggested to effect gonadal development by functioning in the somatic gonad (Vandamme *et al.* 2012), we re-examined GeCo efficiency upon *utx-1* RNAi in the *rrf-1 (pk1417)* background. Importantly, in *rrf-1* mutants, RNAi is impaired in the somatic gonad, including the distal tip cell (DTC), which constitutes the germline stem cell niche (Kumsta and Hansen 2012). Because the suppression of GeCo+ upon *utx-1* RNAi was observed also in the *rrf-1* background, UTX-1 does not seem to enhance GeCo by functioning in the somatic gonad (Figure 4–figure supplement 1A).

Importantly, *utx-1* encodes a conserved H3K27me3 demethylase, an enzyme erasing the repressive mark deposited by PRC2 (Agger *et al.* 2007; Jin *et al.* 2011; Maures *et al.* 2011), potentially explaining how its depletion impairs GeCo efficiency. However, a number

of other H3K27me3 demethylases exist in *C. elegans* which prompted us to test whether depletion of these demethylases might have an effect on GeCo in the *glp-1(ar202)* gonads. We RNAi-depleted *jmjd-1.2*, encoding a H3K9/27me2 demethylase (Kleine-Kohlbrecher *et al.* 2010), *jmjd-3.1*, *jmjd-3.2*, and *jmjd-3.3*, which were reported to demethylate H3K27me2/3 (Agger *et al.* 2007; Kleine-Kohlbrecher *et al.* 2010; Zuryn *et al.* 2014), and, as a control, *jmjd-2,* encoding a H3K9/36 demethylase (Whetstine *et al.* 2006; Greer *et al.* 2014) (Figure 4B, Figure 4–source data 1). Only the depletion of JMJD-1.2 suppressed GeCo+ significantly, though to a lesser degree than the depletion of UTX-1 (Figure 4B, Figure 4–source data 1). The suppression of GeCo by the depletion of UTX-1 or JMJD-1.2 stresses the importance of counteracting PRC2 in reprograming. However, only the expression of *utx-1* is activated by the GLP-1^{Notch} signaling, suggesting that it is the activity of UTX-1, which is key for the reprograming dependent on GLP-1^{Notch} signaling.

GLP-1^{Notch} and PRC2 regulate expression of the H3K27 demethylase UTX-1

The inhibition of GeCo enhancement upon *utx-1* RNAi in the *rrf-1* background suggested that UTX-1 functions in the germline. To test the potential expression of *utx-1* in the germline, we constructed a strain expressing single copy-integrated, FLAG and GFP-tagged, functional UTX-1 (expressed from the endogenous *utx-1* promoter under the control of endogenous *utx-1* 3'UTR). We found that this protein was indeed expressed in the germline (Figure 5–figure supplement 1). To examine the potential transcriptional regulation of *utx-1* expression by GLP-1^{Notch} and PRC2, we also created a strain expressing GFP-tagged histone H2B from the *utx-1* promoter (*putx-1* reporter), under the control of an unregulated (*tbb-2*) 3'UTR. This construct was also single-copy integrated into a defined genomic location. With both the UTX-1 fusion protein and the *putx-1* reporter, we expected expression patterns similar to that of other reported GLP-1^{Notch} target genes (Lamont *et al.* 2004; Lee *et al.* 2006; Kershner *et al.* 2014). Among these, *lst-1* and *sygl-1* account for the role of GLP-1^{Notch} in stem cell maintenance, and both genes are expressed in the distal-most stem cells/progenitors (Kershner *et al.* 2014). By contrast, both the UTX-1 fusion protein and the *putx-1* reporter were little or

not expressed in the distal-most, proliferative part of the germline (Figure 5A-C; Figure 5–figure supplement 1). Concomitantly with progression through meiosis, their expression increased toward the proximal end of the gonad (Figure 5A-C). When examining the existing mRNA hybridization patterns of Notch-activated and PRC2-repressed genes (33 genes), we noticed that half of these (18, all X-linked) are similarly expressed in the medial and/or proximal, but not the distal-most, gonads (Supplementary file 2), arguing against direct transcriptional activation of these genes by GLP-1^{Notch} in the wild type. Nevertheless, in agreement with the expression analyses, we observed increased expression of the *putx-1* reporter in PRC2-depleted gonads; this increase occurred throughout the gonad, including the distal-most region (Figure 5A). *In situ* hybridization for the endogenous *utx-1* transcript also showed increased expression throughout the gonad in the absence of PRC2 (Figure 5–figure supplement 2). Moreover, expression of the *putx-1* reporter was higher upon increased GLP-1^{Notch} activity in *glp-1(ar202)* mutants, including the distal-most region where, in the wild-type, *utx-1* is little or not expressed (Figure 5B). Importantly, we found that the activation of the *utx-1* promoter by Notch signaling was depended on the putative LAG-1/CSL binding sites within the promoter (Yoo *et al.* 2004), as deleting those sites reduced reporter expression by approximately one-fourth (Figure 5C). The interaction between LAG-1 and *utx-1* was also tested by chromatin immunoprecipitation (ChIP), performed on a strain expressing FLAG-tagged LAG-1 in either wild-type or *glp-1(ar202)* background (Figure 5D and Figure 5–figure supplement 3); the previously identified GLP-1^{Notch} targets, *lst-1* and *sygl-1* (Kershner *et al.* 2014), served as positive controls for the ChIP. Expectedly, we observed the enhanced binding of LAG-1 to the *utx-1* promoter, indicating that *utx-1* is a transcriptional target of GLP-1^{Notch} signaling. Summarizing, based on the observations in mutant backgrounds, PRC2 and GLP-1^{Notch} signaling have antagonistic effects on *utx-1* transcription. However, in wild type, the endogenous levels of GLP-1^{Notch} signaling are apparently insufficient to overcome PRC2-mediated repression of *utx-1* in the distal-most part of the gonad.

Discussion

In the *C. elegans* germline, GLP-1^{Notch} signaling is essential for maintaining a pool of undifferentiated stem cells/progenitors. Here, we report an unexpected role of GLP-1^{Notch} signaling in promoting cell fate reprograming. To understand this phenomenon, we identified genes activated upon increased GLP-1^{Notch} signaling. While the identified genes include the physiological GLP-1^{Notch} targets, *sygl-1* and *lst-1*, many other genes, including *utx-1*, appear to be only weakly or not expressed in the distal-most region of the wild-type gonad, where both *sygl-1* and *lst-1* are induced by GLP-1^{Notch} (Kershner *et al.* 2014). Thus, the wild-type levels of GLP-1^{Notch} signaling are either insufficient to induce expression of many potential target genes (see below), or their expression is controlled by additional mechanisms, perhaps similarly to *lip-1* mRNA, which, while induced by GLP-1^{Notch}, is post-transcriptionally degraded in the distal-most gonad (Lee *et al.* 2006). In addition to its major proliferation-promoting function, GLP-1^{Notch} has been suggested to have a lesser role in promoting germ cell differentiation (Hansen *et al.* 2004). Some of the identified Notch-activated genes appear to promote germ cell differentiation, potentially explaining the proposed differentiation-promoting function of GLP-1^{Notch}. However, whether these genes are activated by GLP-1^{Notch} and promote differentiation under physiological conditions remains to be determined.

Many of the Notch-activated genes are repressed by PRC2, suggesting that the expression of these genes is determined by the crosstalk between the extrinsic intercellular signaling pathway, Notch, and the intrinsic chromatin modifier PRC2. Indeed, at least in the case of *utx-1*, PRC2 appears to prevent its inappropriate expression in the distal-most gonad, which, nevertheless, can be overcome upon increased GLP-1^{Notch} signaling. Our findings suggest that GLP-1^{Notch} antagonizes PRC2, at least in part, by stimulating expression of the H3K27 demethylase UTX-1, which is essential for the enhancement of cellular reprograming. Previously, it was suggested that UTX-1 influences the germline by functioning in the somatic gonad (Vandamme *et al.* 2012.) However, by using the *rrf-1* background, which displays defective RNAi in the somatic gonad, including DTC (Kumsta and Hansen 2012), we found that the reprogramming-promoting role of UTX-1 is unlikely to dependent on its function in the somatic gonad. Although we cannot fully exclude the possibility that the

reprograming-facilitating role of UTX-1 depends on its expression in another somatic tissue (such as the intestine, in which RNAi remains functional in the *rrf-1* mutant; Kumsta and Hansen 2012), the germline expression of UTX-1 reported here suggests a germline-autonomous function. Consistent with this hypothesis, manipulating either PRC2 or GLP-1^{Notch} affected the germline expression of *utx-1*.

Although additional factors, such as the uncharacterized C07G1.6 and the ortholog of the human Aldolase A (Kuwabara and O'Neil 2001; Shaye and Greenwald 2011) might contribute to reprograming, they appear to be less critical. In addition to UTX-1, another H3K27/H3K9-demethylating enzyme, JMJD-1.2 (Kleine-Kohlbrecher *et al.* 2010), is required for enhanced reprograming. Similar to UTX-1, JMJD-1.2 is likely to be directly involved in regulating chromatin accessibility, since its depletion results in increased levels of the repressive H3K9me2 and H3K27me2 modifications (Kleine-Kohlbrecher *et al.* 2010). The reprograming-promoting role of JMJD-1.2 might indicate that, besides further demethylation of H3K27me2, perhaps also the removal of H3K9me2 facilitates GeCo. Future studies will shed light on this interesting question.

UTX-1 orthologs in other species contribute to tissue-specific chromatin signatures, for example during myogenesis or in cardiac development (Seenundun *et al.* 2010; Lee *et al.* 2012), and have been implicated in germ cell and somatic reprograming (Mansour *et al.* 2012). Together with our data, these findings underscore the importance of UTX-1 in cellular reprograming. Here, we suggest that one way the activity of UTX-1 may be stimulated to promote reprograming is through its Notch signaling-dependent transcriptional activation. Interestingly, an antagonistic relationship between Notch and PRC2 has been also observed in T-cell leukemia (Ntziachristos *et al.* 2012). A fascinating possibility is that a regulatory principle described here could help explain the etiology of this and perhaps other human diseases linked to a pathological increase in Notch signaling.

MATERIALS AND METHODS

Nematode culture and mutants

Standard procedures were used to maintain animals. Worms (RRID:WB_DL226) were grown at 25 °C unless stated otherwise. All heat-shock and temperature-sensitive strains were kept at 15 °C. The *C. elegans* lines used in this study are listed and described in detail in the Supplementary file 3A.

RNA interference Experiments

The Enhancer-Suppressor screen on Notch targets was performed by feeding the animals with bacteria containing RNAi clones from the Ahringer and Vidal RNAi libraries. The clones not present in either of these libraries were cloned using primers as described in detail in the Supplementary file 3B. Experiments were performed at 15 °C, 20 °C or 25 °C using bleached embryos or overnight-synchronized L1 animals as stated in Supplementary file 1. The percentage of adult animals with the germline tumor phenotype was scored. To test germ cell autonomy, RNAi clones that induced significant suppression or enhancement in either setting were re-tested in a strain carrying the *glp-1*(*ar202*) (RRID:WB_GC833) allele and, additionally the *rrf-1*(*pk1417*) (RRID:WB_NL2098) mutation, which impairs RNAi primarily in the soma (Sijen *et al.* 2001). For this test, gravid adults were picked to RNAi plates and allowed to lay eggs over night at the semi-permissive temperature of 20 °C. Progeny was scored for enhancement or suppression of the germline tumorous phenotype at the young adult stage by DAPI staining of dissected gonads and scoring gonads as either wild type, as containing a proximal or distal tumor but still some eggs, or as completely tumorous.

Reprograming experiments were carried out as F1-RNAi. Worms were put on RNAi plates and the following F1 generation was screened for phenotypes. Used RNAi clones are described in the Supplementary file 3B. The genotype of the worms used for germ cell reprogramming assays is BAT28 (*otIs305 ntIs1,* RRID:WB_OH9846, details in Supplemental Material an Methods). Animals were synchronized by bleaching and eggs were put on NGM-

agar containing *E.coli* OP50 (RRID:WB_OP50) as food source to grow at 15 °C until worms reached the L4-stage. At this stage 15-20 worms were put per well of a 6-well plate, containing bacteria expressing dsRNA or carrying an empty RNAi vector, and grown at 15 °C until most of the F1 progeny reached the L3/L4 stage. The plates were heat-shocked at 37 °C for 30 min followed by an overnight incubation at 25 °C. Next day (~16 h post heat-shock) the plates were screened for progeny showing ectopic GFP induction in the germline. To induce the Glp-phenotype in *glp-1(ar202)*, the animals were shifted to room temperature 9 h before the heat-shock. For double RNAi, bacteria were grown as saturated culture. The OD_{600} was measured to ensure that the bacteria were mixed in an appropriate 1:1 ratio and subsequently seeded on RNAi 6-well plates. The RNAi screen was performed as described above. The p-values were calculated using Student's *t*-test.

Cell cycle arrest by HU treatment and EdU staining

Hydroxyurea (HU) treatment was carried out as previously described (Fox *et al.* 2011; Patel *et al.* 2012). HU was added to seeded RNAi-plates at a final concentration of 250 µM. L4 worms (strain BAT32, details in Supplementary file 3A) grown on RNAi-plates were transferred to HU plates and incubated at room temperature for 5 h prior to heat-shock in order to induce CHE-1 expression. To test HU efficiency, control animals were treated with HU for 12 h with subsequent staining for DAPI and H3Ser10ph (pH3) antibody (Abcam #ab5176). After overnight incubation, the worms were assessed for GFP induction in the germline as described above. To assess the efficiency of the HU treatment, the *E. coli* strain of MG1693 (*E. coli* stock center), with incorporated 5-ethynyl-20-deoxyuridine (EdU), was used to feed L3/L4 worms. EdU in combination with DAPI staining was performed similar to the procedure described previously (Ito and McGhee 1987) and according to the manufacturers instructions (Invitrogen) of the EdU labeling kit. The Click-iT® EdU reaction buffer (Invitrogen) was mixed with Alexa Fluor® azide (‘click’ reaction) dye to detect cells that were replicating DNA. Staining was performed by freeze cracking worms after fixation with 2% formaldehyde.

413

414 ***C. elegans* tiling array analysis**

415 Parental animals were raised at 15 °C and shifted to 25 °C for egg laying. Offspring was
416 dissected after the L4-adult transition. Fifty gonads per analyzed genotype in triplicates were
417 dissected in M9 containing levamisole. RNA was isolated using the PicoPure RNA Isolation
418 Kit (Applied Biosystems) according to the manufacturer's recommendations. Total RNA (200
419 ng for the Notch ON/OFF experiments or 100 ng for the *mes*/wild-type experiments) was
420 amplified using the Affymetrix GeneChip WT Amplified Double Stranded cDNA Synthesis
421 Kit according to the manufacturer's instructions. The Affymetrix GeneChip WT Double-
422 Stranded cDNA Terminal Labeling Kit was used for the fragmentation and labeling of 7.5 µg
423 cDNA. The labeled material was loaded onto Affymetrix GeneChip C. elegans Tiling 1.0R
424 Arrays and hybridized at 65ºC for 16 h. The arrays were washed in an Affymetrix Fluidics
425 station with the protocol FS450_0001 and scanned in an Affymetrix GeneChip Scanner 3000
426 with autoloader using Affymetrix GCC Scan Control v. 3.0.0.1214 software. All tiling arrays
427 were processed in R (32,33) using Bioconductor (34) and the packages tilingArray and
428 preprocessCore. The arrays were RMA background corrected and log2 transformed on the
429 oligo level using the following command:
430 expr <- log2 (rma.background.correct (exprs (readCel2eSet (filenames,rotated = TRUE)))).
431 We mapped the oligos from the tiling array (bpmap file from www.affymetrix.com) to the
432 *C.elegans* genome assembly ce6 (www.genome.ucsc.edu) using bowtie (Langmead *et al.*
433 2009), allowing no error and unique mapping position. Expressions for individual transcripts
434 were calculated by intersecting the genomic positions of the oligos with transcript annotation
435 (WormBase WS190) and averaging the intensity of the respective oligos. For the *mes-4*/wt
436 experiment, no quantile normalization was performed as the distributions for the *mes-4*
437 mutant and the wt differed substantially. In the case of the Notch ON/OFF dataset quantile
438 normalization was performed on the level of transcripts. The p-values were calculated in R
439 with the hypergeometric distribution function "phyper".
440

Validation of array analysis by RT-qPCR:

RNA was isolated as described above. cDNA was synthesized with oligo dT primer using the ImProm II Reverse Transcription System from Promega according to the manufacturer's instructions. cDNA was used for qPCR with the Absolute QPCR SYBR Green ROX Mix (AbGene) on an ABI PRISM 7700 system (Applied Biosystems). qPCR reactions were performed as described previously (Biedermann *et al.* 2009). At least one primer in each pair is specific for an exon-exon junction. Sequences of the used primers are described in detail in the Supplementary file 3C. Mouse RNA was added before RNA isolation and reverse transcription, allowing for normalization to *cyt-c* and thereby correcting for variations in RNA isolation and reverse transcription. Standard curves for quantification were generated from a serial dilution of input cDNA for each primer pair. The amount of target present in each replicate was derived from the standard curve; an average was calculated for each of the triplicates. To compare total mRNA levels, the qPCR results were normalized to mouse *cyt-c* and to the *C. elegans* tubulin gene *tbb-2*, and fold enrichments were calculated.

In-situ* hybridization for *utx-1

RNA *in situ* hybridization was performed and analyzed as previously described (Biedermann *et al.* 2009). Description of the primer pairs to generate probes from cDNA can be found in the Supplementary file 3C. Images were captured with a Zeiss AxioImager Z1 microscope, equipped with a Zeiss AxioCam MRc camera. Images were taken in linear mode of the Axiovision software (Zeiss) and processed with Adobe Photoshop CS4 in an identical manner.

Chromatin Immunoprecipitation and qPCR (ChIP-qPCR)

ChIP was performed as described (Askjaer *et al.* 2014). In brief, worms (strains OP591, RRID:WB_OP591, and BAT890) were washed with M9 buffer and frozen as 'worm popcorn' in liquid nitrogen prior to pulverization with a mortar and pestle. The powder was dissolved in 10 volumes of 1,1 % formaldehyde in PBS + 1mM PMSF and incubated 10 min

with gentle rocking at room temperature with subsequent quenching for 5 min at room temperature by adding 2,5 molar glycine (final concentration 125 mM). After centrifugation with 4.000 g at 4 °C the pelleted was washed with ice-cold PBS+1mM PMSF and resuspended in 50 mM FA buffer (50 mM HEPES/KOH pH 7,5; 1mM EDTA; 1 % Triton-X 100; 0,1% Sodium deoxycholate; 150 mM NaCl) + 1% sarkosyl + protease-inhibitors. Samples where sonicated twice using the Biorupter (15 times 30 sec ON, 30 sec OFF) on high settings at 4 °C followed by spinning at 13.000 g, 15 min, 4 °C. The supernatant corresponding to 4 mg of protein measured by Bradford assay was used for ChIPs. Samples were incubated with 50 µl of FLAG or HA antibodies coupled to µMACS^{TM} microbeads (Milteny) (all blocked with 5% milk in FA-buffer). After incubating 1 h at 4 °C, the beads where washed in µMACS matrix columns in a magnetic rack with FA buffer containing 1M and 0.5 M NaCl and subsequent wash with TE and TEL buffer (0,25 M LiCl; 1 % Sodium deoxycholate; 1 mM EDTA; 10 mM Tris pH 8,0). Bound material was eluted with 65 °C pre-warmed 125 µl ChIP elution buffer (1% SDS, 250 mM NaCl, 10 mM Tris pH 8.0, 1 mM EDTA) and fixation was reversed using 2 µl of 10 mg/ml Proteinase K at at 50 °C for 1 h followed by 65 °C incubation overnight. DNA was purified using the Quiaquick PCR purification kit in a final volume of 40 µl and 1 µl was used for qPCR. Negative controls were used which were taken to assess the quality of the ChIP and fold enrichment of the target genes: lysates (N2 worms) which do not express the recombinant target protein with specific antibody (anti-FLAG coupled to µMACS beads) and lysates of worms expressing the recombinant target protein with unspecific antibody (anti-HA coupled to µMACS beads) controls, respectively. Primer for qPCRs were designed using Primer3Plus (Untergasser *et al.* 2007) with the following settings: amplified region min. 100 bp - max. 200 bp; GC content: 50-60 %; min. primer length: 18 nt - max. length 24 nt; melting temperature: min. 58 °C - max. 63 °C; max.; 3' self complementary allowance set to 1; max. allowed length of a mononucleotide repeat (max. poly-x): 3. Sequences of the used primers are listed in in the Supplementary file 3C. The qPCRs were run on CFX96 Touch™ Real-Time PCR Detection System from BioRad using the Maxima SYBR Green/ROX qPCR Master Mix (2X). The data

analysis was performed by calculating the ΔΔCt-values. Differences were assessed using Student's *t*-test.

DAPI staining and counting of germ cells

Worms were transferred to a slide and fixed by adding 10 - 20 µl 95% ethanol and letting evaporate the ethanol. The ethanol fixation was repeated 2 more times before adding the DAPI solution in microscopy mounting media (vectashield from Vector or similar). The samples were sealed with a coverslip and nail polish before microscopy. Fluorescent micrographs were recorded with Zeiss AxioImager Z1 microscope and the SensicamII camera (PCO) and the micromanager software was used to capture Z-stack images with 0.5 µm slice steps. Images subject to direct comparison were taken at identical exposure times. Counting of germ cells within the range from the DTC to the turn of gonadal arms of *glp-1(ar202); hsp::che-1; gcy-5::gfp* animals treated with either mock or *lin-53* RNAi was performed using the Z-stacks. Micromanager was used to control the Z-stack levels and the ImageJ plugin for cell counting for scoring the number of germ cells. Germ cell counts in gonads of Notch ON: *gld-2(q497) gld-1(q485) glp-1(ar202)* and Notch OFF: *gld-2(a497) gld-1(q485) glp-1(e2144)* (Figure 1–supplemental figure 2) and germline tumor phenotype in *glp-1(ar202)* and *glp-1(ar202); rrf-1(pk1417)* were scored after dissection, formaldehyde fixation and DAPI staining. For Notch ON and Notch OFF mutants, the central plane of the gonads was imaged and germ cells in the entire dissected gonad were counted using the CellCounter plugin with ImageJ. For each of the two strains, germ cells in the entire gonad of 15 dissected gonads were counted.

Immunostaining and Antibodies

Antibody staining of intact worms were performed using a freeze-crack procedure as described (Duerr 2006). In brief, after washing, worms were resuspended in 0.025% glutaraldehyde, and frozen between two frost-resistant glass slides on dry ice. Separating the glass slides while frozen creates additional cracks in the cuticle. Acetone/methanol or 4%

paraformaldehyde in 0.1M Phosphate buffer for 1 hour on ice fixation was used. Worms were washed off the slides in PBS, blocked with 0.2% gelatin + 0.25% Triton in PBS, and stained. Primary antibodies were diluted in PBS with 0.1% gelatin and 0.25% Triton and fixed worms were incubated 4 h - overnight at 4 C. After PBS washes secondary antibody was applied for 3 h. After PBS washes worms were mounted with DAPI-containing mounting medium (Dianova, #CR-38448) on glass slides. The primary antibodies used were anti-H3K27me3 (1:400; gift from Dr. Hiroshi Kimura); anti-HA (1:100, Roche #12CA5; acetone fixation); anti-H3Ser10ph (1:400, Abcam, #ab14955; acetone fixation). Secondary antibodies were Alexa Fluor dyes applied at 1:1000 dilution.

Stainings for H3K27me3 on dissected gonads were performed using anti-H3K27me3 from Millipore (catalogue number 07-449, Lot 1959680; courtesy of Jan Padeken, Gasser laboratory) on dissected gonads. Adult animals were dissected in M9 containing Levamisole, fixed with 2% paraformaldehyde in PBS on poly-lysine coated slides, snap-frozen on dry ice, freeze-cracked, incubated for 5 minutes in ice-cold DMF at -20°, washed for 5 min in PBS 0.1% Tween-20 at room temperature, blocked for 20 min in PBS 0.1% Tween-20 + 5% BSA and incubated with the primary antibody over night at 4 °C. Secondary antibodies (Alexa 488, goat anti rabbit, 1:500) were applied for 2h at room temperature. Slides were then washed three times for 5 min in PBS 0.1% Tween-20 at room temperature and mounted with Vectashield mounting medium containing DAPI.

Transgenic animals and reporter GFP quantifications

The transcriptional reporter gene *putx-1::gfp-h2b (rrrSi185)* was constructed from the 1302 bp putative promoter region of the gene *utx-1* (*human UTX (Ubiquitously transcribed TPR on X) homolog - 1*) fused to sequences encoding for GFP-H2B and the ubiquitously expressed *tbb-2* 3'UTR using the Gateway Reporter Cloning System (Merritt *et al.* 2008). The reporter gene *putx-1::gfp-h2b (rrrSi185* and *rrrSi281)* was constructed with the following primers:

putx-attB4:

GGGGACAACTTTGTATAGAAAAGTTGGGATTTTATCTTCATCGGACCTG

putx-attB1 : GGGGACTGCTTTTTTGTACAAACTTGTGGCGGTGTGAGAAGCGATAC

The full-length functional transgene *putx-1::flag-gfp-utx-1::utx-1 3'UTR (rrrSi189)* was constructed with the following primers: utx-1+3UTR+attB2 L ggggacagctttcttgtacaaagtggACGACGAATCAGAACCTCTGCCGGAGGAGCGTCATgtaag utx-1+3UTR+attB3 R ggggacaactttgtataataaagttgaatgcggatactgccttctc

The functional UTX-1 transgene *putx-1::flag-gfp-tev::utx-1::utx-1 3'utr(rrrSi189)* contains the same promoter as the transcriptional reporter, the full-length *utx-1* genomic sequence as well as the endogenous 3'UTR, and was equipped with N-terminal GFP, FLAG, and TEV tags. Transgenic animals were produced by single copy integration using the MosSCI direct insertion protocol (Frøkjaer-Jensen *et al.* 2008). The *rrrSi189* transgene is functional, as it rescues the *utx-1* mutant (*ok3553* allele). For GFP quantification, gonads were dissected from live animals in M9 buffer containing levamisole and mounted to glass microscopy slides (Frøkjaer-Jensen *et al.* 2008). Fluorescent micrographs were recorded with Zeiss AxioImager Z1 microscope and a Zeiss Axioncam MRm REV 2 CCD camera was used to capture images. Fluorescence intensities were quantified using ImageJ. GFP intensities were normalized to the picture background and corrected with the average autofluorescences measured in wild type (N2) gonads at the corresponding temperatures. Images subject to direct comparison were taken at identical exposure times and were processed with Adobe Photoshop CS4 in an identical manner. The numbers of analyzed gonads were as follows: n = 44 for wild-type reporter; n = 36 for *glp-1(gf^{ts})*; n = 55 for wild-type reporter on control RNAi; n = 48 for *mes-2(RNAi)*; n = 15 for *mes-3(RNAi)*; n = 29 for *mes-6(RNAi)*, and n = 20 for LAG-1 binding sites deleted reporter.

Genetic interaction of *glp-1* and *mes-2*

Alleles used were *glp-1(ar202)* and *mes-2(bn11)*. Worms were grown at the semi-permissive temperature of 20 °C and gonads were dissected and DAPI-stained shortly after the L4-young adult transition.

The experiment was performed twice. In a first round, a low number of gonads was examined to identify whether the double mutant had a phenotype and to define phenotypic categories to score. Based on the observation of a clear and penetrant phenotype, gonads were scored in a second round according to the categories defined in the first round.

ACKNOWLEDGMENTS

We thank Sergej Herzog, Alina El-Khalili, Mei He, S. Muehlhaeusser and Iskra Katic for technical assistance, and the following FMI technology platforms: functional genomics, bioinformatics, advanced imaging and microscopy. We also thank the CGC, supported by the NIH, Tim Schedl and Dave Hansen for providing strains. We thank S. Gasser, J. Priess, D. Schübeler, G. Merdes and members of the Tursun and Ciosk groups for discussion and comments on the manuscript. This work was partly sponsored by the SBFI grant Nr. C15.0038 to RC. Friedrich Miescher Institute for Biomedical Research is sponsored by the Novartis Research Foundation. BT receives funding from ERC-StG-2014-637530 and ERC CIG PCIG12-GA-2012-333922 and is supported by the Max Delbrueck Center for Molecular Medicine in the Helmholtz Association.

REFERENCES

Agger K, Cloos PAC, Christensen J, Pasini D, Rose S, Rappsilber J, Issaeva I, Canaani E, Salcini AE, Helin K (2007) UTX and JMJD3 are histone H3K27 demethylases involved in HOX gene regulation and development. *Nature* **449**, 731–734. doi:10.1038/nature06145.

Altun-Gultekin Z, Andachi Y, Tsalik EL, Pilgrim D, Kohara Y, Hobert O (2001) A regulatory cascade of three homeobox genes, ceh-10, ttx-3 and ceh-23, controls cell fate specification of a defined interneuron class in C. elegans. *Development (Cambridge, England)* **128**, 1951–1969.

Artavanis-Tsakonas S, Rand MD, Lake RJ (1999) Notch signaling: cell fate control and signal integration in development. *Science (New York, NY)* **284**, 770–776.

Askjaer P, Ercan S, Meister P (2014) Modern techniques for the analysis of chromatin and nuclear organization in C. elegans. *WormBook : the online review of C elegans biology* 1–35. doi:10.1895/wormbook.1.169.1.

612 Austin J, Kimble J (1987) glp-1 is required in the germline for regulation of the decision
613 between mitosis and meiosis in C. elegans. *Cell* **51**, 589–599.

614 Bender LB, Cao R, Zhang Y, Strome S (2004) The MES-2/MES-3/MES-6 Complex and
615 Regulation of Histone H3 Methylation in C. elegans. *Current Biology* **14**, 1639–1643.
616 doi:10.1016/j.cub.2004.08.062.

617 Biedermann B, Wright J, Senften M, Kalchhauser I, Sarathy G, Lee M-H, Ciosk R (2009)
618 Translational repression of cyclin E prevents precocious mitosis and embryonic gene
619 activation during C. elegans meiosis. *Developmental Cell* **17**, 355–364.
620 doi:10.1016/j.devcel.2009.08.003.

621 Christensen S, Kodoyianni V, Bosenberg M, Friedman L, Kimble J (1996) lag-1, a gene
622 required for lin-12 and glp-1 signaling in Caenorhabditis elegans, is homologous to
623 human CBF1 and Drosophila Su(H). *Development (Cambridge, England)* **122**, 1373–
624 1383.

625 Ciosk R, DePalma M, Priess J (2006) Translational regulators maintain totipotency in the
626 Caenorhabditis elegans germline. *Science (New York, NY)* **311**, 851.

627 Djabrayan NJV, Dudley NR, Sommermann EM, Rothman JH (2012) Essential role for Notch
628 signaling in restricting developmental plasticity. *Genes & Development* **26**, 2386–2391.
629 doi:10.1101/gad.199588.112.

630 Doyle TG, Wen C, Greenwald I (2000) SEL-8, a nuclear protein required for LIN-12 and
631 GLP-1 signaling in Caenorhabditis elegans. *Proceedings of the National Academy of*
632 *Sciences of the United States of America* **97**, 7877–7881.

633 Duerr JS (2006) Immunohistochemistry. *WormBook : the online review of C elegans biology*
634 1–61. doi:10.1895/wormbook.1.105.1.

635 Egli D, Birkhoff G, Eggan K (2008) Mediators of reprogramming: transcription factors and
636 transitions through mitosis. *Nature Reviews Molecular Cell Biology* **9**, 505–516.
637 doi:10.1038/nrm2439.

638 Fong Y, Bender L, Wang W, Strome S (2002) Regulation of the different chromatin states of
639 autosomes and X chromosomes in the germline of C. elegans. *Science (New York, NY)*
640 **296**, 2235–2238. doi:10.1126/science.1070790.

641 Fox PM, Vought VE, Hanazawa M, Lee M-H, Maine EM, Schedl T (2011) Cyclin E and
642 CDK-2 regulate proliferative cell fate and cell cycle progression in the C. elegans
643 germline. *Development (Cambridge, England)* **138**, 2223–2234.
644 doi:10.1242/dev.059535.

645 Frøkjaer-Jensen C, Davis MW, Hopkins CE, Newman BJ, Thummel JM, Olesen S-P, Grunnet
646 M, Jorgensen EM (2008) Single-copy insertion of transgenes in Caenorhabditis elegans.
647 *Nature Genetics* **40**, 1375–1383. doi:10.1038/ng.248.

648 Fukushige T, Krause M (2005) The myogenic potency of HLH-1 reveals wide-spread
649 developmental plasticity in early C. elegans embryos. *Development (Cambridge,*
650 *England)* **132**, 1795–1805. doi:10.1242/dev.01774.

651 Fukushige T, Hawkins MG, McGhee JD (1998) The GATA-factor elt-2 is essential for
652 formation of the Caenorhabditis elegans intestine. *Developmental Biology* **198**, 286–302.

Gaydos LJ, Rechtsteiner A, Egelhofer TA, Carroll CR, Strome S (2012) Antagonism between MES-4 and Polycomb Repressive Complex 2 Promotes Appropriate Gene Expression in C. elegans Germ Cells. *Cell Reports* **2**, 1169–1177. doi:10.1016/j.celrep.2012.09.019.

Greenwald I, Kovall R (2013) Notch signaling: genetics and structure. *WormBook : the online review of C elegans biology* 1–28. doi:10.1895/wormbook.1.10.2.

Greer EL, Beese-Sims SE, Brookes E, Spadafora R, Zhu Y, Rothbart SB, Aristizábal-Corrales D, Chen S, Badeaux AI, Jin Q, Wang W, Strahl BD, Colaiácovo MP, Shi Y (2014) A Histone Methylation Network Regulates Transgenerational Epigenetic Memory in C. elegans. *Cell Reports* **7**, 113–126. doi:10.1016/j.celrep.2014.02.044.

Hajnal A, Berset T (2002) The C.elegans MAPK phosphatase LIP-1 is required for the G(2)/M meiotic arrest of developing oocytes. *The EMBO Journal* **21**, 4317–4326.

Hanna J, Saha K, Pando B, Zon JV, Lengner CJ, Creyghton MP, Oudenaarden AV, Jaenisch R (2009) Direct cell reprogramming is a stochastic process amenable to acceleration. *Nature* **462**, 595–601. doi:10.1038/nature08592.

Hansen D, Albert Hubbard EJ, Schedl T (2004) Multi-pathway control of the proliferation versus meiotic development decision in the Caenorhabditis elegans germline. *Developmental Biology* **268**, 342–357. doi:10.1016/j.ydbio.2003.12.023.

Hansen D, Wilson-Berry L, Dang T, Schedl T (2004) Control of the proliferation versus meiotic development decision in the C. elegans germline through regulation of GLD-1 protein accumulation. *Development (Cambridge, England)* **131**, 93.

Horner MA, Quintin S, Domeier ME, Kimble J, Labouesse M, Mango SE (1998) pha-4, an HNF-3 homolog, specifies pharyngeal organ identity in Caenorhabditis elegans. *Genes & Development* **12**, 1947–1952.

Ichida JK, T C W J, Williams LA, Carter AC, Shi Y, Moura MT, Ziller M, Singh S, Amabile G, Bock C, Umezawa A, Rubin LL, Bradner JE, Akutsu H, Meissner A, Eggan K (2014) Notch inhibition allows oncogene-independent generation of iPS cells. *Nature chemical biology* **10**, 632–639. doi:10.1038/nchembio.1552.

Ito K, McGhee JD (1987) Parental DNA strands segregate randomly during embryonic development of Caenorhabditis elegans. *Cell* **49**, 329–336.

Jarriault S, Schwab Y, Greenwald I (2008) A Caenorhabditis elegans model for epithelial-neuronal transdifferentiation. *Proceedings of the National Academy of Sciences of the United States of America* **105**, 3790–3795. doi:10.1073/pnas.0712159105.

Jin C, Li J, Green CD, Yu X, Tang X, Han D, Xian B, Wang D, Huang X, Cao X, Yan Z, Hou L, Liu J, Shukeir N, Khaitovich P, Chen CD, Zhang H, Jenuwein T, Han J-DJ (2011) Histone demethylase UTX-1 regulates C. elegans life span by targeting the insulin/IGF-1 signaling pathway. *Cell metabolism* **14**, 161–172. doi:10.1016/j.cmet.2011.07.001.

Kadyk LC, Kimble J (1998) Genetic regulation of entry into meiosis in Caenorhabditis elegans. *Development (Cambridge, England)* **125**, 1803–1813.

Kershner AM, Shin H, Hansen TJ, Kimble J (2014) Discovery of two GLP-1/Notch target genes that account for the role of GLP-1/Notch signaling in stem cell maintenance. *PNAS*

695 **111**, 3739–3744. doi:10.1073/pnas.1401861111.

696 Kimble J, Crittenden S (2007) Controls of germline stem cells, entry into meiosis, and the
697 sperm/oocyte decision in Caenorhabditis elegans. *Annual review of cell and*
698 *developmental biology* **23**, 405.

699 Kleine-Kohlbrecher D, Christensen J, Vandamme J, Abarrategui I, Bak M, Tommerup N, Shi
700 X, Gozani O, Rappsilber J, Salcini AE, Helin K (2010) A Functional Link between the
701 Histone Demethylase PHF8 and the Transcription Factor ZNF711 in X-Linked Mental
702 Retardation. *Molecular Cell* **38**, 165–178. doi:10.1016/j.molcel.2010.03.002.

703 Kumsta C, Hansen M (2012) C. elegans rrf-1 Mutations Maintain RNAi Efficiency in the
704 Soma in Addition to the Germline. *PLoS ONE* **7**, e35428.
705 doi:10.1371/journal.pone.0035428.s007.

706 Kuwabara PE, O'Neil N (2001) The use of functional genomics in C. elegans for studying
707 human development and disease. *Journal of inherited metabolic disease* **24**, 127–138.

708 Lamont LB, Crittenden SL, Bernstein D, Wickens M, Kimble J (2004) FBF-1 and FBF-2
709 regulate the size of the mitotic region in the C. elegans germline. *Developmental Cell* **7**,
710 697–707. doi:10.1016/j.devcel.2004.09.013

711 Langmead B, Trapnell C, Pop M, Salzberg SL (2009) Ultrafast and memory-efficient
712 alignment of short DNA sequences to the human genome. *Genome Biology* **10**, R25.
713 doi:10.1186/gb-2009-10-3-r25.

714 Lee M-H, Hook B, Lamont LB, Wickens M, Kimble J (2006) LIP-1 phosphatase controls the
715 extent of germline proliferation in Caenorhabditis elegans. *The EMBO Journal* **25**, 88–
716 96. doi:10.1038/sj.emboj.7600901.

717 Lee S, Lee JW, Lee S-K (2012) UTX, a histone H3-lysine 27 demethylase, acts as a critical
718 switch to activate the cardiac developmental program. *Developmental Cell* **22**, 25–37.
719 doi:10.1016/j.devcel.2011.11.009.

720 Lessard JA, Crabtree GR (2010) Chromatin regulatory mechanisms in pluripotency. *Annual*
721 *review of cell and developmental biology* **26**, 503–532. doi:10.1146/annurev-cellbio-
722 051809-102012.

723 Liu J, Sato C, Cerletti M, Wagers A (2010) 'Notch Signaling in the Regulation of Stem Cell
724 Self-Renewaland Differentiation.'. (Elsevier Inc.) doi:10.1016/S0070-2153(10)91012-7.

725 Mansour AA, Gafni O, Weinberger L, Zviran A, Ayyash M, Rais Y, Krupalnik V, Zerbib M,
726 Amann-Zalcenstein D, Maza I, Geula S, Viukov S, Holtzman L, Pribluda A, Canaani E,
727 Horn-Saban S, Amit I, Novershtern N, Hanna JH (2012) The H3K27 demethylase Utx
728 regulates somatic and germ cell epigenetic reprogramming. *Nature* **488**, 409–413.
729 doi:10.1038/nature11272.

730 Maures TJ, Greer EL, Hauswirth AG, Brunet A (2011) The H3K27 demethylase UTX-1
731 regulates C. elegans lifespan in a germline-independent, insulin-dependent manner.
732 *Aging Cell* **10**, 980–990. doi:10.1111/j.1474-9726.2011.00738.x.

733 Merritt C, Rasoloson D, Ko D, Seydoux G (2008) 3' UTRs are the primary regulators of gene
734 expression in the C. elegans germline. *Current biology : CB* **18**, 1476–1482.
735 doi:10.1016/j.cub.2008.08.013.

Meshorer E, Misteli T (2006) Chromatin in pluripotent embryonic stem cells and differentiation. *Nature Reviews Molecular Cell Biology* **7**, 540–546. doi:10.1038/nrm1938.

Ntziachristos P, Tsirigos A, Van Vlierberghe P, Nedjic J, Trimarchi T, Flaherty MS, Ferres-Marco D, da Ros V, Tang Z, Siegle J, Asp P, Hadler M, Rigo I, De Keersmaecker K, Patel J, Huynh T, Utro F, Poglio S, Samon JB, Paietta E, Racevskis J, Rowe JM, Rabadan R, Levine RL, Brown S, Pflumio F, Dominguez M, Ferrando A, Aifantis I (2012) Genetic inactivation of the polycomb repressive complex 2 in T cell acute lymphoblastic leukemia. *Nature Medicine* **18**, 298–303. doi:doi:10.1038/nm.2651.

Orkin SH, Hochedlinger K (2011) Chromatin connections to pluripotency and cellular reprogramming. *Cell* **145**, 835–850. doi:10.1016/j.cell.2011.05.019.

Patel T, Tursun B, Rahe DP, Hobert O (2012) Removal of Polycomb Repressive Complex 2 Makes C. elegans Germ Cells Susceptible to Direct Conversion into Specific Somatic Cell Types. *Cell Reports*. doi:10.1016/j.celrep.2012.09.020.

Pepper AS-R, Killian DJ, Hubbard EJA (2003) Genetic analysis of Caenorhabditis elegans glp-1 mutants suggests receptor interaction or competition. *Genetics* **163**, 115–132.

Priess J, Schnabel H, Schnabel R (1987) The glp-1 locus and cellular interactions in early C. elegans embryos. *Cell* **51**, 601–611.

Riddle MR, Weintraub A, Nguyen KCQ, Hall DH, Rothman JH (2013) Transdifferentiation and remodeling of post-embryonic C. elegans cells by a single transcription factor. *Development (Cambridge, England)* **140**, 4844–4849. doi:10.1242/dev.103010.

Sawey ET, Johnson JA, Crawford HC (2007) Matrix metalloproteinase 7 controls pancreatic acinar cell transdifferentiation by activating the Notch signaling pathway. *Proceedings of the National Academy of Sciences of the United States of America* **104**, 19327–19332. doi:10.1073/pnas.0705953104.

Seenundun S, Rampalli S, Liu Q-C, Aziz A, Palii C, Hong S, Blais A, Brand M, Ge K, Dilworth FJ (2010) UTX mediates demethylation of H3K27me3 at muscle-specific genes during myogenesis. *The EMBO Journal* **29**, 1401–1411. doi:10.1038/emboj.2010.37.

Sekiya S, Suzuki A (2012) Intrahepatic cholangiocarcinoma can arise from Notch-mediated conversion of hepatocytes. *The Journal of clinical investigation* **122**, 3914–3918. doi:10.1172/JCI63065.

Shaye DD, Greenwald I (2011) OrthoList: a compendium of C. elegans genes with human orthologs. *PLoS ONE* **6**, e20085. doi:10.1371/journal.pone.0020085.

Sijen T, Fleenor J, Simmer F, Thijssen KL, Parrish S, Timmons L, Plasterk RH, Fire A (2001) On the role of RNA amplification in dsRNA-triggered gene silencing. *Cell* **107**, 465–476.

Singh K, Chao MY, Somers GA, Komatsu H, Corkins ME, Larkins-Ford J, Tucey T, Dionne HM, Walsh MB, Beaumont EK, Hart DP, Lockery SR, Hart AC (2011) C. elegans Notch Signaling Regulates Adult Chemosensory Response and Larval Molting Quiescence. *Current Biology* **21**, 825–834. doi:10.1016/j.cub.2011.04.010.

Spivakov M, Fisher AG (2007) Epigenetic signatures of stem-cell identity. *Nature Reviews Genetics* **8**, 263–271. doi:10.1038/nrg2046.

778 Tian X, Hansen D, Schedl T, Skeath JB (2004) Epsin potentiates Notch pathway activity in
779 Drosophila and C. elegans. *Development (Cambridge, England)* **131**, 5807–5815.
780 doi:10.1242/dev.01459.

781 Tocchini C, Keusch JJ, Miller SB, Finger S, Gut H, Stadler MB, Ciosk R (2014) The TRIM-
782 NHL Protein LIN-41 Controls the Onset of Developmental Plasticity in Caenorhabditis
783 elegans (J Ahringer, Ed.). *PLoS genetics* **10**, e1004533.
784 doi:10.1371/journal.pgen.1004533.

785 Tursun B, Patel T, Kratsios P, Hobert O (2011) Direct conversion of C. elegans germ cells
786 into specific neuron types. *Science (New York, NY)* **331**, 304–308.
787 doi:10.1126/science.1199082.

788 Untergasser A, Nijveen H, Rao X, Bisseling T, Geurts R, Leunissen JAM (2007)
789 Primer3Plus, an enhanced web interface to Primer3. *Nucleic Acids Research* **35**, W71–4.
790 doi:10.1093/nar/gkm306.

791 Vandamme J, Lettier G, Sidoli S, Di Schiavi E, Nørregaard Jensen O, Salcini AE (2012) The
792 C. elegans H3K27 demethylase UTX-1 is essential for normal development, independent
793 of its enzymatic activity. *PLoS genetics* **8**, e1002647. doi:10.1371/journal.pgen.1002647.

794 Whetstine JR, Nottke A, Lan F, Huarte M, Smolikov S, Chen Z, Spooner E, Li E, Zhang G,
795 Colaiacovo M, Shi Y (2006) Reversal of Histone Lysine Trimethylation by the JMJD2
796 Family of Histone Demethylases. *Cell* **125**, 467–481. doi:10.1016/j.cell.2006.03.028.

797 Yoo AS (2004) Crosstalk Between the EGFR and LIN-12/Notch Pathways in C. elegans
798 Vulval Development. *Science (New York, NY)* **303**, 663–666.
799 doi:10.1126/science.1091639.

800 Yuzyuk T, Fakhouri THI, Kiefer J, Mango SE (2009) The polycomb complex protein mes-
801 2/E(z) promotes the transition from developmental plasticity to differentiation in C.
802 elegans embryos. *Developmental Cell* **16**, 699–710. doi:10.1016/j.devcel.2009.03.008.

803 Zhu J, Fukushige T, McGhee JD, Rothman JH (1998) Reprogramming of early embryonic
804 blastomeres into endodermal progenitors by a Caenorhabditis elegans GATA factor.
805 *Genes & Development* **12**, 3809–3814.

806 Zuryn S, Ahier A, Portoso M, White ER, Morin MC, Margueron R, Jarriault S (2014)
807 Sequential histone-modifying activities determine the robustness of transdifferentiation.
808 *Science (New York, NY)* **345**, 826–829. doi:10.1126/science.1255885.

809

FIGURE LEGENDS

Figure 1. GLP-1^{Notch} signaling promotes reprograming of germ cells.

(A) GLP-1^{Notch} enhances germ cell conversion (GeCo) into neuronal-like cells. Left: fluorescent (top) and combined fluorescent/differential interference contrast (DIC) micrographs (bottom) of adult animals. All animals ectopically expressed the pro-neuronal transcription factor CHE-1 from a heat-shock promoter. *glp-1(ar202)* is a temperature-sensitive gain-of-function allele of the Notch receptor. Animals were subjected to either mock (control) or *lin-53* RNAi. Reprogrammed cells expressed a GFP reporter driven from the neuronal *gcy-5* promoter (here an in other figures nGFP) and are outlined here and elsewhere in yellow. Any signal outside the outlined region comes from somatic tissues. GeCo+ indicates animals that displayed a strongly enhanced GeCo phenotype. Scale bars = 10 µm. The cartoons depicting the GeCo and GeCo+ phenotypes are on the top right. The gonads are shaded in grey and GFP-positive converted germ cells are green. Fractions of animals displaying GeCo and GeCo+ are indicated below. At least 250 animals were quantified per condition. P-values were calculated using Student's t-test: $p^1 < 0{,}0001$; $p^2 = 0{,}0006$. Error bars represent SEM. (B) The transcriptional effector of the GLP-1^{Notch} signaling pathway, LAG-1, is required for the GLP-1^{Notch}–mediated enhancement of GeCo. Left: fluorescent micrographs of adults expressing CHE-1–induced nGFP as explained above. GeCo is diminished upon the depletion of LAG-1. White dashed lines outline the animal body. Scale bars = 10 µm. Right: the corresponding quantifications. At least 400 animals were quantified per condition. P-values were calculated using Student's t-test: $p^1 < 0{,}0001$; $p^2 = 0{,}0018$. Error bars represent SEM. (C) GLP-1^{Notch} signaling enhances GeCo independently from germ cell proliferation. Shown are DAPI-stained gonads of *glp-1(ar202)* animals, expressing CHE-1–induced nGFP, treated with either mock or *lin-53* RNAi. Germ cells were counted from the DTC (yellow asterisk) to the turn of the gonad arm (dashed yellow line). 15 gonad arms per condition were counted. Scale bars = 10 µm. Quantifications are on the right. While greatly inhibiting GeCo,

lag-1 RNAi did not change the number of germ cells. P-values were calculated using Student's t-test: p^1 = 0,89. Error bars represent SEM. (D) GLP-1^{Notch} enhances GeCo independently from proliferation. Left: fluorescent micrographs of adults (with indicated genotypes), expressing CHE-1–induced nGFP. The first panel on the left shows a control, heterozygous (wild-type) *gld-1 gld-2/ ++; glp-1/ +* animal. The other panels show the homozygous *gld-1(q497)*, *gld-2(q485)* mutants, carrying either a loss-of-function (center) or a wild-type (right) allele of *glp-1*. Despite proliferating, germ cells in the *gld-1 gld-2; glp-1* gonads have lost the ability to undergo GeCo. Scale bars = 10 μm. Right: the corresponding quantifications. At least 250 animals were quantified per condition. P-values were calculated using Student's t-test: p^1 = 0,0478; p^2 = 0,0201. Error bars represent SEM.

Figure 2. GLP-1^{Notch} and PRC2 regulate common targets and are functionally connected.

(A) Notch-activated genes are biased for the sex chromosome linkage. Left: changes in transcript abundance in the 'Notch ON' versus 'OFF' dissected gonads (genotypes explained in Figure 2–supplemental figure1A-B) were analyzed by microarrays. Transcripts upregulated at least 2-fold in the 'Notch ON' gonads are marked in red, those downregulated at least 2-fold in blue. Selected transcripts verified by RT-qPCR in Figure 2–supplemental figure 2A are additionally circled in black. Right: 5426 genes can be considered expressed in the gonad, based on the bimodal distribution of expression values. Only 3% of those expressed genes are X-linked. In contrast, nearly half (46%) of the expressed and Notch-activated transcripts are X-linked (see Figure 2–supplemental figure 2B for numbers). (B) GLP-1^{Notch} and the Polycomb Repressive Complex 2 interact genetically. Left: DAPI-stained gonads from animals of the indicated genotypes. The *mes-2(bn11)* M+Z- single mutant gonads have wild-type appearance at 20 °C. The *glp-1(ar202)* gain-of-function mutants have an almost wild-type appearance at this temperature, except for an extended proliferative zone in the gonad, referred to as "distal tumor". At the same temperature, *mes-2(bn11)* M+Z-*; glp-1(ar202)*

865 double mutants developed extensive germline tumors in 32/32 of the examined gonads. The
866 insets show close-ups from the indicated gonadal regions: the distal-most regions contain
867 undifferentiated, proliferative germ cells in all mutants (a, c, e). However, while the single
868 mutants contain oocytes with characteristically condensed chromosomes in the proximal
869 gonads (b, d), the proximal gonads of the double mutants harbor proliferative germ cells (f).
870 Scale bar = 30 μm. Right: quantification of the phenotypes. "Distal tumor" indicates the
871 presence of an elongated distal proliferative zone (approximately ½ of the distal gonad arm).
872 "Extended" tumor indicates an extended distal tumor, few oocytes, and frequently also a
873 proximal tumor. "Fully tumorous" indicates the absence of all differentiated cell types except
874 for sperm produced during larval development. (C) GLP-1^{Notch} and PRC2 target the same
875 genes on the X chromosomes. The plots correlate changes in gene expression in M+Z- *mes-2*
876 mutants with changes in gene expression changes in M+Z- *mes-6* mutants. Results are shown
877 separately for X-linked (left) and autosomal (right) transcripts. Notch-activated genes (red in
878 Figure 2A) are marked in red. Lightly shaded areas indicate transcripts that are at least 2-fold
879 upregulated. The overlap between transcripts upregulated by GLP-1^{Notch} and transcripts
880 upregulated by the loss of CePRC2 is highly significant, particularly for the X-linked genes.
881 The significance of the correlation was measured by hypergeometric distribution; X-linked
882 Notch-activated vs. *mes-2* derepressed: p=1.31e-31; X-linked Notch-activated vs. *mes-6* de-
883 repressed: p=7.41e-25; autosomal Notch-activated vs. *mes-2* derepressed: p=1.47e-22;
884 autosomal Notch-activated vs. *mes-6* de-repressed: p=1.8e-12.
885
886 **Figure 3. GLP-1^{Notch} enhances reprograming upon the depletion of PRC2.**
887 (A) Notch and PRC2 genetically interact in GeCo. Left: fluorescent micrographs of *glp-*
888 *1(ar202)* gain-of-function mutants expressing CHE-1–induced neuronal GFP. The animals
889 were subjected to control RNAi or RNAi against CePRC2 components (MES-2, 3, and 6), as
890 indicated. Increased GLP-1^{Notch} signaling enhanced the GeCo+ phenotype upon PRC2
891 depletion. Control RNAi (mock) for each genetic background did not result in any GeCo

892 (images not shown – see quantification). Right: the corresponding quantifications. P-values
893 were calculated using Student's t-test: $p^1 = 0{,}0006$; $p^2 < 0{,}0001$; $p^3 = 0{,}0536$; $p^4 = 0{,}0001$; $p^5 =$
894 0,4035; $p^6 = 0{,}0003$. At least 200 animals were scored per condition. Error bars represent
895 SEM. (B) GLP-1^{Notch} is required for GeCo in PRC2-depleted animals independently from
896 proliferation. Left: fluorescent micrographs of adults expressing CHE-1–induced nGFP, with
897 the genotypes indicated above the panels. The animals were subjected to RNAi as indicated
898 on the left. The first column shows heterozygous, the other two homozygous animals carrying
899 the loss of function alleles *gld-1(q497)*, *gld-2(q485)* and, in the central panel, *glp-1(q175).*
900 The animals were subjected to control RNAi or RNAi against PRC2 components (MES-2, 3,
901 and 6). In the absence of GLP-1^{Notch}, depletion of PRC2 components did not induce GeCo.
902 Scale bars = 10 µm. Right: the corresponding quantifications. P-values were calculated using
903 Student's t-test: $p^1 < 0{,}0456$; $p^2 = 0{,}0337$; $p^3 = 0{,}0070$; $p^4 = 0{,}0637$; $p^5 = 0{,}0080$; $p^6 = 0{,}1259$.
904 At least 70 animals were scored per condition. Error bars represent SEM.
905
906 **Figure 4. The H3K27 demethylase UTX-1 is required for GeCo enhancement**
907 (A) UTX-1 is critical for GeCo enhancement. Candidate Notch-activated genes, selected from
908 Supplementary file 2 with available RNAi clones, were assayed for a role in GeCo in *glp-*
909 *1(ar202)* animals, expressing CHE-1–induced nGFP and treated with *lin-53* RNAi. While the
910 additional depletion of *utx-1* had the strongest impact on GeCo+ and GeCo, the depletion of
911 C07G1.6 and *aldo-1* had a weaker effect. Representative fluorescence micrographs are below
912 the quantification chart. White dashed line outline the animal body, yellow lines outline
913 gonad areas with GeCo. P-values for GeCo+ were calculated using Student's t-test: $p^1 =$
914 $0{,}000013$; $p^2 = 0{,}026$; $p^3 = 0{,}021$; $p^4 > 0{,}1$. At least 250 animals were scored per condition.
915 Error bars represent SEM. nGFP = *gcy-5::gfp.* Scale bars = 10 µm. (B) As in A, but RNAi
916 was performed against *jmjd-1.2* (H3K9/27me2 demethylase); *jmjd-3.1*, *jmjd-3.2*, and *jmjd-*
917 *3.3*, (H3K27me2/3 demethylase); and *jmjd-2* (H3K9/36 demethylases). Only RNAi against
918 *jmjd-1.2* suppresses GeCo+, though to a lesser degree compared to *utx-1* RNAi.

Representative fluorescence micrographs are below the quantification chart. P-values for GeCo+ were calculated using Student's t-test: $p^1 = 0{,}0042$; $p^2 = 0{,}035$; $p^3 > 0{,}2$. At least 190 animals were scored per condition. Error bars represent SEM. Scale bars = 10μm.

Figure 5. UTX-1 is regulated by GLP-1^{Notch} and PRC2.

(A - C) Expression of *utx-1* is regulated by PRC2 and GLP-1^{Notch}. Top: dissected gonads expressing a GFP reporter, driven from the *utx-1* promoter (*putx-1::GFP,* fused to Histone 2B for nuclear localization to facilitate quantification), subjected to the indicated RNAi (A), crossed into the indicated genetic background (B) or carrying the indicated mutations in the reporter gene (C). a, b, and c indicate gonadal regions containing germ cells in mitosis (a), and leptotene/zygotene (b) or pachytene (c) stages of meiosis. Below: the corresponding GFP quantifications. The diagrams show GFP intensities relative to the control (indicated by green arrow) in regions a-c. Results are represented as average changes in the GFP intensity (relative to mock RNAi-ed or untreated animals). The error bars represent SEM. The numbers of analyzed gonads were as follows: n = 44 for wild-type reporter; n = 36 for *glp-1(ar202)*; n = 55 for wild-type reporter on control RNAi; n = 48 for *mes-2* (RNAi); n = 15 for *mes-3* (RNAi); n = 29 for *mes-6* (RNAi), and n = 20 for the LAG-1 binding sites deleted reporter. (A) The *putx-1::GFP* reporter is repressed by PRC2. In all *mes*-depleted gonads, the reporter was de-repressed in proliferating cells (a) as well as in more proximal gonadal regions (b-c). (B) The *putx-1::GFP* reporter is upregulated by GLP-1^{Notch}. In the gain-of-function *glp-1(ar202)* mutant, the reporter was strongly derepressed in the proliferating cells in the distal-most gonad (a). Its expression was also increased in the more proximal regions (b-c), which, in this mutant background, contain proliferating cells instead of meiotic cells. (C) *putx-1::GFP* expression depends on the predicted LAG-1/CSL binding sites in the promoter. Upon deletion of putative LAG-1/CSL binding sites, the reporter expression was abolished. The changes in GFP intensities were highly significant (p-values were measured by independent t-tests) $p^1=4.85^{-13}$, $p^2=1.38^{-20}$, $p^3=1.18^{-7}$. (D) LAG-1 binds the *utx-1* promoter. Lysates of animals expressing FLAG-tagged LAG-1 (strain *wgIs591; lag-1::TY1::EGFP::3xFLAG*),

either in wild-type or *glp-1(ar202)* background, were subjected to ChIP-qPCR analysis of the indicated genes. Negative controls and additional tested genes are shown in Figure 5–supplemental figure 3. The qPCR amplicons were tested in at least three independent experiments. The results are shown as fold enrichment in anti-FLAG IP compared to IP with unspecific antibody. The 3'UTR of *lst-1* serves as a negative control. Interestingly, LAG-1 binding in the *glp-1(ar202)* gain-of-function background is stronger to the *utx-1* promoter than to the reported GLP-1^{Notch} targets *lst-1* and *sygl-1*. The asterisks indicate p-values < 0.05 (Students *t*-test). Error bars represent SEM.

SUPPLEMENTARY FIGURE LEGENDS

Figure 1–figure supplement 1. *glp-1(gf)* gonads contain more than twice the number of converted cells which display neuronal characteristics.

(A) For the quantification of *gcy-5::gfp*-positive cells per gonadal arm only the GeCo category of *wt* vs. *glp-1(gf)* was used because GeCo+ animals already show an extensive area of the gonad filled with *gcy-5::gfp*-positive cells with usually >100 cells/gonad making reliable counting impossible. Notably, animals with a seemingly similar extend of GeCo in *wt* vs. *glp-1(gf)* show a clear increase of *gcy-5::gfp*-positive cells per gonadal arm from approx. 10 in *wt* to > 30 in *glp-1(gf)*. n(wt) = 75 gonaldal arms, n (*glp-1(ar202)*) = 221 gonadal arms. The background of the loss of function allele *glp-1(q175)* leads to a significant decrease in GeCo as shown previously (Tursun *et al.* 2011). (B) A magnified view of *gcy-5::gfp*-positive (nGFP) cells, in a GeCo+ gonad from a *glp-1(gf)* animal. The converted cells show axo-dendritic projections (white arrow heads). The inset in the corresponding DIC image, magnified in the right-bottom corner, shows the nuclear morphology of a converted germ cell, which has lost the germ cell-specific 'fried-egg'-like shape and instead shows nuclear speckles characteristic of a neuronal cell. Scale bar = 1 µm.

Figure 1–figure supplement 2. Germ cell numbers are similar between *gld-1 gld-2* double and *gld-1 gld-2*; *glp-1* triple mutants.

DAPI-stained gonads of *gld-1(q497) gld-2(q485)* or *gld-1(q497) gld-2(q485); glp-1(q175)* mutants, carrying the *hsp::che-1* and *gcy-5::gfp* transgenes. The gonads were imaged by fluorescent microscopy using Z-stack acquisitions. Germ cells from the DTCs (yellow asterisks) to the turn of the gonad arm (dashed lines) were counted. Below:15 gonad arms per condition of L4 animals were counted. The numbers of germ cells differ only slightly (15%) in the double mutant vs. triple mutants background. Scale bars = 10 µm. Error bars represent SEM.

Figure 1–figure supplement 3. Blocking the cell cycle with Hydroxyurea does not inhibit GeCo+.

(A) We used hydroxyurea (HU) treatment for 5 h to chemically block the cell cycle, which makes germ cells arrest in the S phase of the cell cycle. This arrest does not diminish the GeCo+ phenotype in *glp-1(gf)* gonads upon *lin-53* RNAi and *che-1(oe)*. At least 150 animals were quantified per condition. P-values were calculated using Student's t-test: $p^1 = 0{,}1409$; $p^2 = 0{,}4583$. Error bars represent SEM. The right panel shows examples of GeCo+ displaying animals based on *gcy-5::gfp* (nGFP) for HU-untreated (-HU) and HU-treated (+HU) animals. (B) The gonads were stained for EdU incorporation. Dashed lines outline gonads. Asterisks indicate distal tips of gonads. Scale bars = 10 µm. (C) The gonads of *glp-1(ar202) gf* animals, which were treated with HU for 12 h and stained with DAPI and H3Ser10ph (pH3) antibody. The pH3-positive cells indicate condensed chromosomes of dividing cells. After 12 h of HU treatment, the gonads contained, as expected, enlargement nuclei (arrowheads) (Gartner *et al.* 2004; Fox *et al.* 2011). The loss of pH3-positive cells indicates a cell cycle arrest. Asterisks indicate distal tips of gonads, dashed lines outline gonad. Scale bars = 10 µm.

Figure 2–figure supplement 1. Examining transcriptional effects of GLP-1^{Notch} signaling.

(A) GLP-1^{Notch} signaling counteracts the meiosis-promoting activity of several RNA binding proteins, of which GLD-1 and -2 are indicated. (B) Mutants that were used in this study: while the the loss-of-function (lf) alleles of *glp-1* cause the loss of germ cells, gain-of-function (gf) alleles result in a constitutive proliferation of germ cells. However, in the absence of the meiosis-promoting GLD-1 and GLD-2 proteins, germ cells continue to proliferate in the absence of GLP-1^{Notch} activity. (C) Three representative gonads of Notch ON: *gld-2(q497) gld-1(q485); glp-1(ar202)* and Notch OFF: *gld-2(a497) gld-1(q485); glp-1(e2144)* animals are shown after dissection and DAPI staining. The central planes of the gonads were imaged. Nuclei were counted from those images using the CellCounter plugin with ImageJ. For each genetic background, germ cells in the entire gonad of 10 dissected gonads were counted. The quantification below revealed that the numbers of germ cells in both backgrounds are not changed. Error bars represent SD. Scale bar = 10 μm.

Figure 2–figure supplement 2. Analysis of Notch**-activated genes.**

(A) Changes in the abundance of several transcripts (marked black in Fig. 2A) were verified independently from the genomic quantification by RT-qPCR. Colors correspond to fold-changes detected by microarrays (green), by RT-qPCR on genetically identical gonads (black), or by RT-qPCR on gonads with a different loss-of-function *glp-1* allele, *q175* (white). *This experiment was performed only once. The error bars represent SEM. (B) Although the number of genes on the arrays is almost equally distributed between the different chromosomes, the expression of X-linked genes is largely silenced in the germline. The table displays the numbers and fractions of genes on the different chromosomes, and the distributions of the Notch-activated genes. The cutoff between "not expressed" and "expressed" genes was set according to the bimodal distribution of expression values in the Notch ON and OFF arrays.

Figure 2-figure supplement 3. The PRC2 component MES-6 and most enhancers/suppressors of *glp-1(ar202)* induced tumors appear to interact genetically with GLP-1/Notch signaling in a germline-autonomous manner.

Each bar indicates the relative proportion of germlines with wild-type morphology (grey), germlines that contain eggs but also a proximal or distal tumor (red), and germlines that are fully tumorous (black). "n" indicates the number of DAPI-stained gonads scored for each column. Empty vector 1 – 3 represent three independent replicates of the empty vector control and demonstrate the robustness of the experiment. We observed that, for an unknown reason, the *rrf-1(pk1417); glp-1(ar202)* double mutants were less likely to produce tumors at the semi-permissive temperature of 20 °C. Nonetheless, the double mutant strain reacts to enhancers, suppressors, and depletion of PRC2 components in a similar manner as the *glp-1(ar202)* single mutant strain, with the exception of *mbk-1* and B0416.5 RNAi. Depletion of *mes-2* and *mes-3* by RNAi was ineffective, since it did not enhance the tumourous phenotype in either of the two strains.

Figure 2–figure supplement 4. Global levels of H3K27me3 are unaffected by neither loss-of-function nor gain-of-function mutations in *glp-1*.

Stainings of wild-type, gain-of-function *glp-1(ar202)*, Notch ON (*gld-2(q497) gld-1(q485); glp-1(ar202)*) and Notch OFF (*gld-2(a497) gld-1(q485); glp-1(q175)*) gonads with antibodies against H3K27me3 performed on whole worms (left panel, scale bars = 10 μm) or dissected gonads (right panel, scale bars = 1 μm). The H3K27me3 levels do not differ globally between the different mutant backgrounds. Asterisks indicate distal tips of gonads, dashed lines outline gonad.

Figure 4–figure supplement 1. UTX-1 is required for the GeCo+ enhancement upon the depletion of PRC2

(A) Adult *glp-1(ar202)* animals treated with *lin-53* or *mes-3* RNAi were additionally subjected to either control or *utx-1* RNAi. Depletion of *utx-1* strongly suppressed the GeCo+ phenotype. Suppression upon *utx-1* co-depletion with *lin-53* is also detectable in the *rrf-1(pk1417)* background which is permissive for RNAi in the germline but not in the somatic gonad and the DTC. Right: quantification: n = 715 were scored for *lin-53; utx-1* RNAi; n = 500 for *mes-3; utx-1* RNAi and n = 270 were scored for *lin-53; utx-1* RNAi in *rrf-1(pk1417)*. P-values were calculated using Student's t-test: p^1 = 0,0588; p^2 = 0,0042; p^3 = 0,2454; p^4 = 0,01713; p^5 = 0,40479; p^6 = 0,00271. Error bars represent SEM. (B) anti-HA antibody staining for the 3xHA-tagged CHE-1 protein, which is being induced after heat-shock treatment in the different genetic backgrounds: *glp-1(ar202); otIs305* (*hsp^{prom}::che-1::3xHA*) *ntIs1* (*gcy-5^{prom}::gfp*) treated with our without RNAi against *lin-53* and *utx-1*. As additional controls the strain *otIs305* (*hsp^{prom}::che-1::3xHA*) *ntIs1* (*gcy-5^{prom}::gfp*) with or without *lin-53* RNAi and heat shock treatment was used. No obvious changes in the induction of CHE-1::3xHA in the germlines of the different genetic backgrounds can be detected. Scale bars = 1 µm.

Figure 5–figure supplement 1. The functional *utx-1* transgene is expressed in the same pattern as a GFP reporter coupled to the *utx-1* promoter.

Shown is an adult with an outlined gonad. The full-length GFP-tagged functional UTX-1 (*rrrSi189)* is repressed in the distal, proliferative part. Nuclei entering meiosis and developing oocytes express the fusion protein progressively stronger. This expression pattern is identical with the pattern seen in the *utx-1* promoter reporter strains (*rrrSi185*, *rrrSi281*).

Figure 5–figure supplement 2. The endogenous *utx-1* mRNA is upregulated in the absence of the PRC2-component MES-6.

Shown are representative *in-situ* hybridisations against endogenous *utx-1* mRNA in dissected gonads. In M+Z- *mes-6(bn66)* mutants, *utx-1* is upregulated throughout the gonads compared to the control wild-type gonads. "AS" and "S" indicate antisense and sense probes.

Figure 5–figure supplement 3. Testing LAG-1 binding to additional genes by ChIP.

Worm lysates (corresponding to 4 mg protein) of animals, with or without *lag-1::TY1::EGFP::3xFLAG* (*wgIs591*) transgene, were used for ChIP. Samples were incubated with 50 µl of FLAG ('specific' FLAG antibody) or HA antibodies ('unspecific' HA antibody) coupled to µMACS^{TM} microbeads (Milteny). As negative control, lysate N2 or *glp-1(ar202)* worm lysates, which do not express the recombinant target protein, were used. Both negative control lysates did not show any differences during the ChIP experiment when tested with either specific antibody (anti-FLAG coupled to µMACS beads) or unspecific antibody (anti-HA coupled to µMACS beads). Lysates of worms expressing the recombinant target protein in N2 or *glp-1(ar202)* background were incubated with specific (anti-FLAG) and unspecific (anti-HA) antibodies coupled to µMACS beads. The qPCR amplicons were tested in a minimum of three independent ChIP-qPCR experiments. Quantification results are shown as fold enrichment of anti-FLAG µMACS™ beads using *wgIs591* lysate over anti-FLAG µMACS™ beads using lysate without *wgIs591* (*no lag-1::TY1::EGFP::3xFLAG*). Primer for qPCRs (sequence details above) were designed using Primer3Plus (Untergasser *et al.* 2007). The FLAG-beads using lysates with *lag-1::TY1::EGFP::3xFLAG* show specific enrichment for tested target genes thereby validating the specificity of the ChIP. The asterisks indicates p-values < 0.05 (Students *t*-test). Error bars represent SEM.

SOURCE DATA LEGENDS

Figure 1-source data 1. Figure 1-source data 1A: Quantification of GeCo+ phenotype upon RNAi against *lin-53* in *glp-1(ar202)* mutants. Figure 1-source data 1B: Quantification of GeCo dependency on LAG-1. Figure 1-source data 1C: Quantification of germ cells in *glp-1 (ar202)* gonads with our without *lag-1* RNAi treatment. Figure 1-source data 1D: Quantification of GeCo in different genetic backgrounds with highly proliferative germlines upon RNAi against *lin-53*. Figure 1–figure supplement 1A source data: Quantification of gfp-positive germ cells. Figure 1–figure supplement 2 source data: Quantification of germ cells in different genetic backgrounds with highly proliferative germlines. Figure 1–figure supplement 3A source data: Quantification of GeCo after cell cycle block with HU treatment. More details can be found in the corresponding figure legends.

Figure 2-source data 1. Figure 2-source data 2A: Microarray results of differentially expressed genes in Notch ON/OFF gonads. Figure 2–figure supplement 3 source data: Quantification of germlines with wild-type morphology versus germlines with tumors upon germline-autonomous RNAi against genetic interactors of PRC2. More details can be found in the corresponding figure legends.

Figure 3-source data 1. Figure 3-source data 3A: Quantification of GeCo+ phenotype upon RNAi against PRC2 subunits in *glp-1(ar202)* mutants. Figure 3-source data 3B: Quantification of GeCo in different genetic backgrounds with highly proliferative germlines upon RNAi against PRC2 subunits. More details can be found in the corresponding figure legends.

Figure 4-source data 1. Figure 4-source data 4A: Quantification of GeCo+ upon RNAi against *lin-53* and Notch-activated genes. Figure 4-source data 4B: Quantification of GeCo+ upon RNAi against *lin-53* and Histone demethylases. Figure 4–figure supplement 1A source

data: Quantification of GeCo+ upon RNAi against *lin-53* and *utx-1* with and without *rrf-1* (*pk1417*) background. More details can be found in the corresponding figure legends.

SUPPLEMENTARY FILES

- Supplementary file 1: Enhancement or suppression of tumorous phenotypes
- Supplementary file 2: In situ hybridization patterns of Notch-activated genes
- Supplementary file 3A: Information on used *C. elegans* strains used in the study
- Supplementary file 3B: Information on RNAi clones used in this study
- Supplementary file 3C: Information on primer design and sequences
- Figure 1-source data 1: Contains Figure 1-source data 1A, Figure 1-source data 1B, Figure 1-source data 1C, Figure 1-source data 1D, Figure 1–figure supplement 1A source data, Figure 1–figure supplement 2 source data**,** Figure 1–figure supplement 3A source data
- Figure 2-source data 1: Contains Figure 2-source data 2A, Figure 2–figure supplement 3 source data
- Figure 3-source data 1: Contains Figure 3-source data 3A, Figure 3-source data 3B
- Figure 4-source data 1: Contains Figure 4-source data 4A, Figure 4-source data 4B, Figure 4–figure supplement 1A source data

A

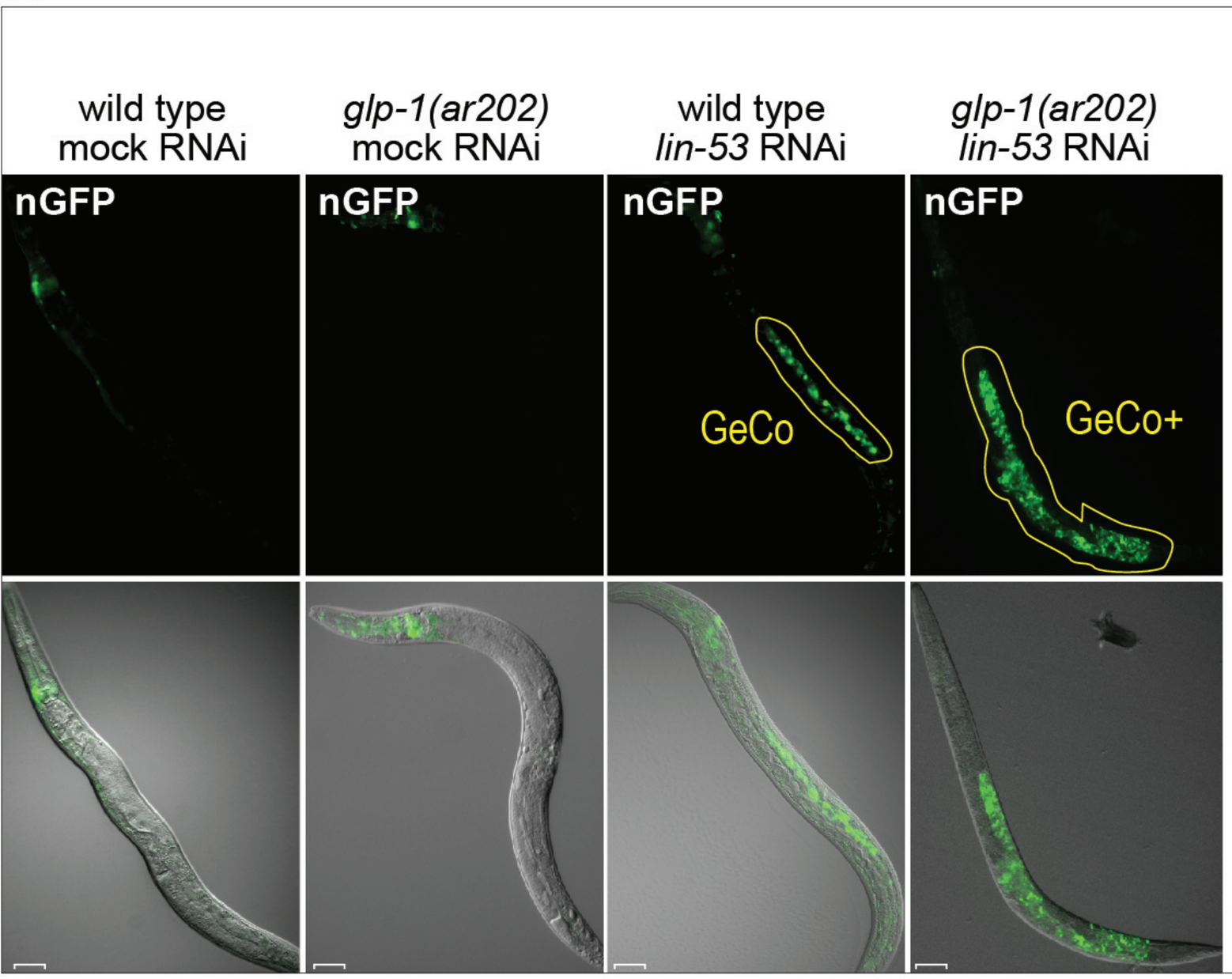
wild type
mock RNAi
glp-1(ar202)
mock RNAi
wild type
lin-53 RNAi
glp-1(ar202)
lin-53 RNAi
nGFP
GeCo
GeCo+

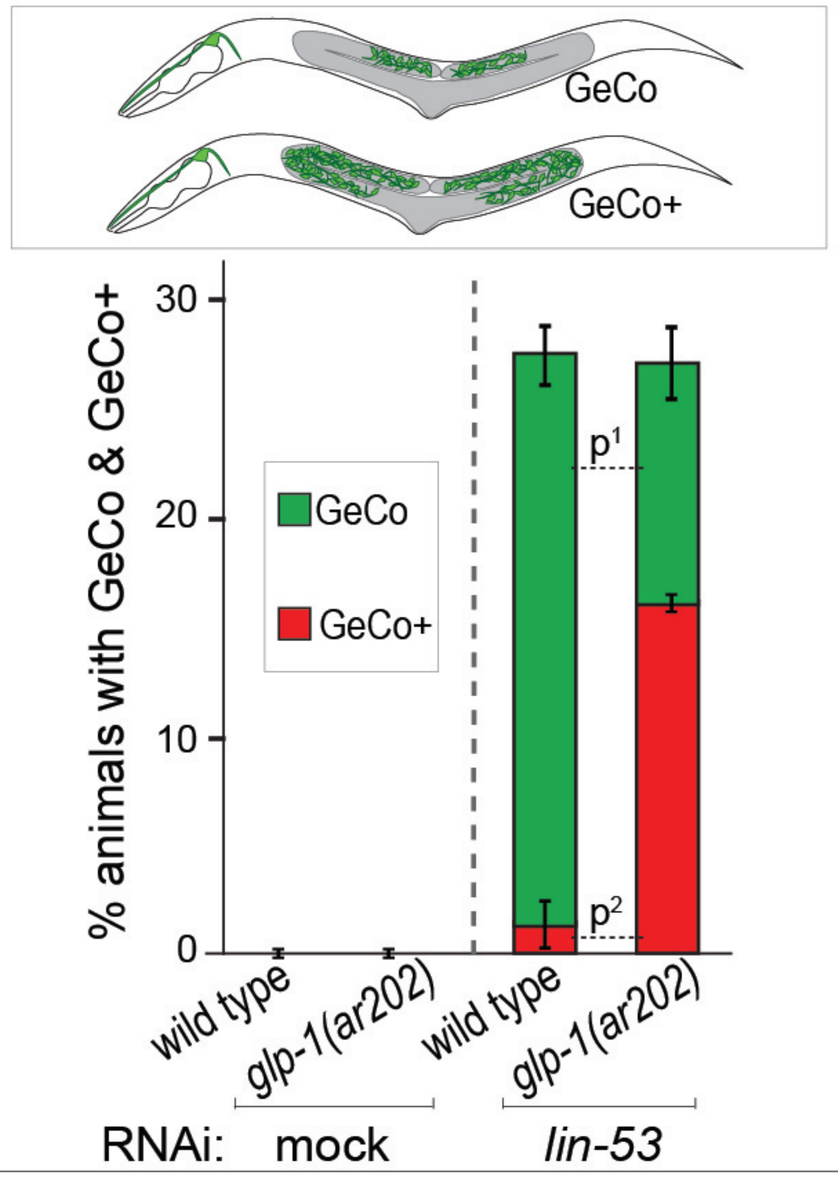
GeCo
GeCo+
% animals with GeCo & GeCo+
30
20
10
0
p1
p2
wild type
glp-1(ar202)
wild type
glp-1(ar202)
RNAi: mock lin-53

B

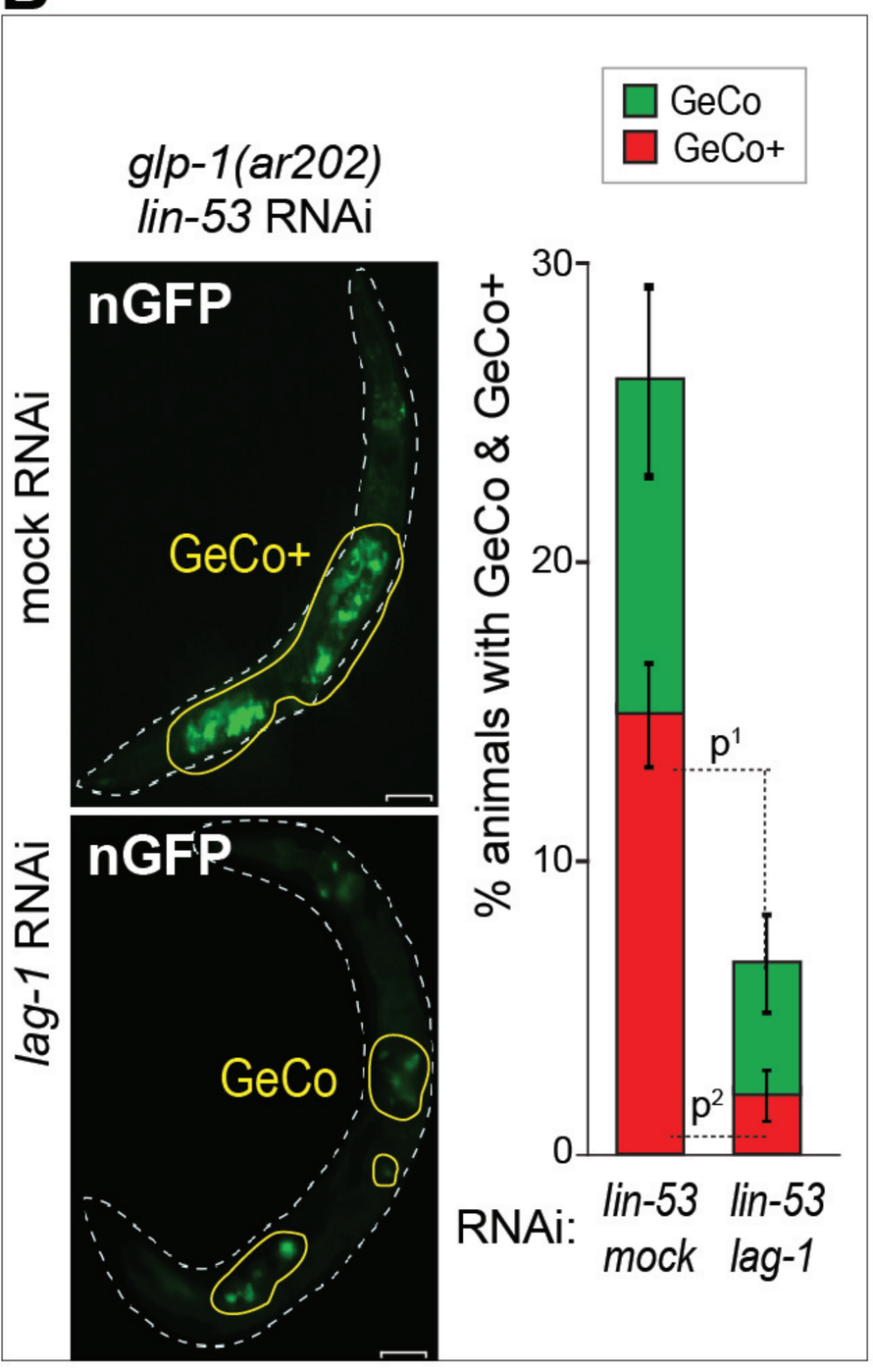
glp-1(ar202)
lin-53 RNAi
GeCo
GeCo+
nGFP
mock RNAi
lag-1 RNAi
% animals with GeCo & GeCo+
30
20
10
0
p1
p2
RNAi: lin-53 mock lin-53 lag-1

C

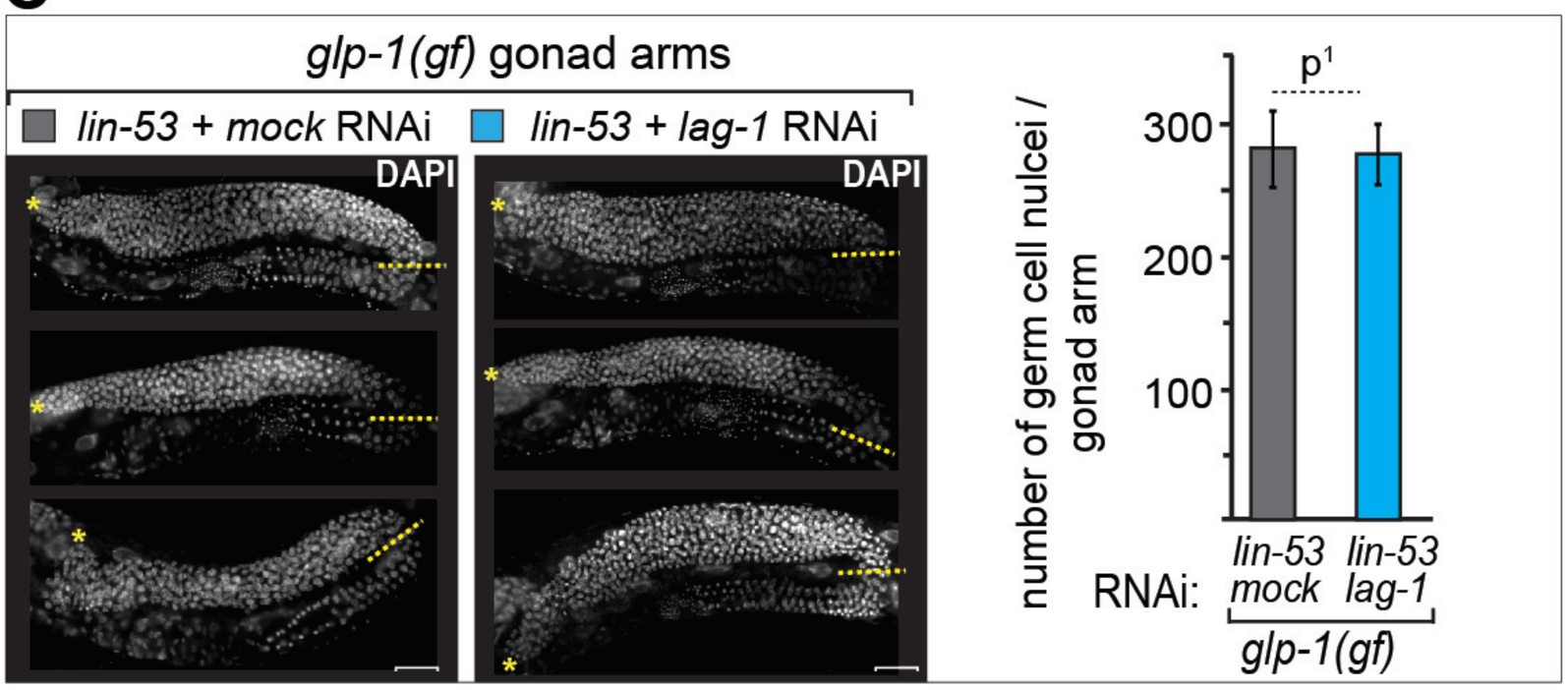
glp-1(gf) gonad arms
lin-53 + mock RNAi
lin-53 + lag-1 RNAi
DAPI
number of germ cell nulcei / gonad arm
300
200
100
p1
RNAi: lin-53 mock lin-53 lag-1
glp-1(gf)

D

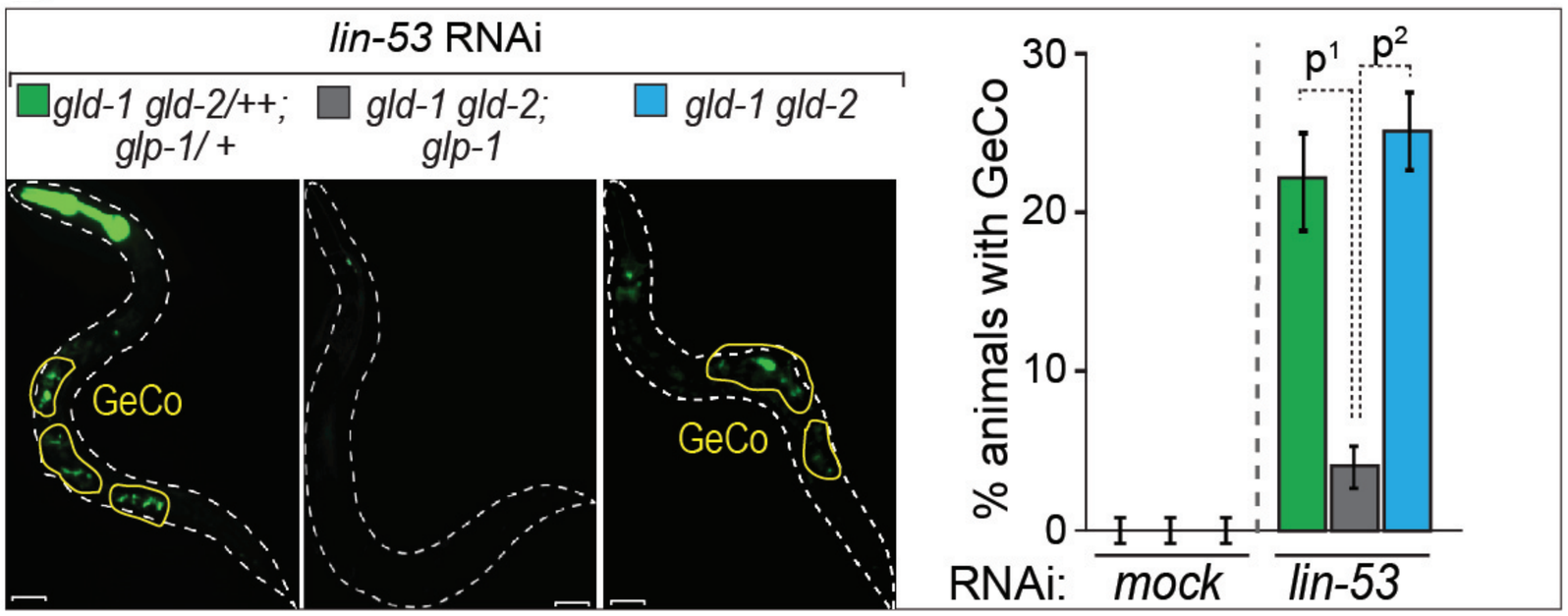
lin-53 RNAi
gld-1 gld-2/++; glp-1/ +
gld-1 gld-2; glp-1
gld-1 gld-2
GeCo
GeCo
% animals with GeCo
30
20
10
0
p1
p2
RNAi: mock lin-53

Seelk et al., Figure 2

A

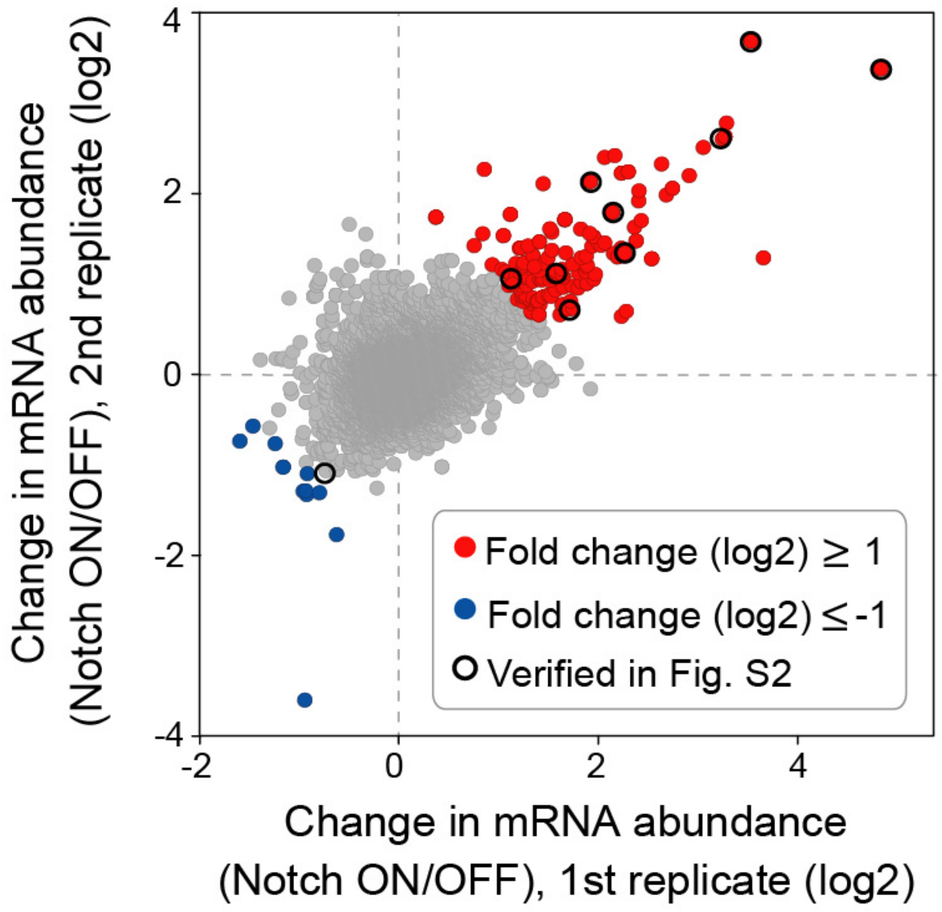

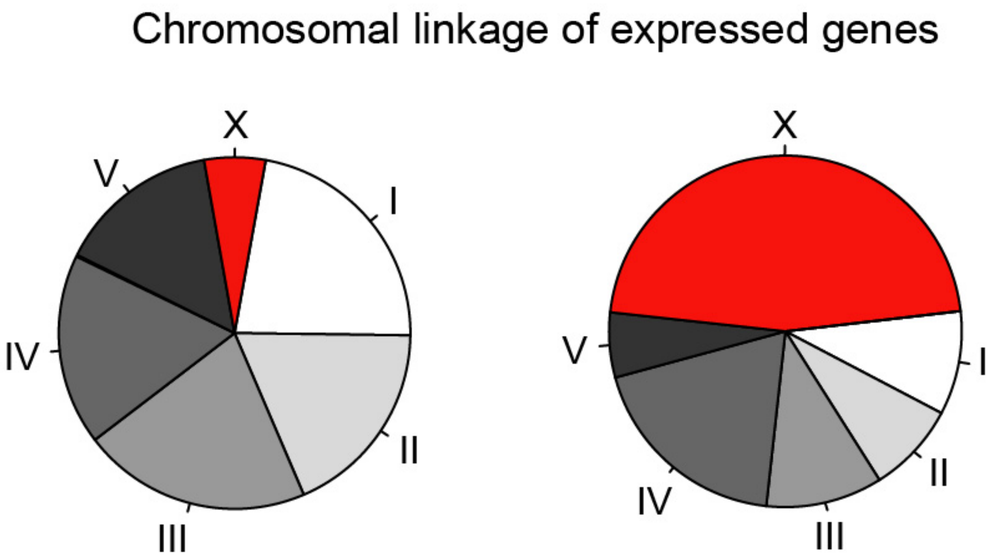

B

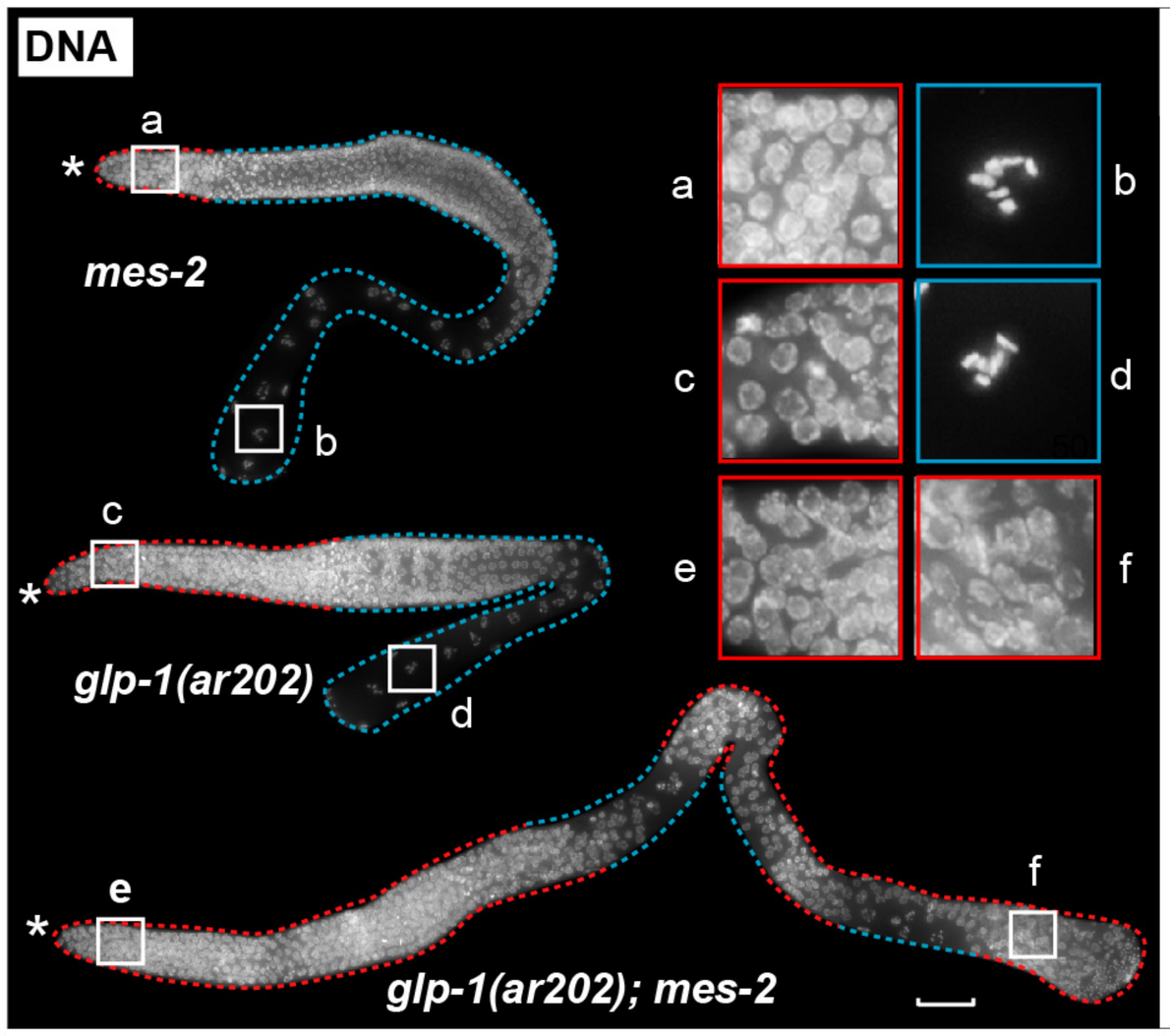

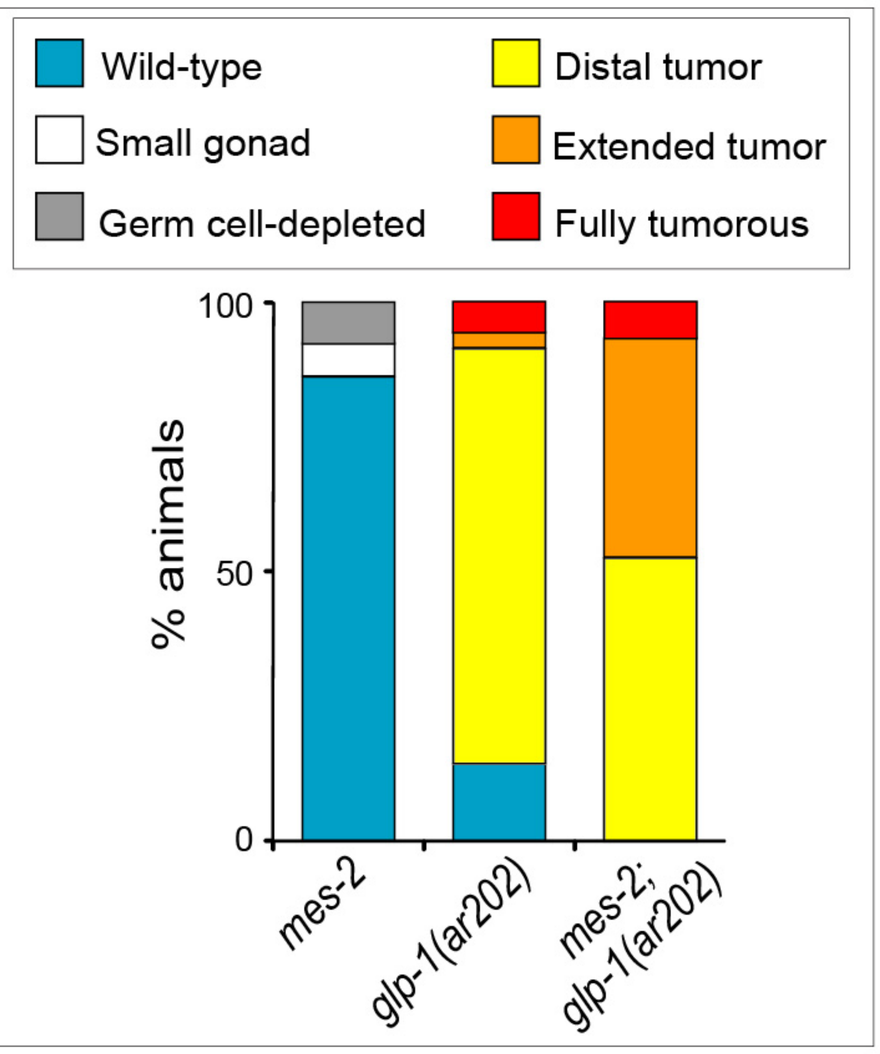

C

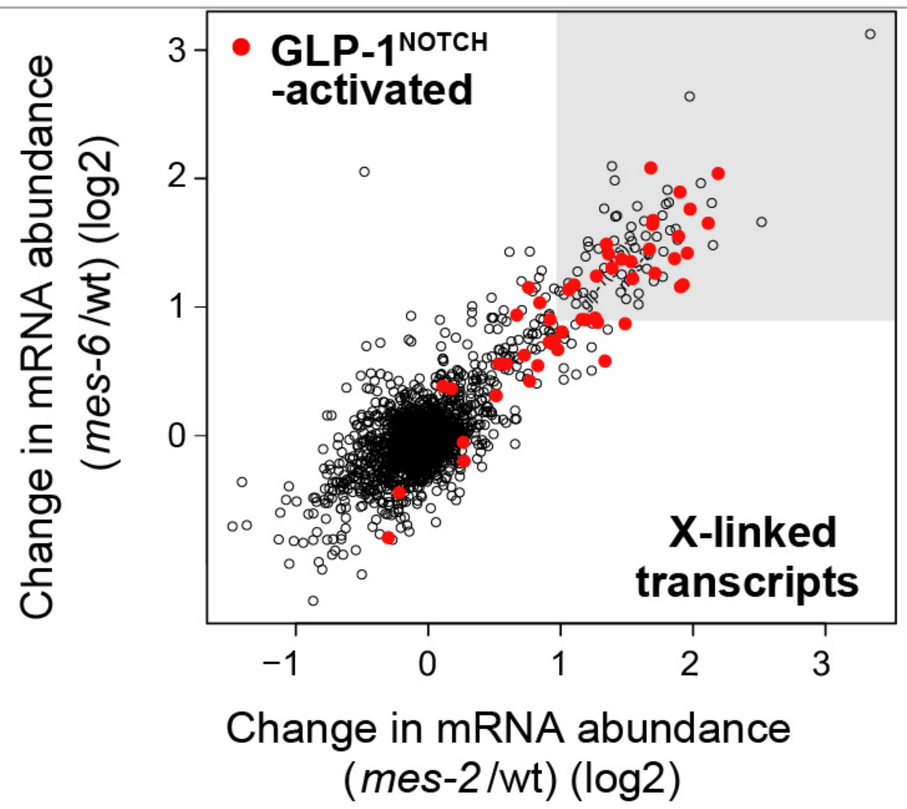

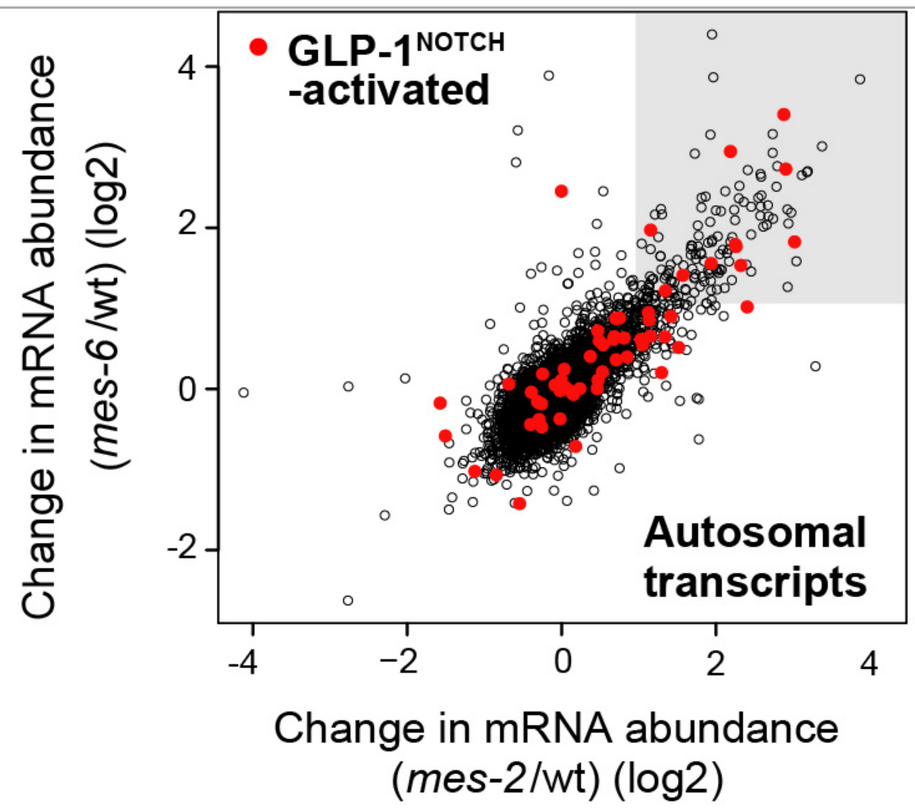

A

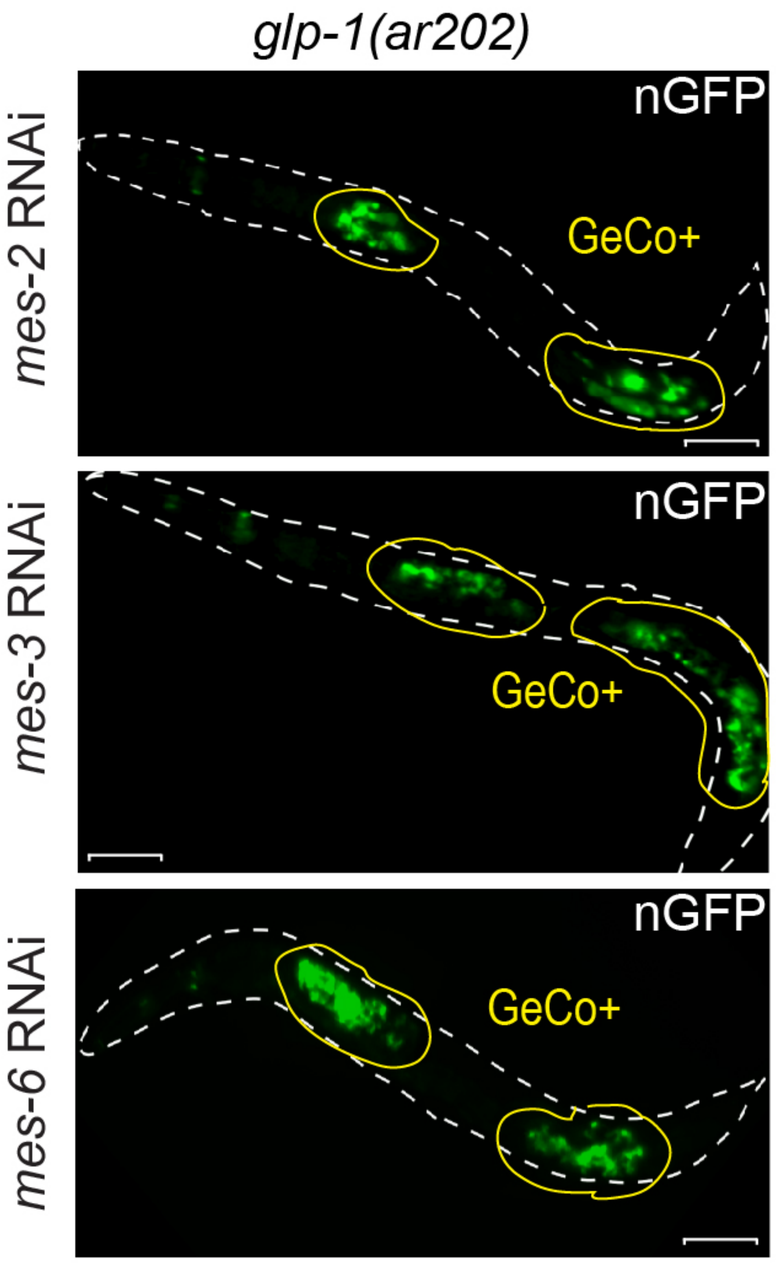
glp-1(ar202)
mes-2 RNAi
mes-3 RNAi
mes-6 RNAi
nGFP
GeCo+

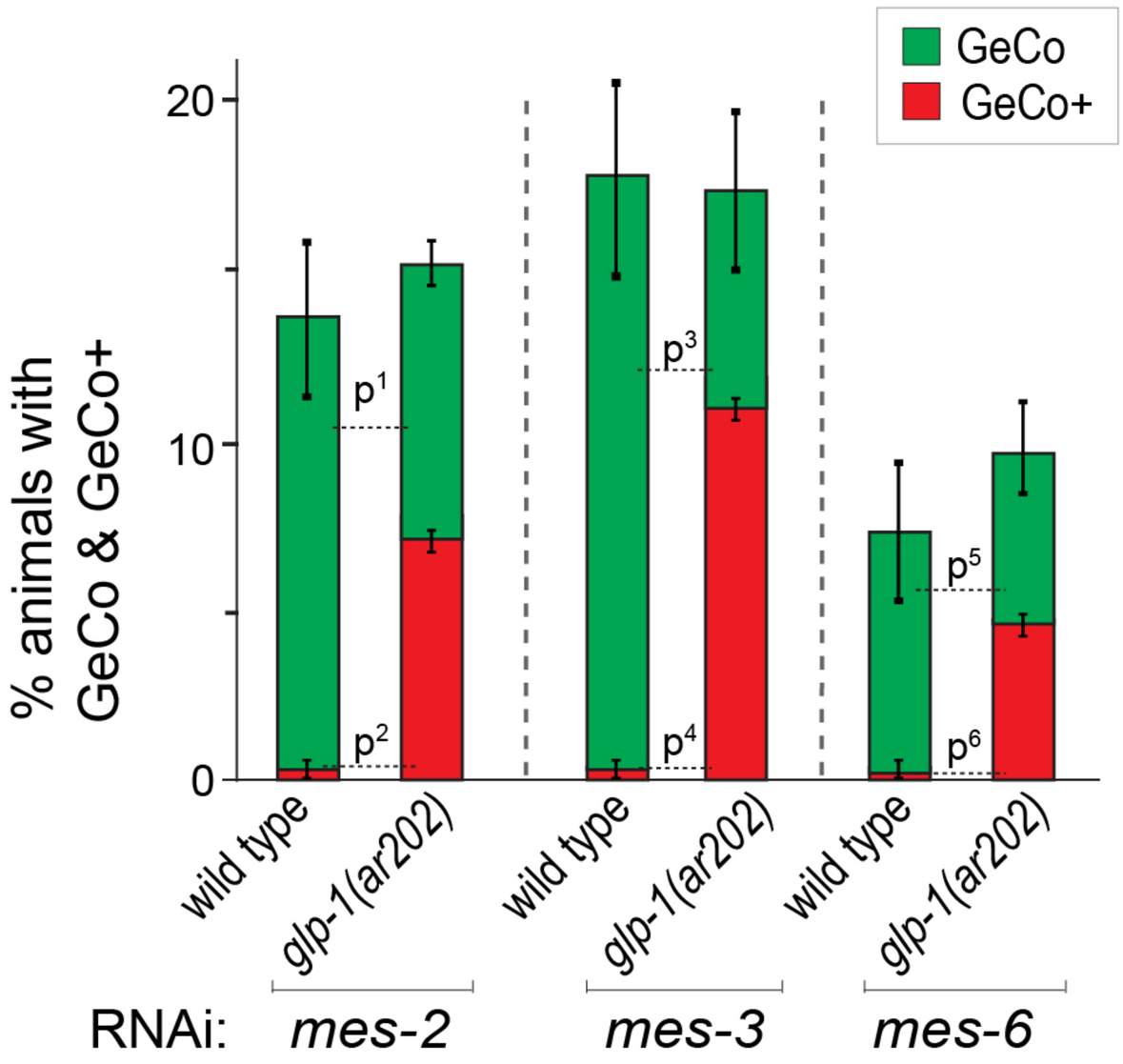
GeCo
GeCo+
% animals with GeCo & GeCo+
20
10
0
p1
p2
p3
p4
p5
p6
wild type
glp-1(ar202)
RNAi:
mes-2
mes-3
mes-6

B

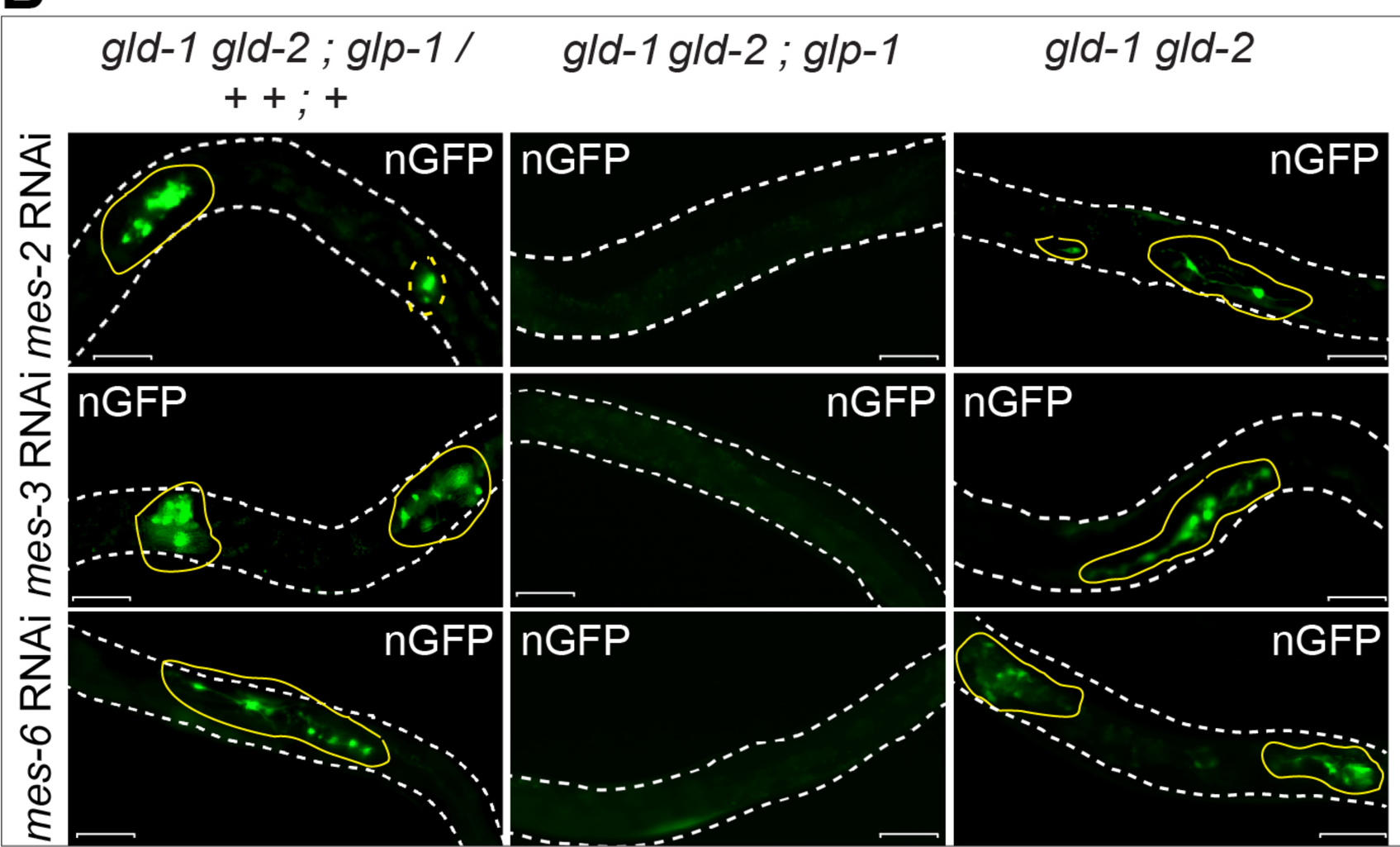
gld-1 gld-2 ; glp-1 / + + ; +
gld-1 gld-2 ; glp-1
gld-1 gld-2
mes-2 RNAi
mes-3 RNAi
mes-6 RNAi
nGFP

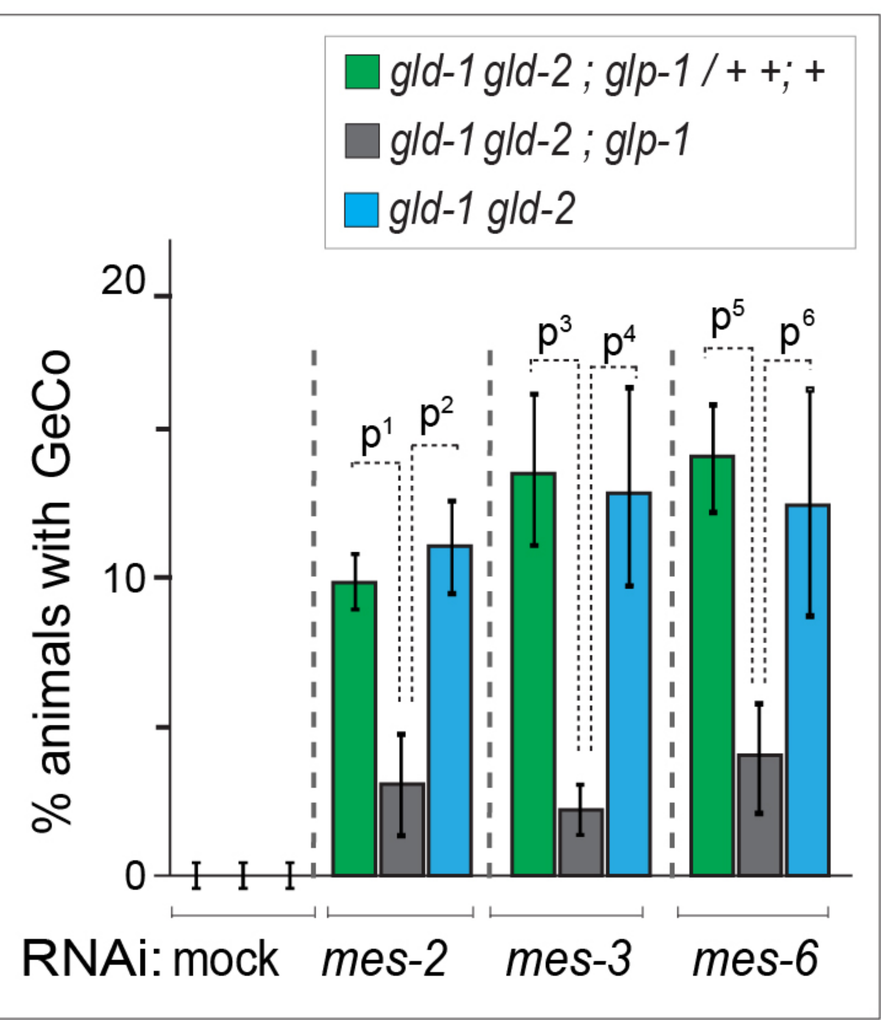
gld-1 gld-2 ; glp-1 / + + ; +
gld-1 gld-2 ; glp-1
gld-1 gld-2
% animals with GeCo
20
10
0
p1
p2
p3
p4
p5
p6
RNAi: mock
mes-2
mes-3
mes-6

A

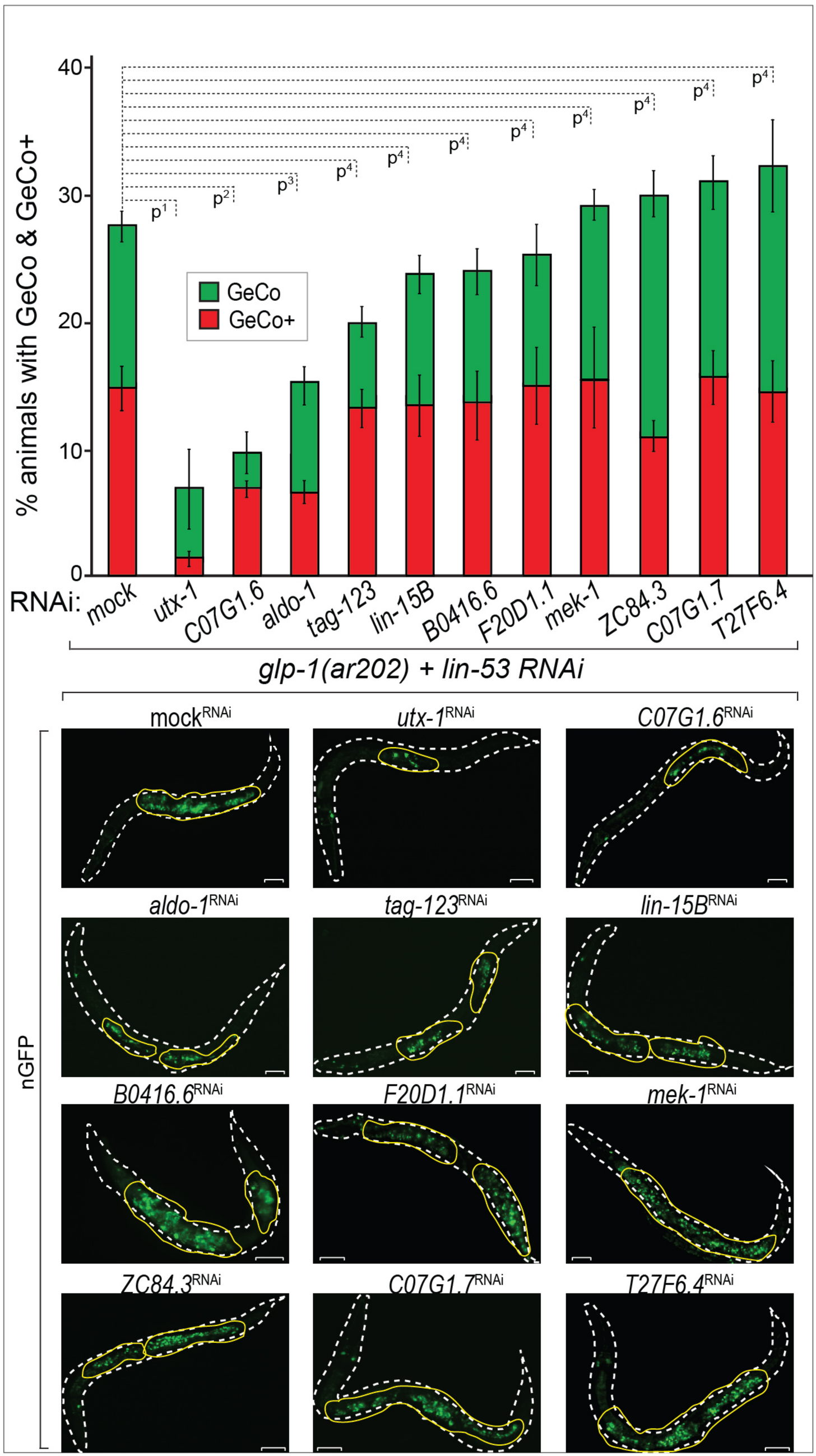
% animals with GeCo & GeCo+
40
30
20
10
0
p1
p2
p3
p4
GeCo
GeCo+
RNAi:
mock
utx-1
C07G1.6
aldo-1
tag-123
lin-15B
B0416.6
F20D1.1
mek-1
ZC84.3
C07G1.7
T27F6.4
glp-1(ar202) + lin-53 RNAi
mockRNAi
utx-1RNAi
C07G1.6RNAi
aldo-1RNAi
tag-123RNAi
lin-15BRNAi
B0416.6RNAi
F20D1.1RNAi
mek-1RNAi
ZC84.3RNAi
C07G1.7RNAi
T27F6.4RNAi
nGFP

B

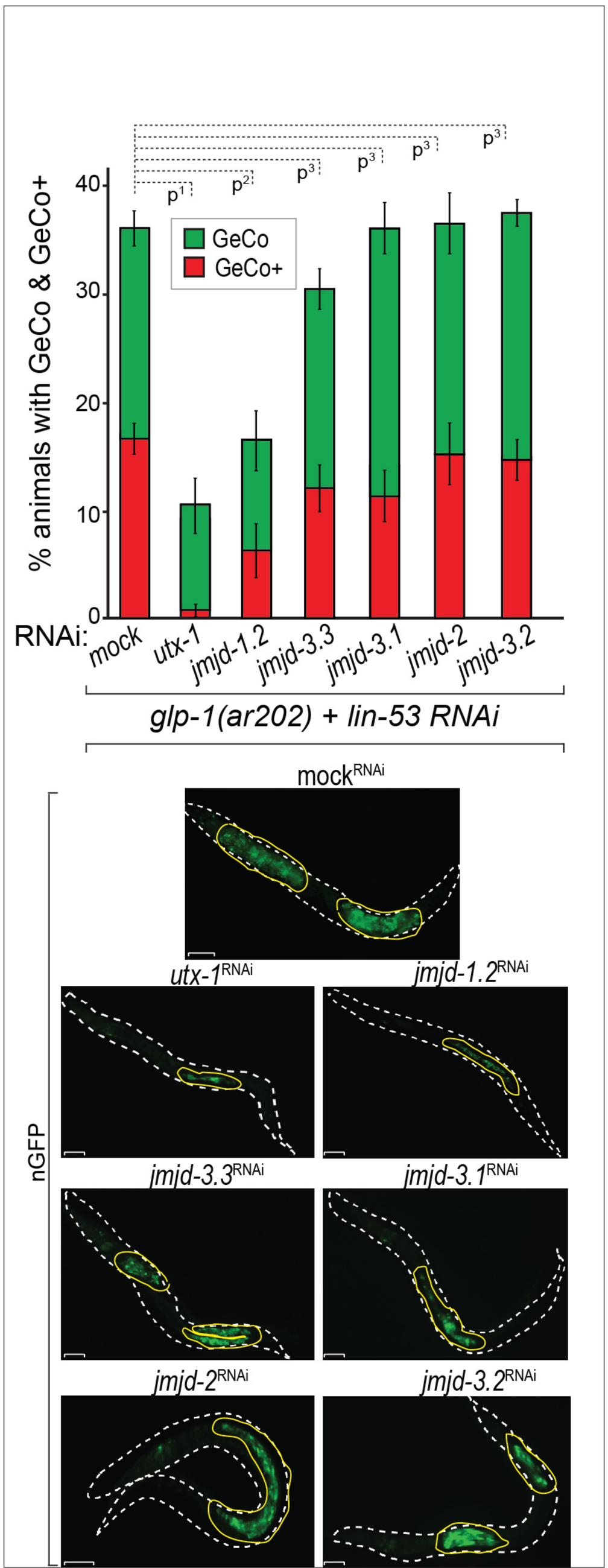
% animals with GeCo & GeCo+
40
30
20
10
0
p1
p2
p3
GeCo
GeCo+
RNAi:
mock
utx-1
jmjd-1.2
jmjd-3.3
jmjd-3.1
jmjd-2
jmjd-3.2
glp-1(ar202) + lin-53 RNAi
mockRNAi
utx-1RNAi
jmjd-1.2RNAi
jmjd-3.3RNAi
jmjd-3.1RNAi
jmjd-2RNAi
jmjd-3.2RNAi
nGFP

Seelk et al., Figure 5

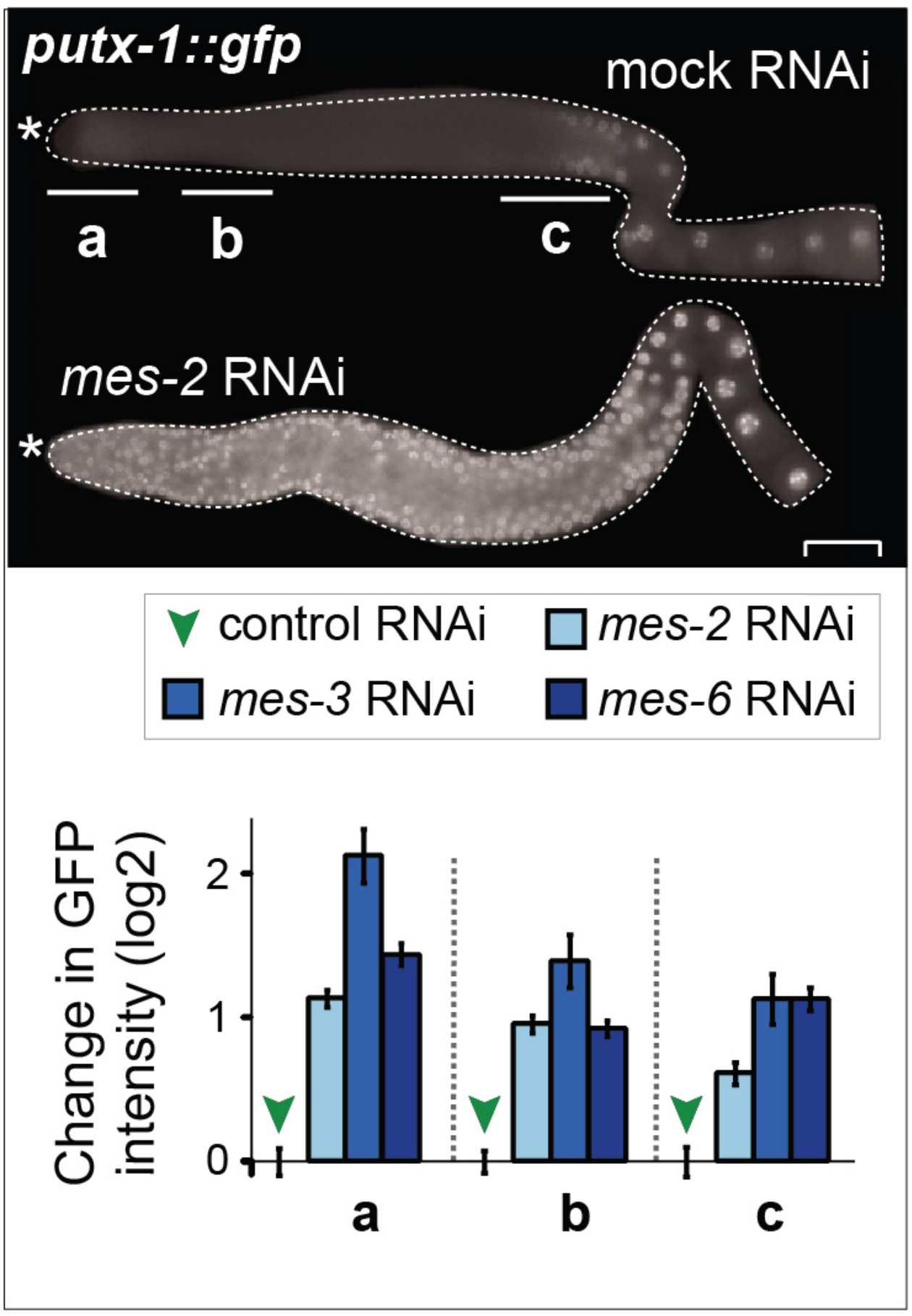

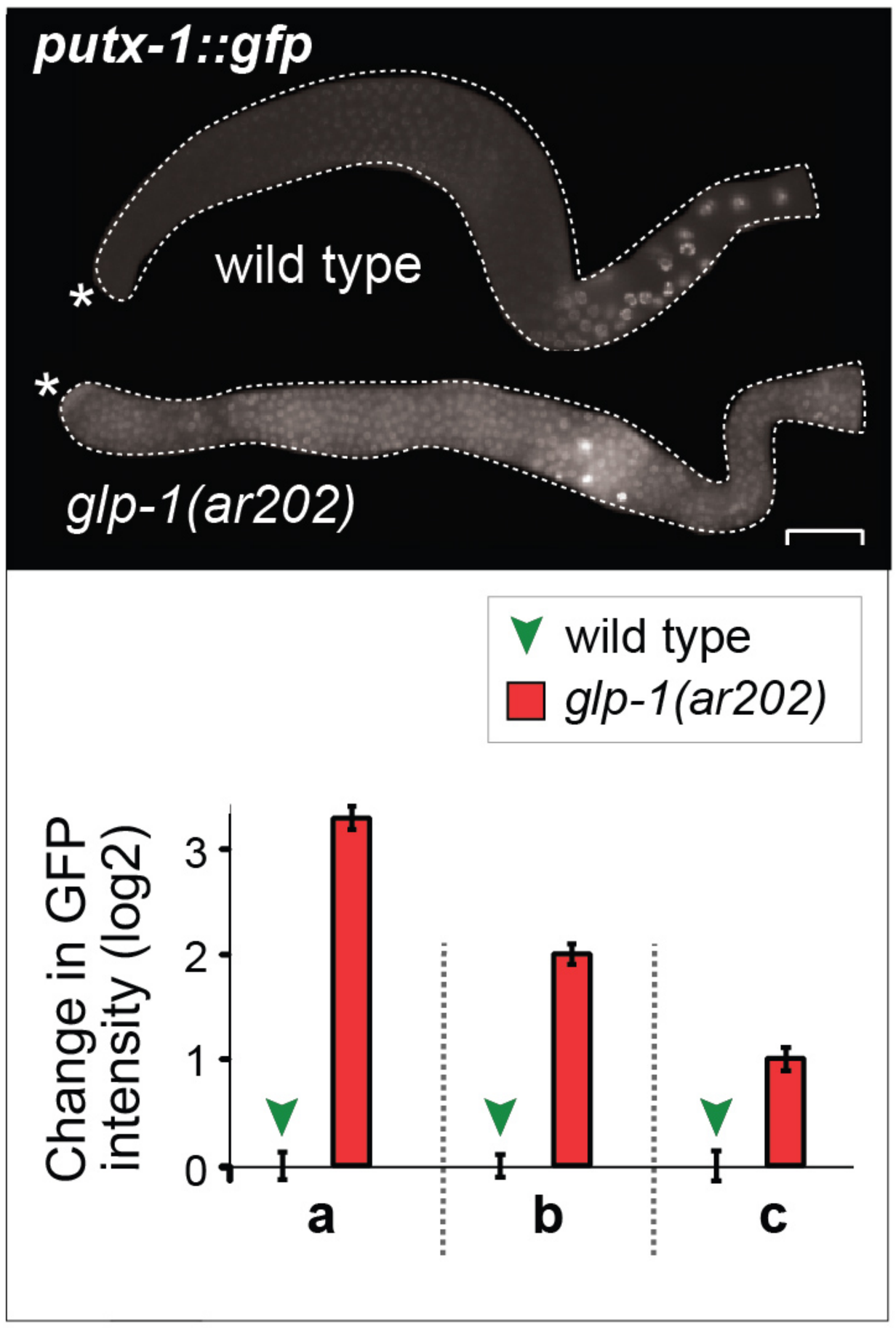

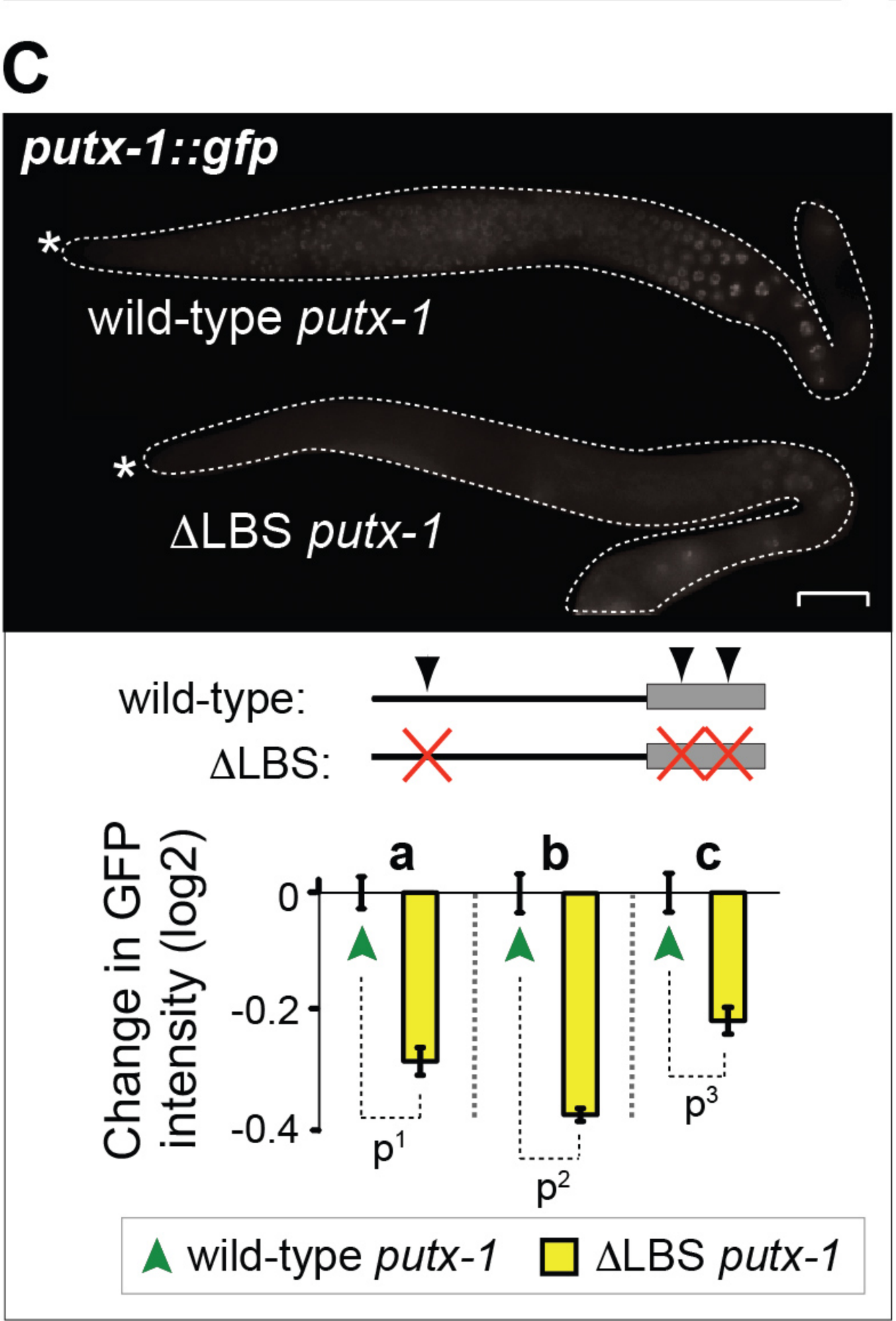

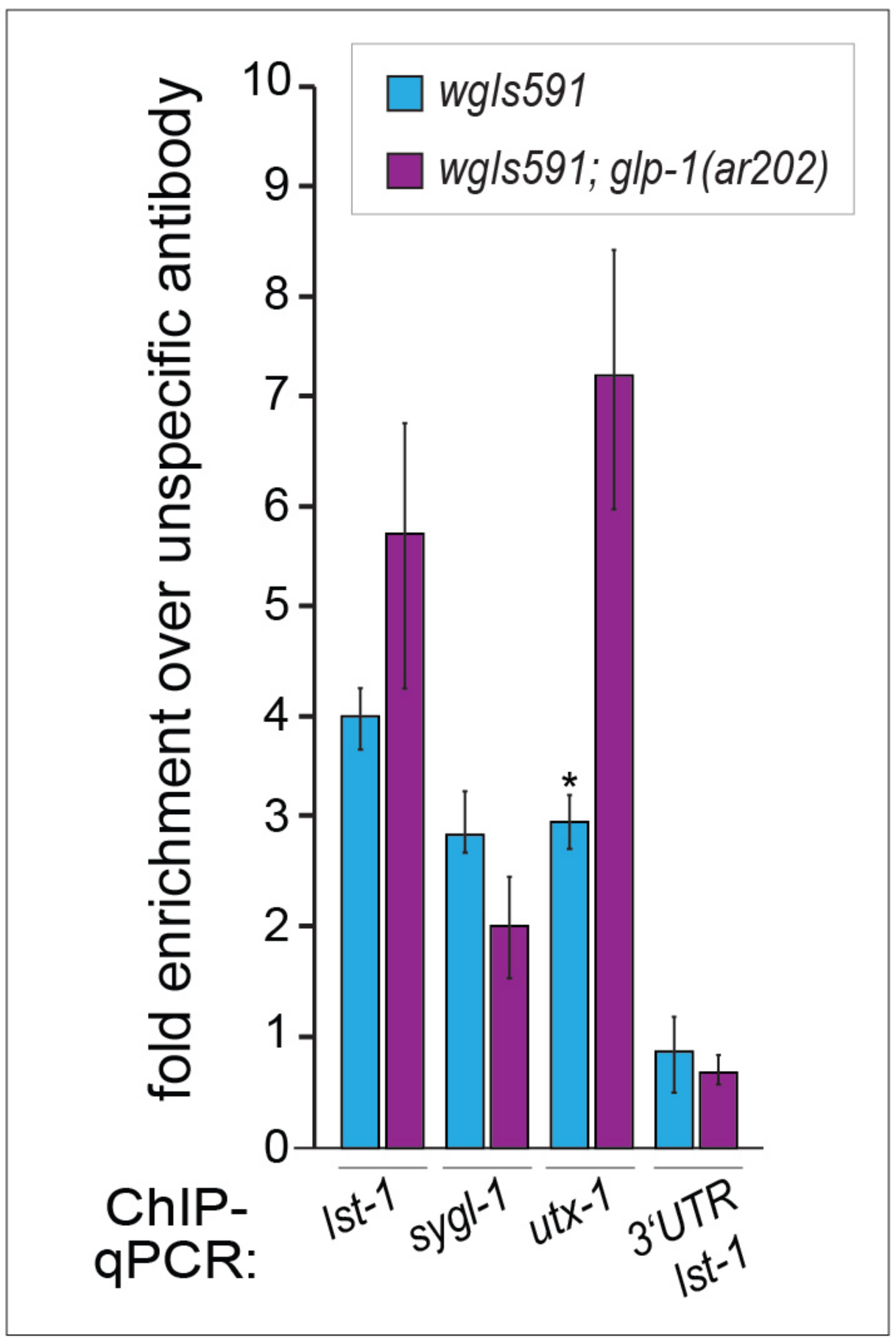

Seelk et al., Figure 1—figure supplement 1

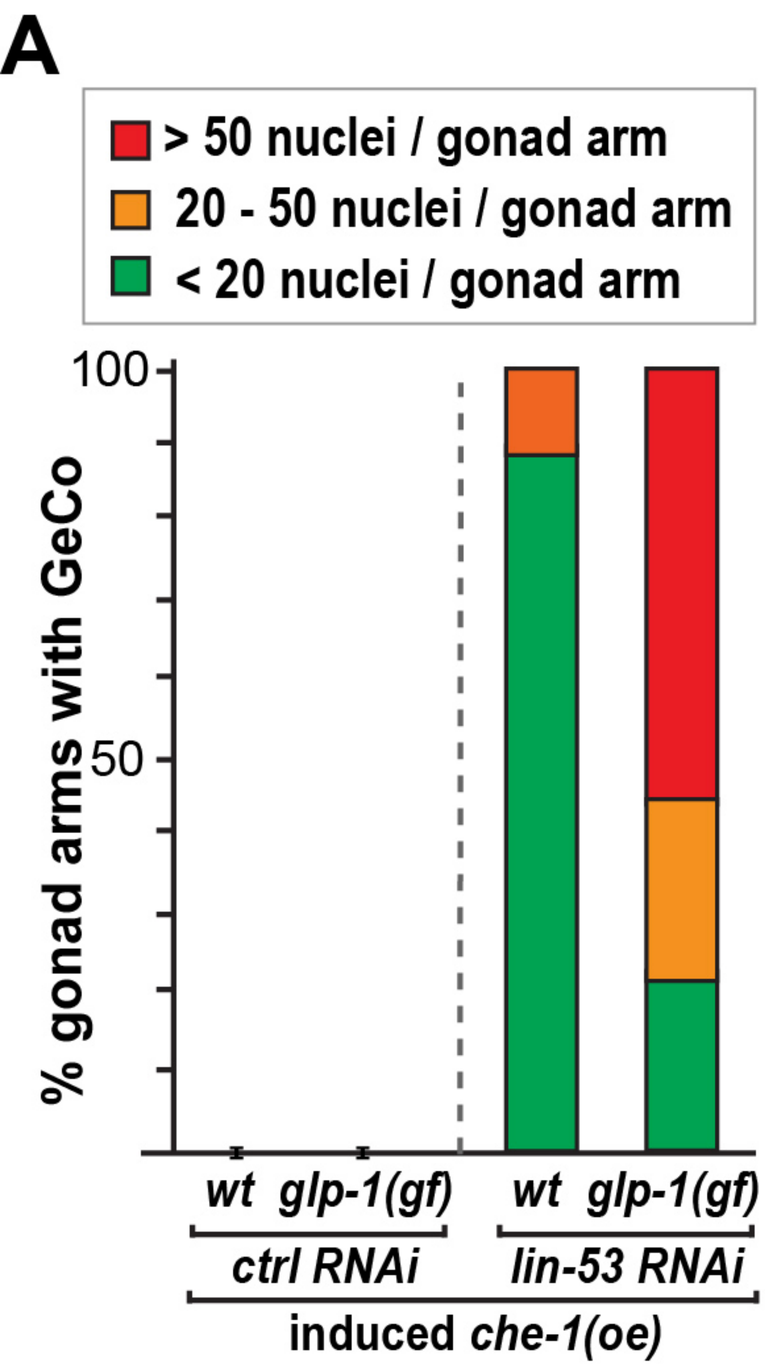

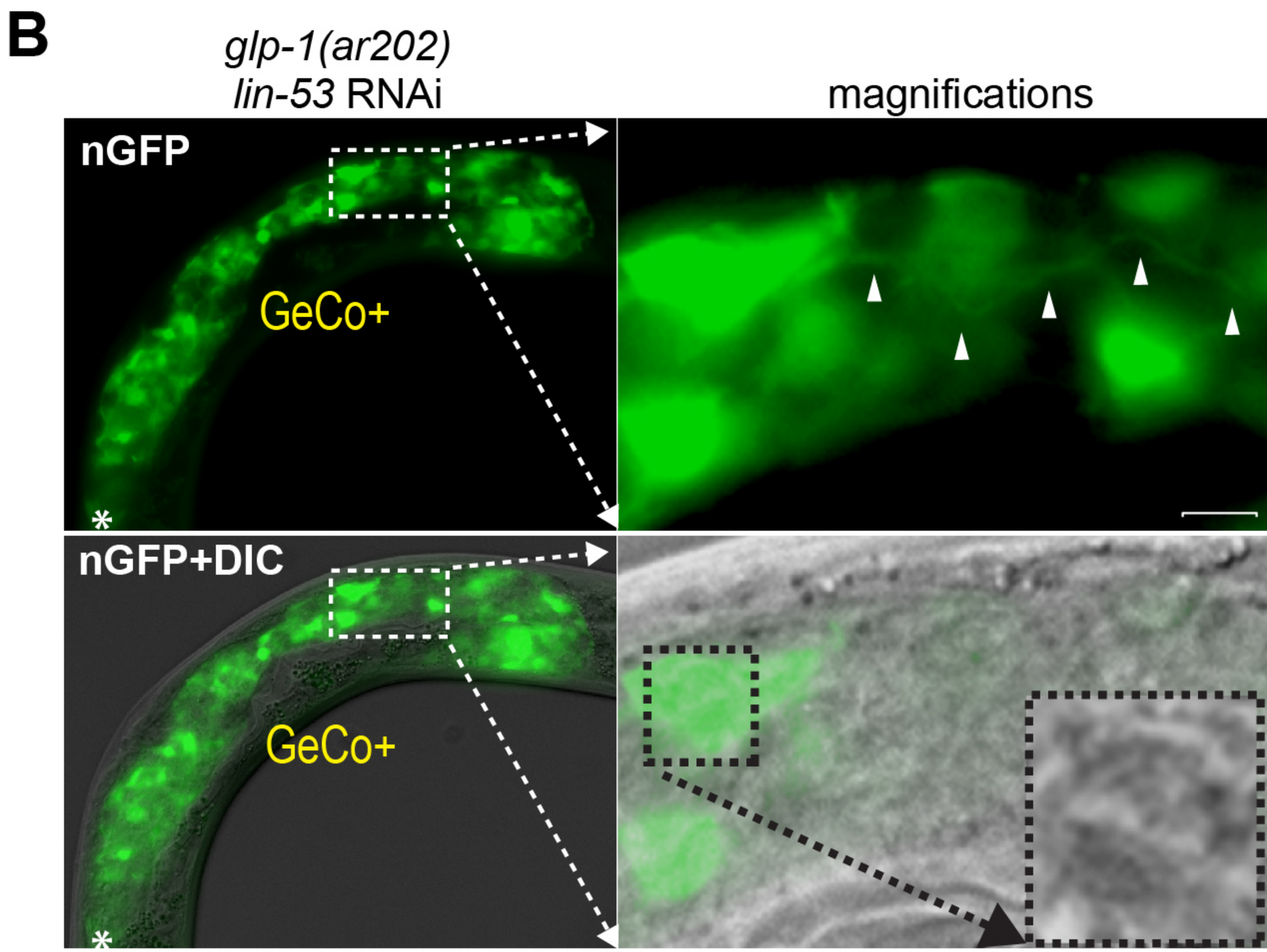

Seelk et al., Figure 1—figure supplement 2

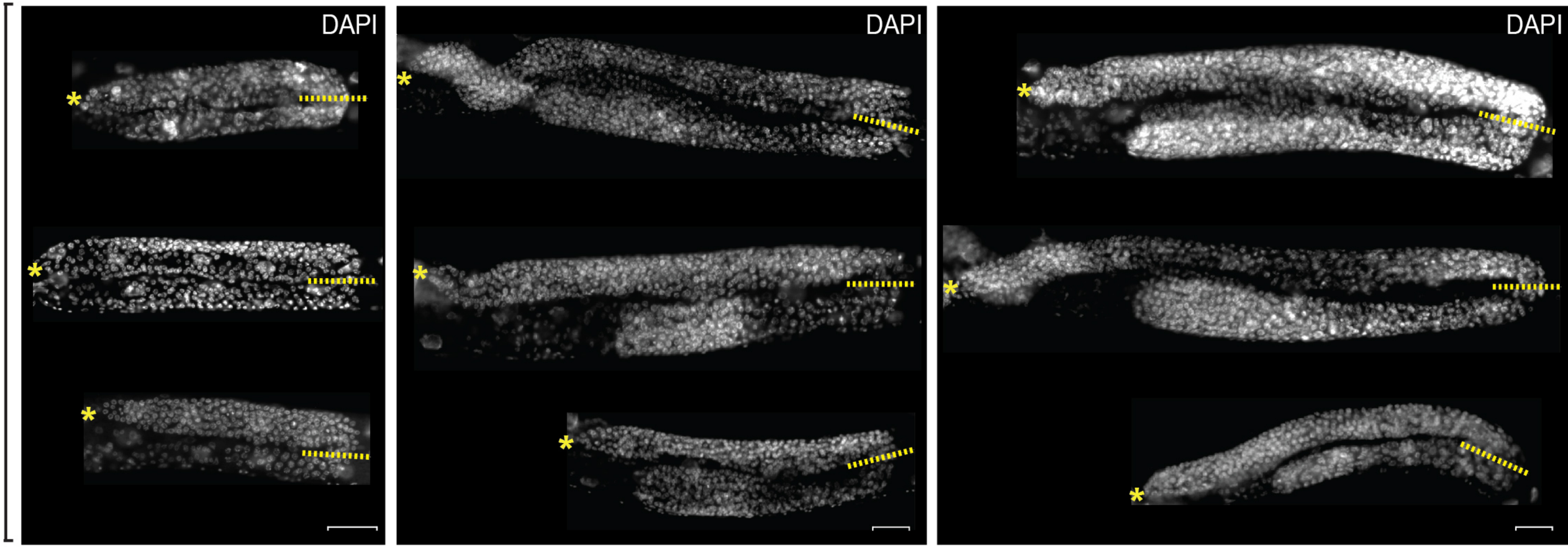

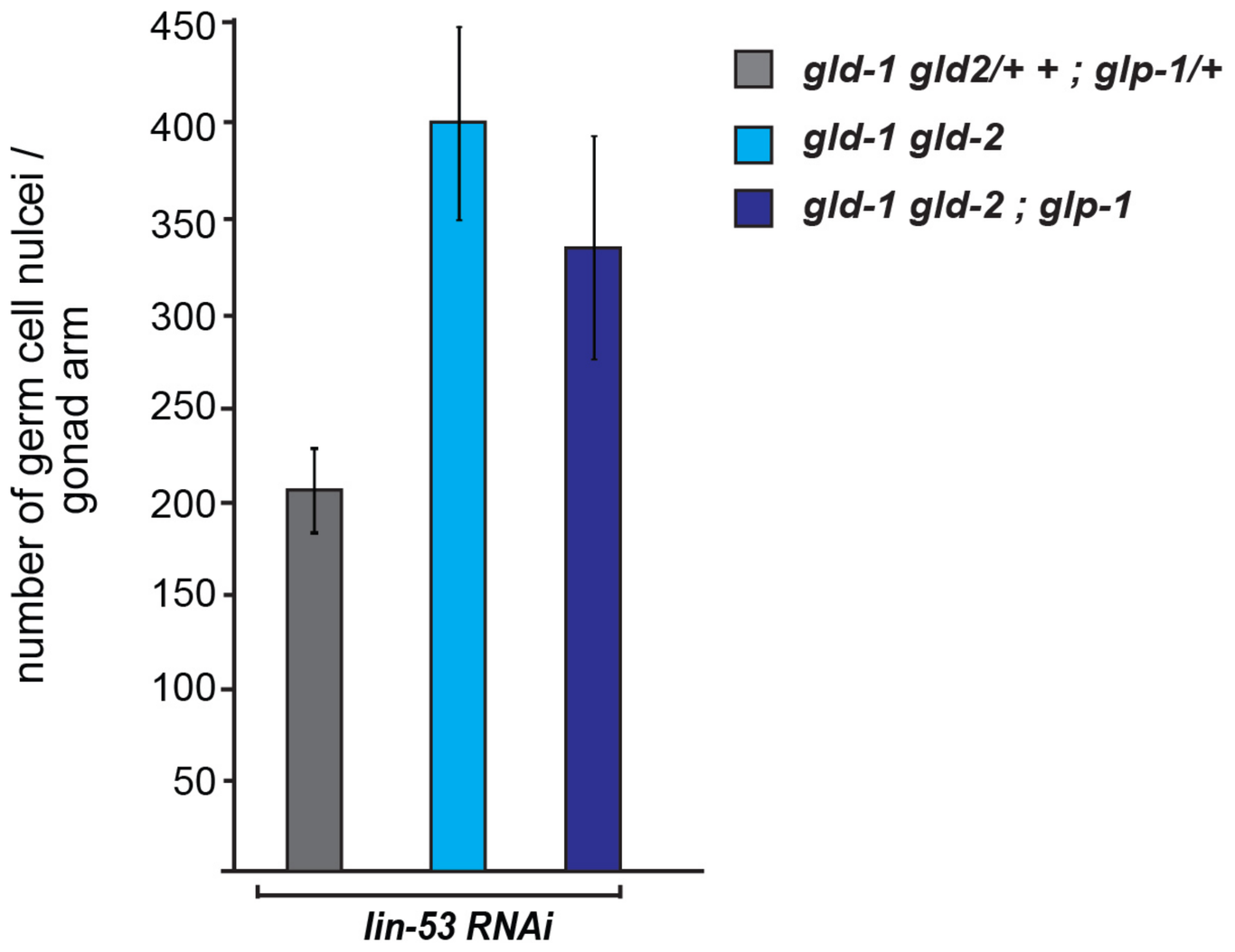

Seelk et al., Figure 1—figure supplement 3

A

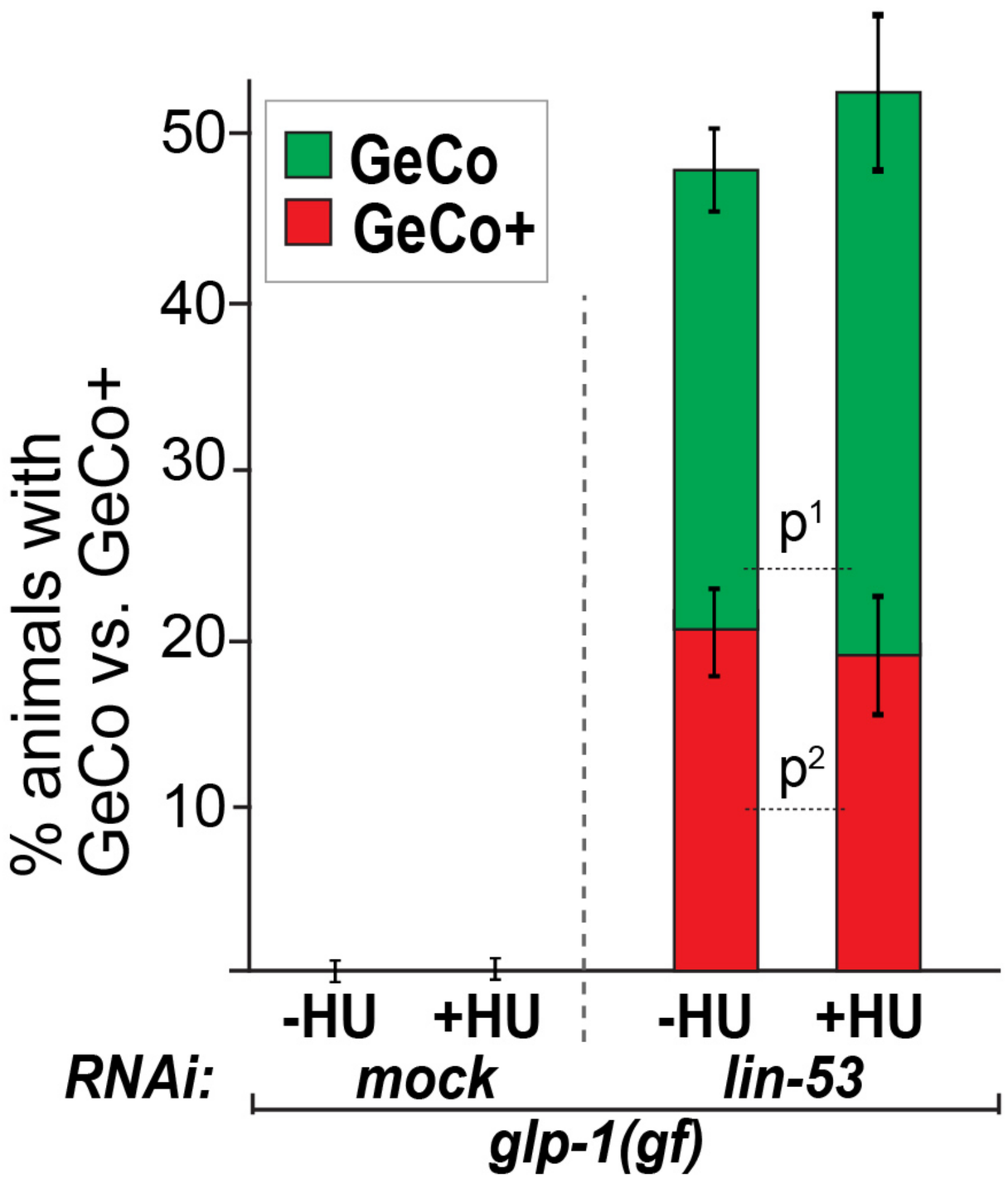

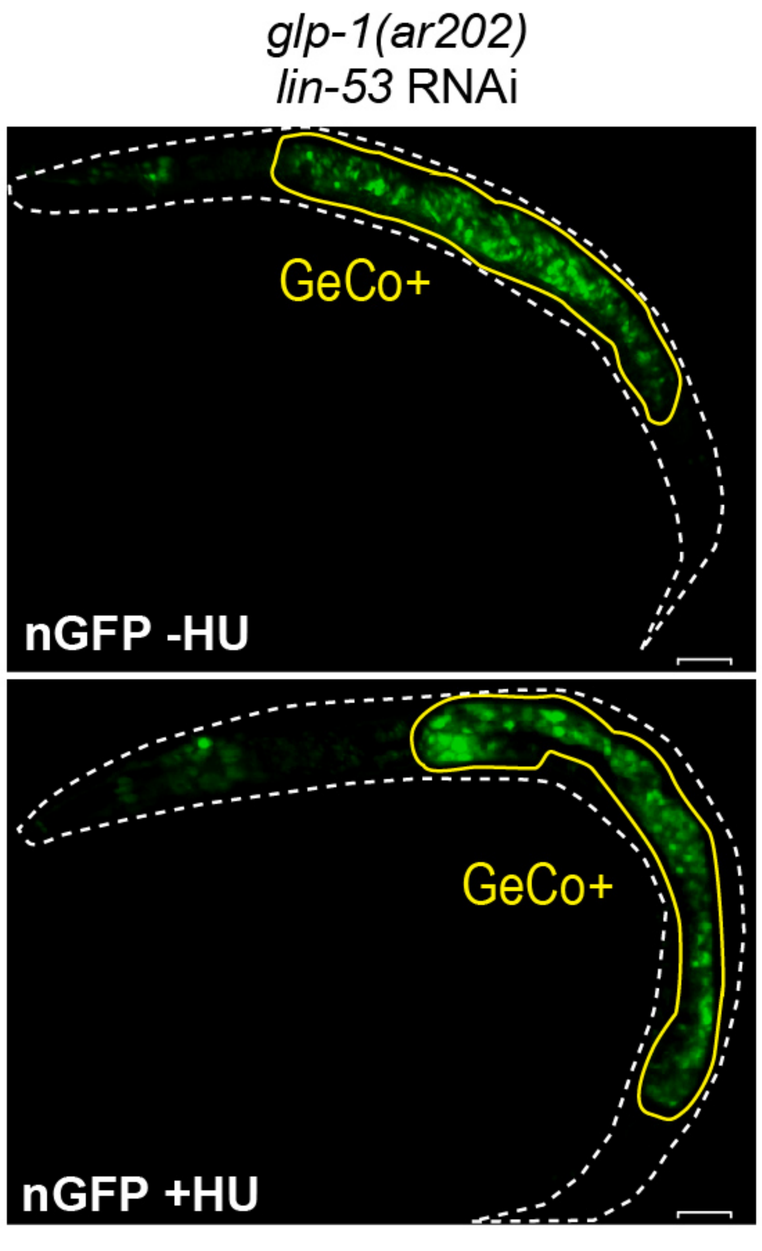

B

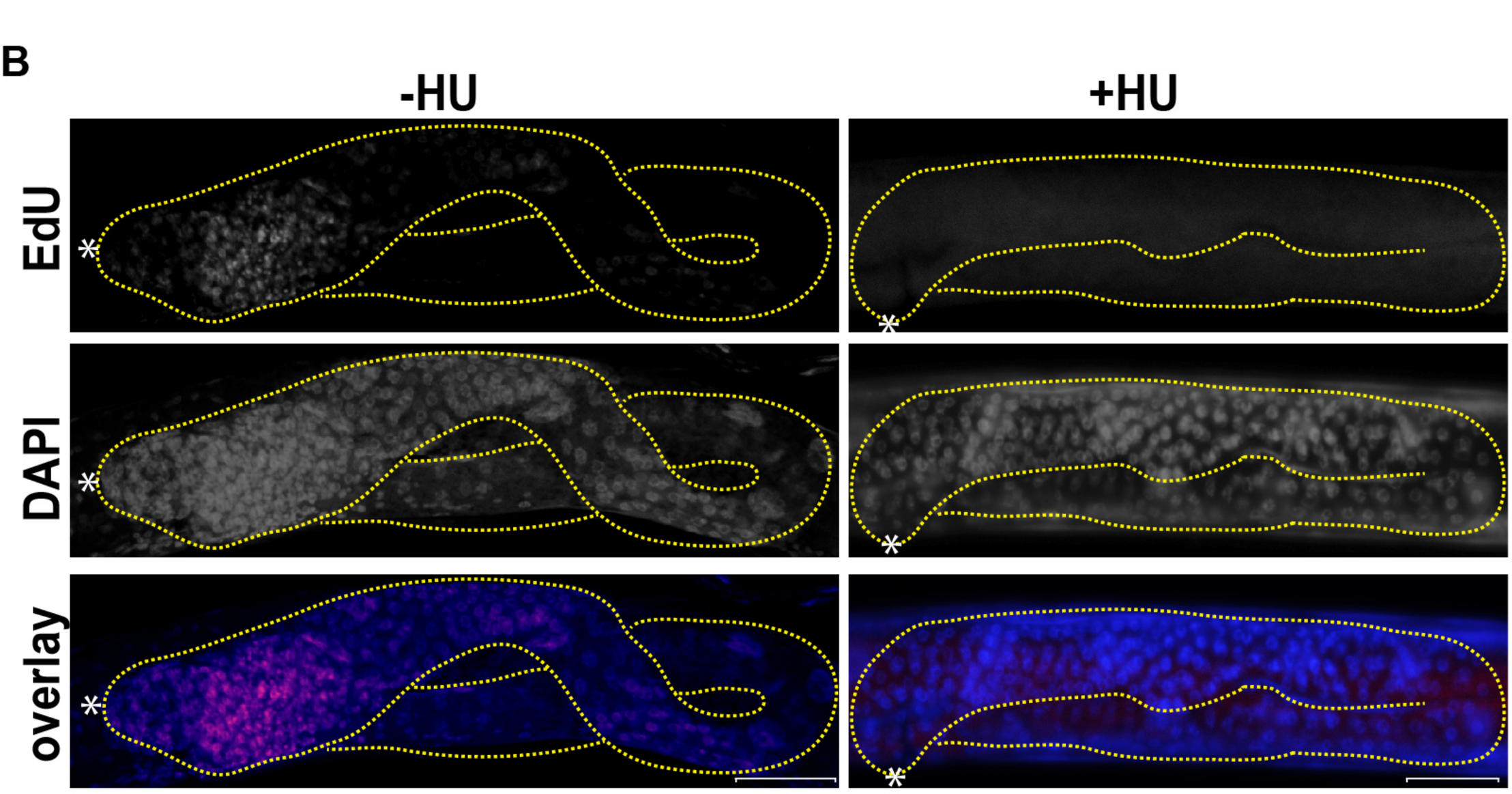

C

glp-1(ar202); otIs305 ntIs1

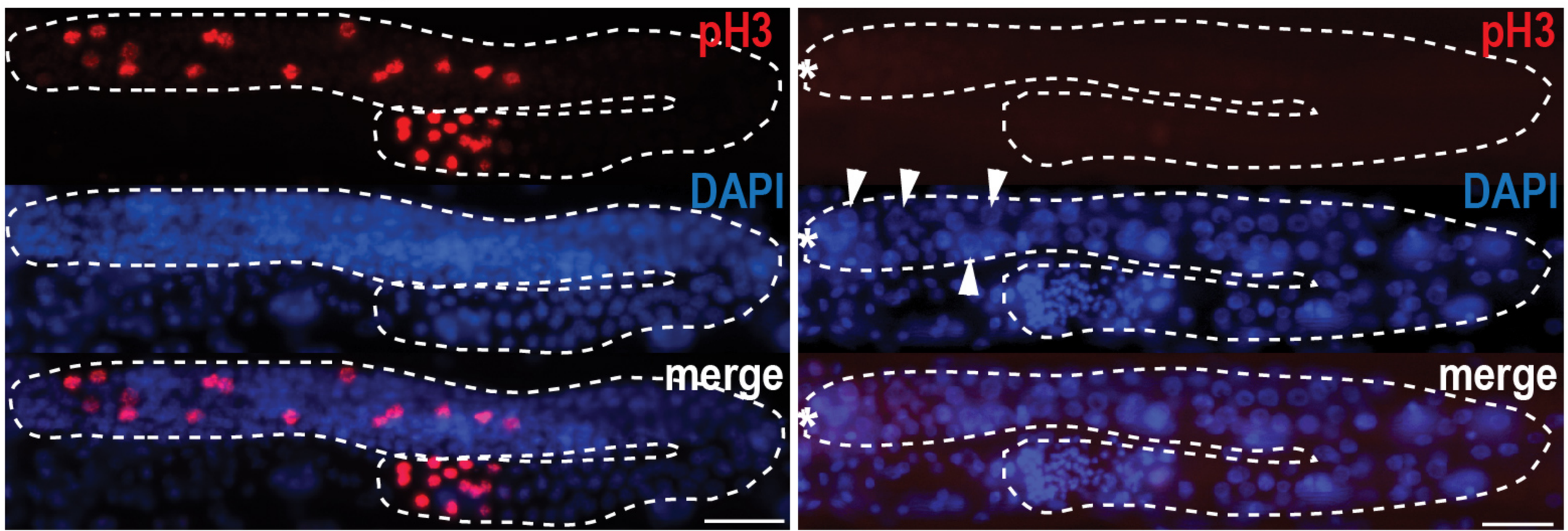

Seelk et al., Figure 2—figure supplement 1

A

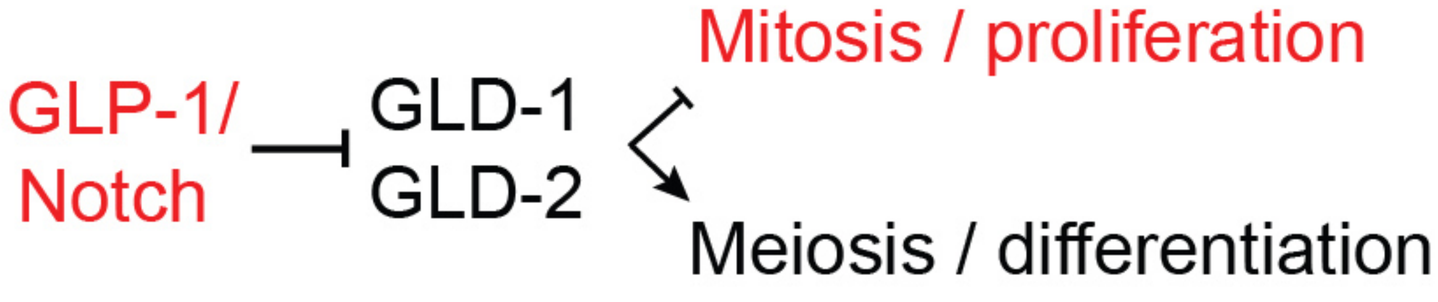

B

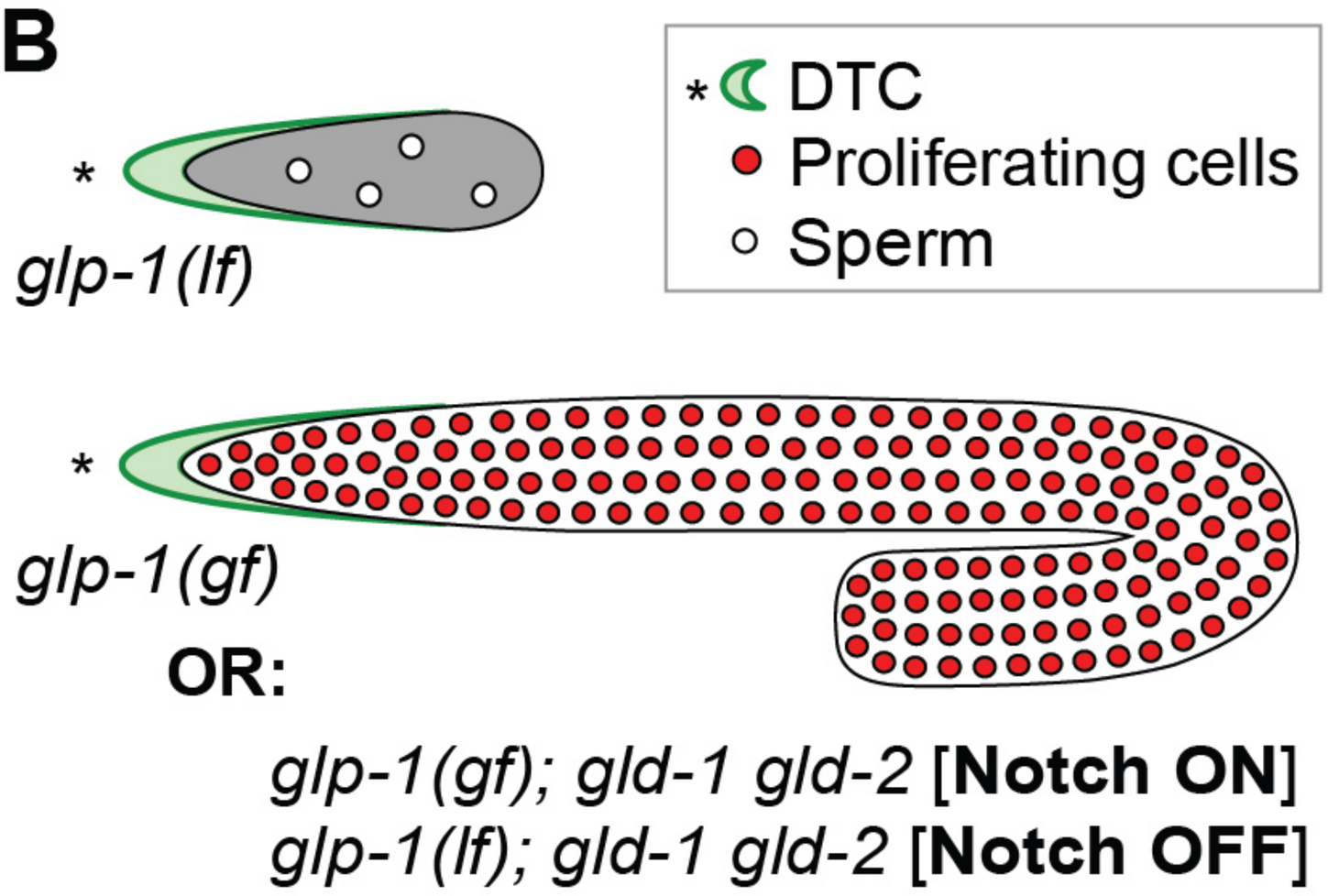

C

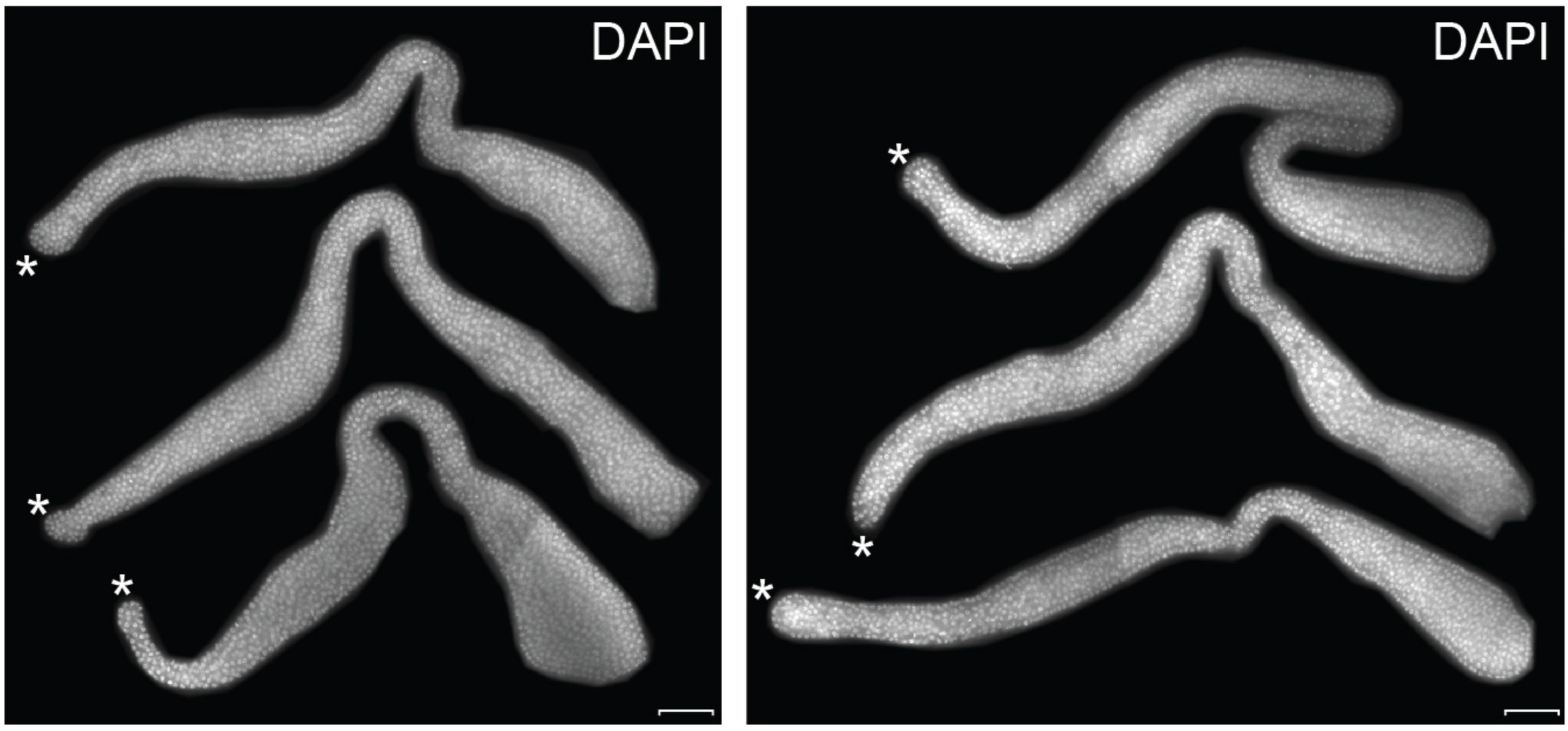

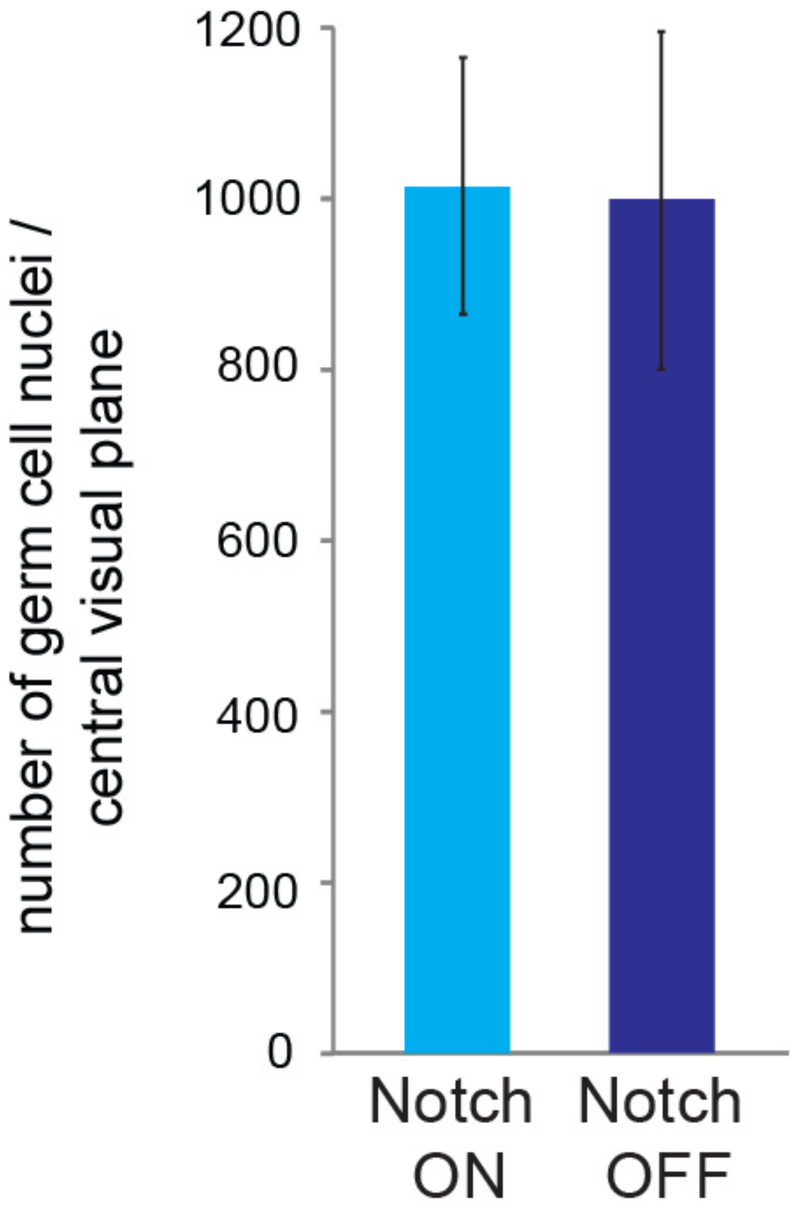

Seelk et al., Figure 2—figure supplement 2

A

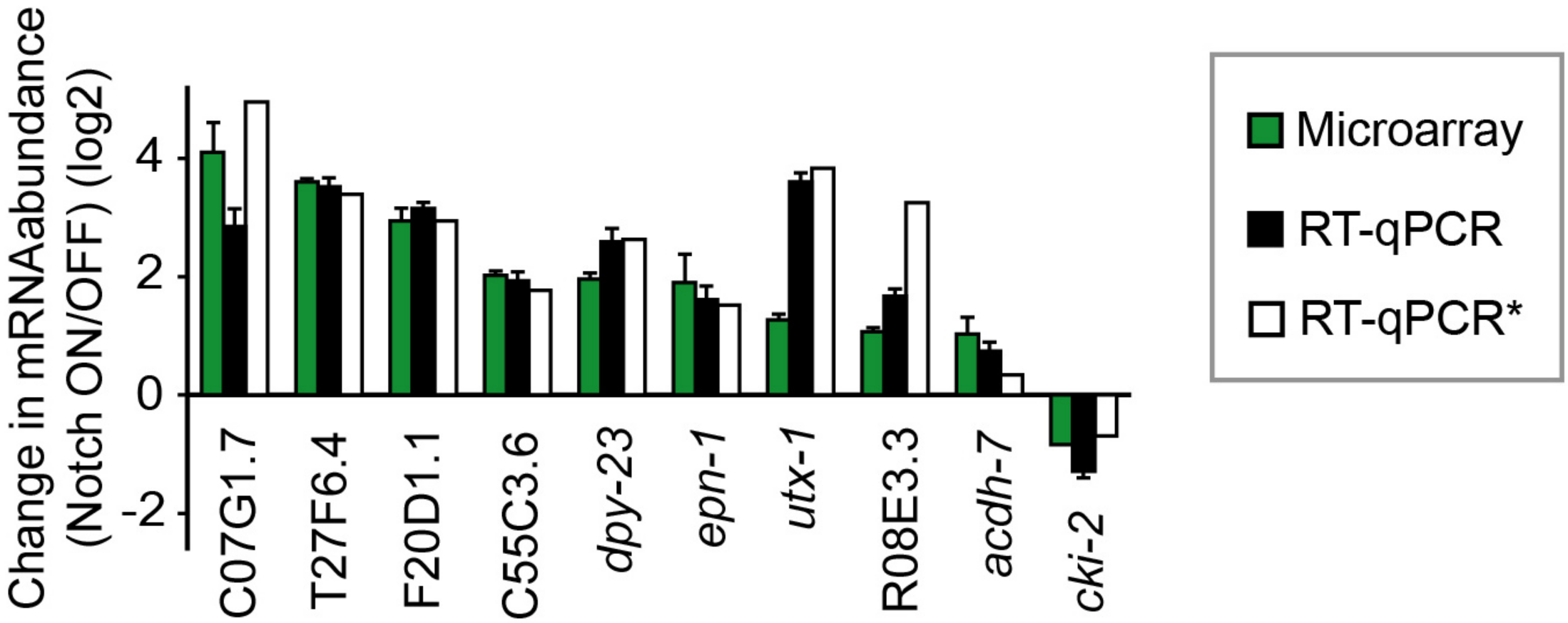

B

Chromosome	All	I.	II.	III.	IV.	V.	X.	Mitochondrial
Total number of genes *(%)*	17986	2623 *(14.58)*	3142 *(17.47)*	2424 *13.48)*	2853 *(15.86)*	4488 *(24.95)*	**2445** *(13.59)*	11 *(0.06)*
Total number of GLP-1 Notch activated genes *(%)*	110	9 *(8.18)*	10 *(9.09)*	12 *(10.91)*	19 *(17.27)*	10 *(9.09)*	50 *(45.45)*	0 *(0)*
Number of 'expressed' genes (cutoff>=4) *(%)*	5426	1281 *(23.61)*	996 *(18.36)*	1219 *(22.47)*	964 *(17.77)*	791 *(14.58)*	164 *(3.02)*	11 *(0.2)*
Number of 'expressed' and GLP-1 Notch activated genes (cutoff>=4) *(%)*	84	8 *(9.53)*	7 *(8.33)*	9 *(10.71)*	16 *(19.05)*	5 *(5.95)*	39 *(46.42)*	0 *(0)*

Seelk et al., Figure 2—figure supplement 3

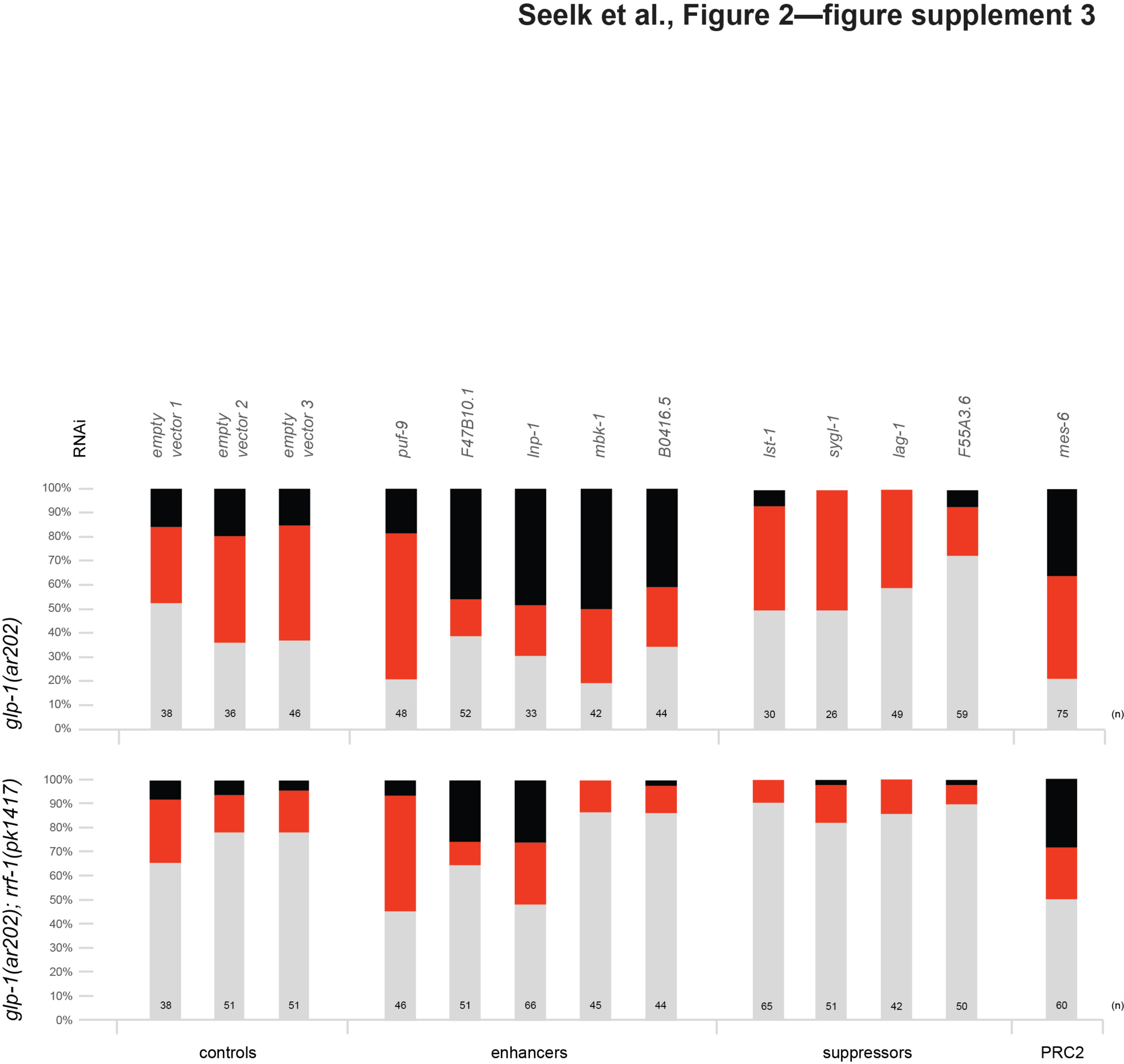

Seelk et al., Figure 2—figure supplement 4

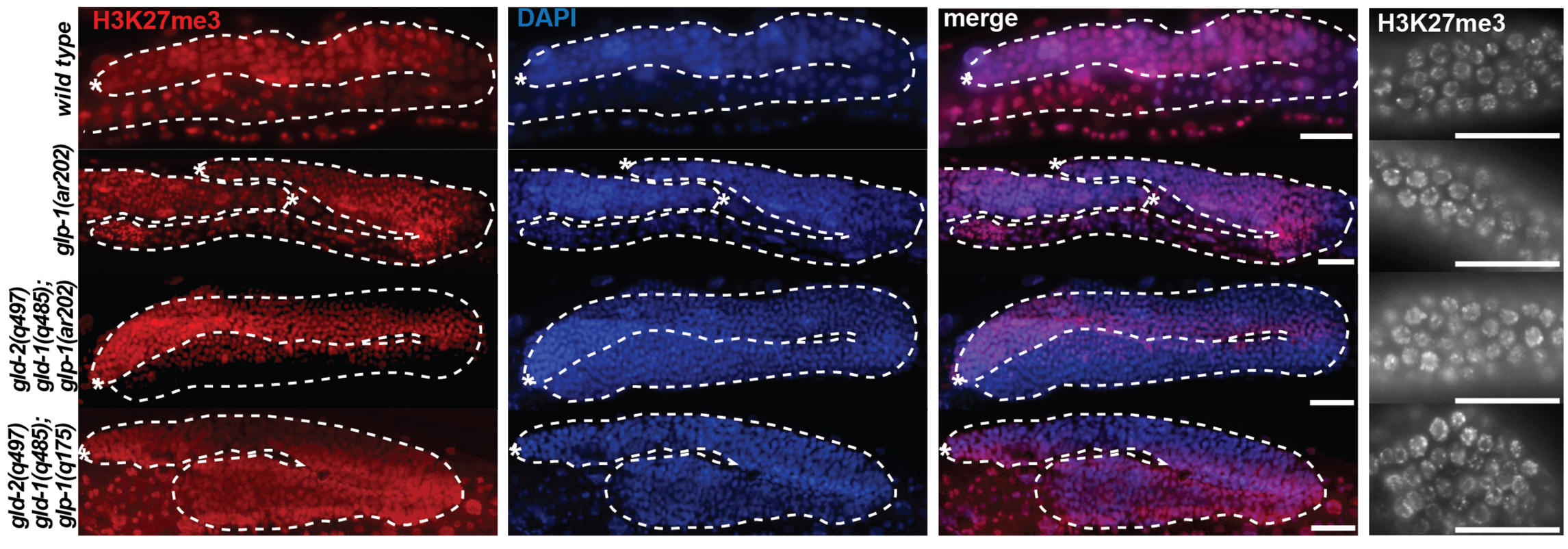

Seelk et al., Figure 4—figure supplement 1

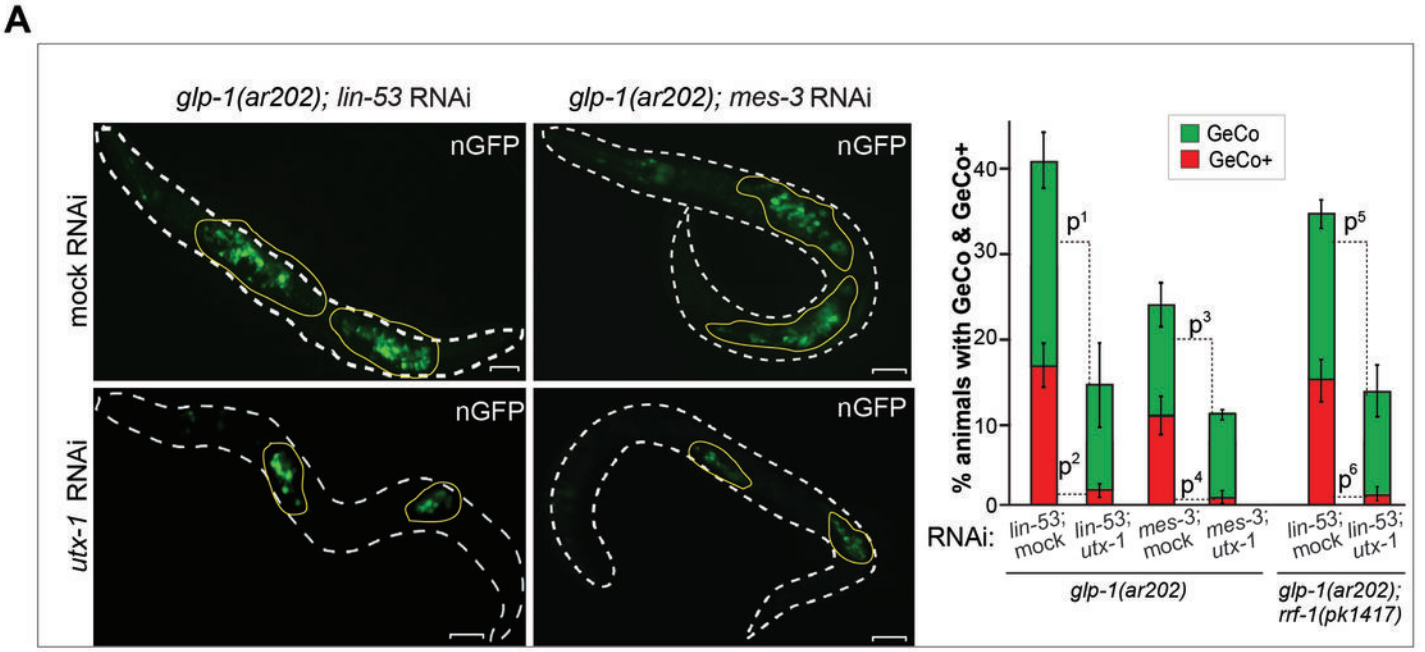

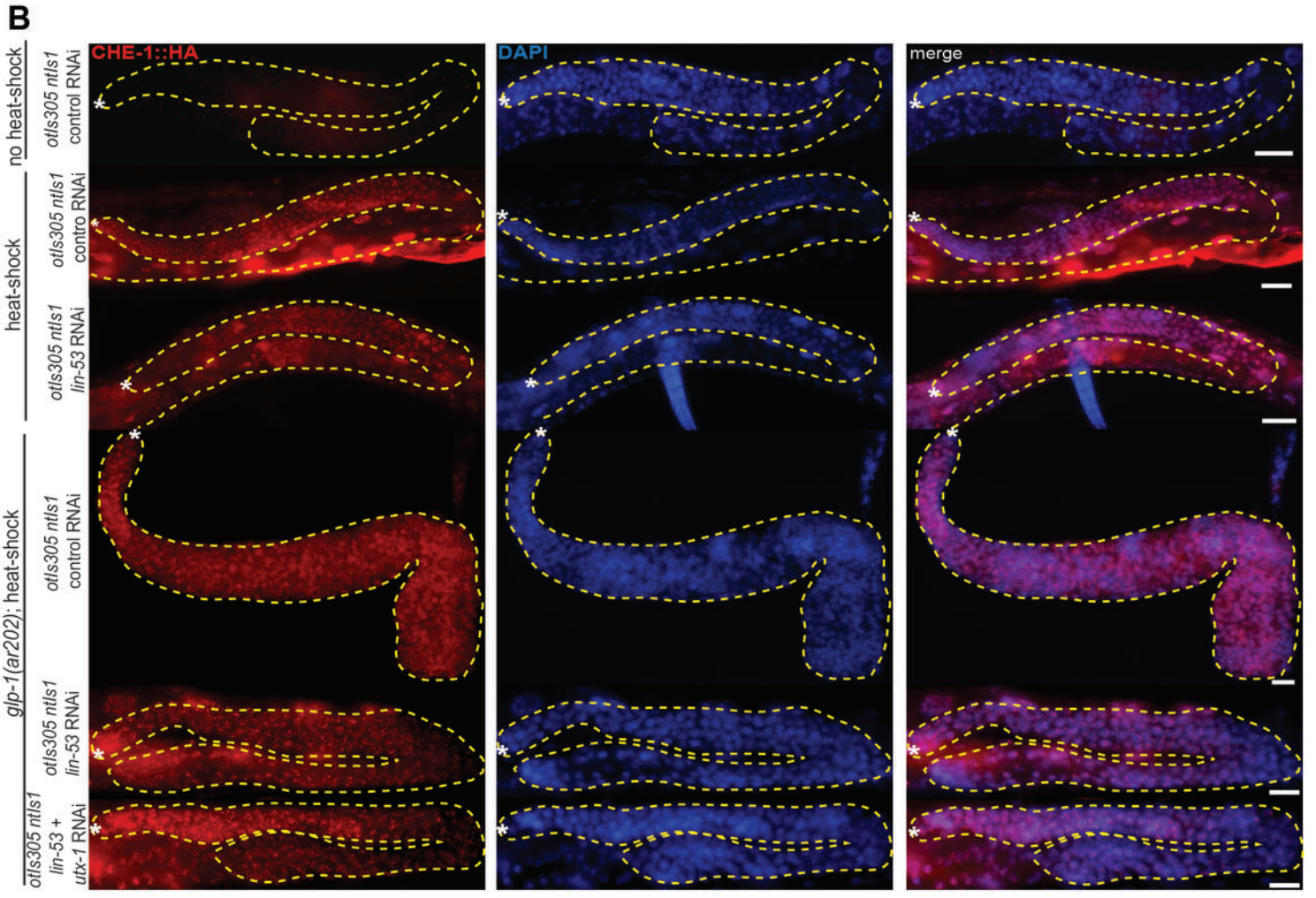

Seelk et al., Figure 5—figure supplement 1

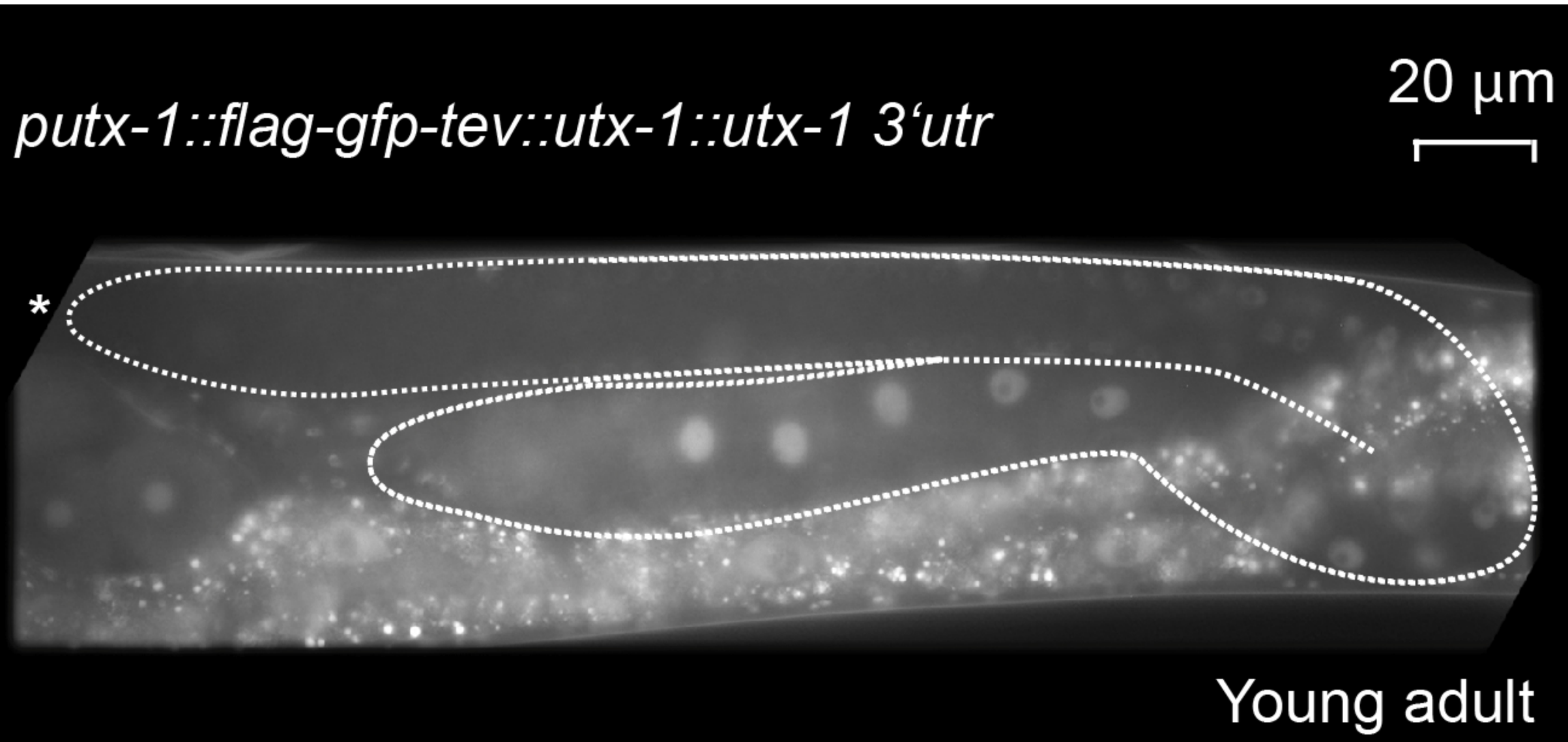

Seelk et al., Figure 5—figure supplement 2

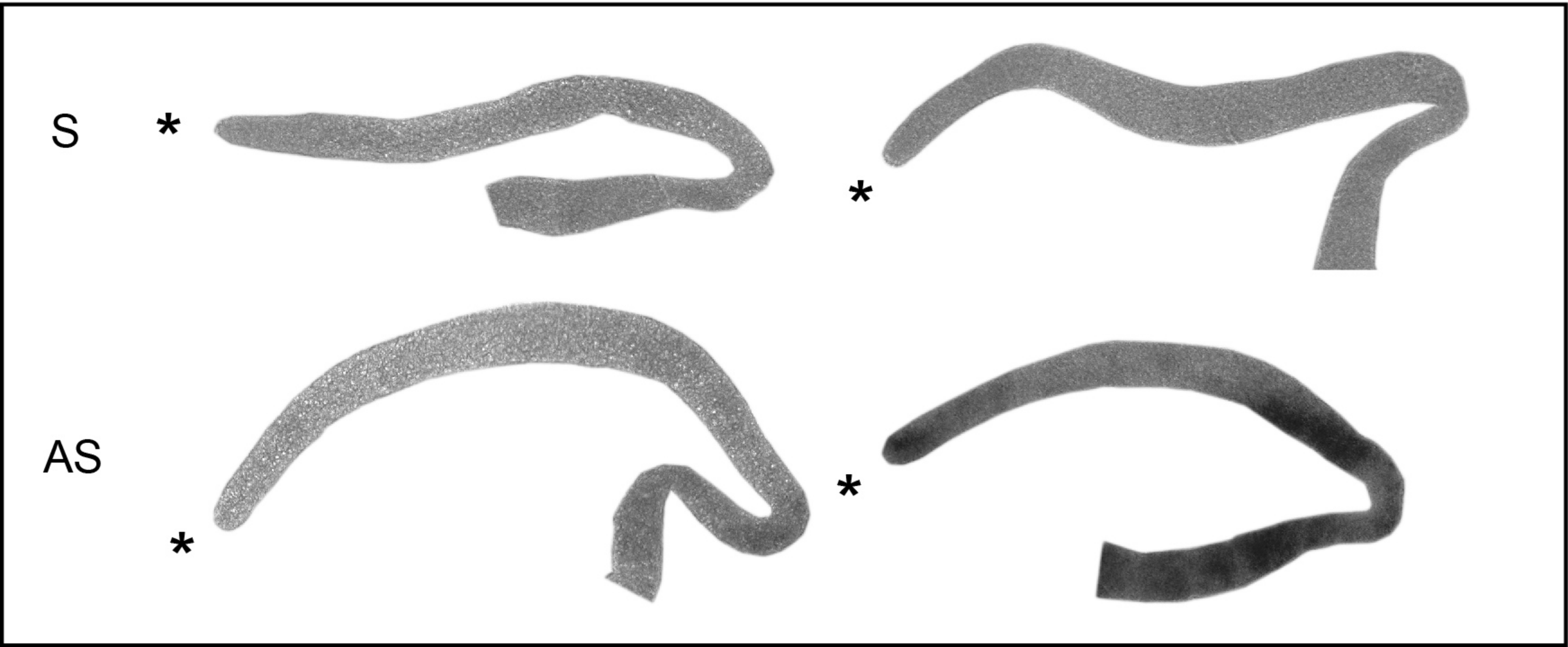

Seelk et al., Figure 5—figure supplement 3